8-8-2007

Surface Optochemical Sensors

Georgeta Crivat
University of New Orleans

Surface Optochemical Sensors

A Dissertation

Submitted to the Graduate Faculty of the
University of New Orleans
in partial fulfillment of the
requirements for the degree of

Doctor of Philosophy
in
Chemistry

by

Georgeta Crivat

B.S. University of Bucharest, 1996

August 2007

ACKNOWLEDGMENTS

I would like to express my appreciation to all those who gave me the opportunity to complete this dissertation.

First and foremost, I am deeply grateful to my supervisor Prof. Zeev Rosenzweig. He has been exceptionally supportive. As my advisor he constantly challenged me not to settle. He taught me to strive for excellence. His suggestions stimulated and encouraged me. After Hurricane Katrina our whole group was displaced. Zeev and Nitsa Rosenzweig opened not only their home but their hearts to our entire group. To have had the experience working with him has truly been a gift that I know could never be repaid.

I would also like to thank Prof. Matthew Tarr, Prof. Richard B. Cole, Prof. Branko S. Jursic, Prof. Guijun Wang, Prof. Kazuya Kikuchi, Dr. Nitsa Rosenzweig, Dr. Laurie Locascio, Dr. Michael Gaitan and Dr. Darwin Reyes for their suggestions and fruitful discussions on my courses and research projects.

I would like to acknowledge my close friends and colleagues: Gabriela Blagoi, Liliana and Mihai Viciu, Doinita Neiner, Speranta Stoian, Simona and Marius Tanasescu, Harry Rees, Paul E. Golder, Louise Golder, Darshita Shah, Brian Hutchison, Silvia Lacerda, Vania de Paoli, Lifang Shi , Ashley Quach, Arriel Wicks, Bryant Johnson for their love, friendship, and support.

I would like to express my sincere gratitude to Laurie Locascio, Michael Gaitan, Steven Choquette and Darwin Reyes of NIST for their kindness and consideration after Hurricane Katrina.

I would like to dedicate this dissertation to my wonderful parents Sevastita and Constantin.

TABLE OF CONTENTS

LIST OF FIGURES

Chapter 1

Chapter 2

Chapter 3

Chapter 4

Chapter 5

LIST OF TABLES

ABSTRACT

The objective of my research is to develop new surface optochemical sensors for studying cellular processes by investigating techniques to modify surface properties. The spectral characteristics of the modified surfaces and coatings are designed to show remarkable changes after interaction with analytes from biological fluids and cells.

My studies focused on pancreatic cells and addressed the need for improved techniques to measure zinc release from pancreatic cells (chapter 3, 4) and to measure the metastasis potential of cancerous pancreatic cells (chapter 5).

Chapter 3 describes the development of zinc sensing glass slides by conjugating a carboxyl-modified ZnAF-2 to an amino functionalized glass surface. The sensor was used for the measurement of glucose-stimulated zinc ion release from cultured beta pancreatic cells with impact in diabetes research. In chapter 4 is described conjugation of the carboxyl-modified ZnAF-2 to antibody molecules (A2B5) that specifically recognize pancreatic cells. This enabled for the first time the use of targeted zinc sensors to monitor zinc release events from pancreatic cells.

Chapter 5 describes development for the first time of a fluorescence sensor to measure the proteolysis activity of pancreatic cancer cells in microfluidic systems. The sensor was fabricated using a Layer by layer (LbL) deposition of polyelectrolyte. The sensor was based on Fluorescence Resonance Energy Transfer (FRET) between luminescent quantum dots (serve as donors) and rhodamine molecules (serve as acceptors) that are separated by multi-layers of polyelectrolytes. The microfluidic platform enables precise delivery of reactants to assemble the sensor and facilitate unique cellular assays of enzymatic activity and enzymatic expression on pancreatic cancer cells. Keywords: Biosensors, Optochemical, Surface Chemistry

CHAPTER 1

BACKGROUND OF SURFACE OPTOCHEMICAL SENSORS FOR PANCREATIC ACTIVITY

An optochemical fluorescence surface sensor employs a recognition component which expresses changes in spectral characteristics upon interaction with a specific analyte. The chemical or physical reaction between analyte and sensor molecule takes place at the solid interface. Changes in absorption, emission quantum yield or shift in the wavelength in the emission spectra are generally used to determine the concentration of specific substances by using spectroscopic methods. Fluorophores which specifically bind corresponding analytes are defined as probes for analyte recognition [1].

As a biosensor, the film is provided with an active biological sensing element inserted in the transduction process. A transducer converts the interaction analyte-sensor in a continuous electrical or optical signal corresponding to the analyte concentration. The sensitivity and selectivity of a biosensor is highly dependent on the affinity of sensor-analyte interaction and transducer performance [2, 3].

Generally, the interaction of fluorescent substances with analytes from biological specimens provides one with information about their particular location on proteins, membranes or conformational changes (e.g., protein folding involving FRET) and their physiological status [41].

There are inherent problems associated with using freely diffusing dyes, such as overloading with fluorescent probes, interference reactions with other analytes from environment, permeability through membranes and lack of site specific information. Covalent immobilization of the sensing molecule to a substrate prevents the dye from leaking in the medium or permeating through membranes.

When a cell is bearing of receptors, surface antigens with specificity for a given antibody or hormone, then incorporating target molecules with specificity for a given substrate, immobilizes the sensor onto the material of interest, and provides with site specific information.

When using freely diffusing probes in intra or extra cellular analysis, cytotoxicity and chemical and photo stability are issues to take into account.

Previously, fluorescent probes were immobilized on particles used as intracellular sensors. These probes were encapsulated by biologically localized embedding (pebbles), liposomes, and lipobeads [4-9]. Toxicity issues were overcome by incorporating the sensor in a hydrophilic polymer matrix or phospholipid layer (liposoms). The sub- micrometer sensors have millisecond response time. However, the leakage rate of fluorophores from liposome affects the accuracy of measurements. Lipobeads, particle based sub-micromiter sensors, coated with a phospholipid membrane, were further developed to enhance the stability of the sensor. They were used to detect intracellular pH and oxygen in physiological conditions [9].

In the development of a surface sensor, the immobilization of the fluorophore to a physical support is a key step in the design of the sensor.

There are several approaches to incorporate the fluorophore in a film using mechanical, electrostatic or covalent immobilization. The advantages of immobilization of fluorescent

molecules on a surface include the elimination of fluorophore leakage into the surrounding solution and enhanced stability and lifetime of the sensors [10].

We investigated two techniques to present the sensor: covalent immobilization of the sensor on modified glass surfaces and electrostatic immobilization of the sensor by processing multilayer thin films.

The covalent immobilizations methods are preceded by a chemical modification step of the glass slide surface such to provide it with nucleophilic functional groups to enable further conjugation with fluorophores.

The development of ultra thin organic films, using electrostatic attraction between polymers as a driving force, is a versatile technology which enables the control of the structure and properties of the films within nanometer scale [11, 12].

It is also described in literature fabrication of ultra thin film optical chemical sensors for pH, metal ions (Fe, Hg); 2, 4-dinitro toluene, organic nitro compounds, i.e. using electrostatic Layer-by-Layer assembly [13].

The goal of these studies was to develop film/coating sensors for detecting pancreatic activity. The pancreas is a gland organ with digestive and endocrine functions. The endocrine pancreas is represented by millions of clusters of cells organized in islets of Langerhans. The most important types of cells localized in these islets are beta cells which secrete insulin, alfa cells which secrete glucagon and delta cells which secrete somatostatin. Unfortunately, it is relatively difficult to discriminate between them using typical staining techniques. [39, 40] Therefore, there is a need for the development of new sensing methods to classify the cells. Because cells within islets have

specialized secretory functions with relevance in their pathology, methods that allows for cell identification using cell-secreted products as the analyte are an obvious choice.

The exocrine pancreas is responsible for the secretion of bicarbonate ions (centroacinar cells) and digestive enzymes (basophilic cells). The most important diseases which affect the pancreas are diabetes mellitus and pancreatic cancer. Diabetes mellitus is a metabolic disorder which is characterized by the inability of the beta cells to secrete adequate amounts of insulin to preclude hyperglycemia. The disease results in severe complications (e.g., acidosis and non ketoacidosis coma, renal failure, blindness, retinal damage). Reports suggest that zinc is associated with the function of beta cells including insulin synthesis, storage and release [14]. Insulin is co-stored as a hexamer complex with two zinc ions within the secretory vesicles of beta pancreatic cells. When pancreatic cells are stimulated by elevated glucose concentration, insulin is co-released with zinc by exocytosis. Dissociation of the insulin-zinc complex occurs in conditions of exposure to extra cellular pH [14, 15]. The dissociation results in the formation of insulin monomers, which are the biologically active form of insulin, and free zinc ions. The role of zinc ions in insulin secretion and in the pathology of diabetes is not entirely understood. However, it is thought that zinc deficiency might affect the capacity of islets to synthesize and release insulin [14]. Complications of diabetes could also originate from the high level of intracellular oxidants associated with decrease in the zinc dependent antioxidant enzymes (e.g., superoxide dismutase SOD) [14].

1.1 Surface Optical Chemical Sensors for Detecting Zinc Ion Release Events from Pancreatic Beta Cells

A variety of analytical techniques are used to detect and quantify zinc in aqueous samples. Inductively coupled plasma atomic emission spectroscopy [21, 22] and atomic absorption spectrophotometry [23] are used extensively to detect zinc at trace levels. Due to the trace level of zinc ions in biological samples a pre-concentration step was required to realize sufficient sensitivity [21]. X- ray fluorescence spectroscopy has been used successfully to detect zinc ions in tissues without a pre-concentration step [24]. Another detection technique, based on using radioisotopes of Zn, is limited by the significant hazardous potential, isotope availability and cost. None of these techniques could be used for real time zinc ion detection in cellular systems.

Miniaturized fluorescence sensors that were developed in the last two decades provided a new analytical tool for the detection of intra- and extra -cellular ion levels.

Among the zinc ion fluorescent indicators that were used for the analysis of zinc ion in beta cells include ultraviolet excitable quinoline-based dyes like 6-methoxy-8-quinolyl-para-toluenesulfonamide (TSQ) [16], zinquin [17] and visible light excitable fluorophores like Fluozin-3 [18]. The basic limitation of these dyes is their narrow zinc ion selectivity, especially in the presence of calcium. Additionally, the diffusion and partitioning of the dye through the cellular membrane affects the accuracy of extra cellular measurements of zinc.

Recently, a new zinc sensitive fluorophore {6-[N- [N', N'-bis (2-pyridinylmethyl)-2-aminoethyl] amino-3', 6'-dihydroxy-spiro [isobenzofuran-1(3H), 9'-[9H] xanthene]-3-one} (ZnAF-2) was synthesized [19]. This dye is structurally and spectroscopically similar to fluorescein and has a superior selectivity and sensitivity toward zinc ions. The cellular permeability of ZnAF-2 like

other zinc ion sensitive dyes still remained a problem. The purpose of the modification of ZnAF-2 with a piperidine carboxylic acid aliphatic chain was to allow conjugation chemistry to various substrates and prevent the permeability issues.

We designed fluorescence based glass slide film sensors for studying zinc release events from pancreatic cells (Chapter 3). The direct application of the sensor is on studies of pathogenesis and pharmacology of diabetes mellitus.

For the targeted measurement of zinc ion release from pancreatic β cells, a coating of beta cells with an antibody sensor was developed (Chapter 4). The sensor was developed by conjugation of antibody A2B5, for targeting of the biological system, with ZnAF2 for zinc release measurements.

1.2 Surface Optical Chemical Nano-Sensor for Detecting Pancreatic Enzymatic Activity

Pancreatic adenocarcinoma is a malignant tumor with a poor prognosis. It is the fifth leading cause of death in United States [20]. This prognosis originates from the high potential of invasiveness and malignancy of pancreatic cancer into neighboring blood vessels. The tumor cell invasion is described as a protease-driven digestion of extra-cellular matrix and basement membrane. In addition to a tumor associated trypsinogen, the cancer cells have also the ability to synthesize a trypsinogen activity stimulating factor (TASF) [20].

Detection of enzymatic activity, in conjunction with detection of CA19-9, lipase, iron and albumin in the serum proved to be sensitive markers in the diagnosis and study of pancreatic cancer [25]. Studies on enzymatic activity are typically performed using transfection,

zymography (electrophoretic technique for measuring proteolytic activity) and western-blott analysis which use gel electrophoresis to discriminate native proteins based on size and net charge and denatured proteins based on size [26, 27]. However, these techniques are invasive and destructive as they necessitate obtaining of samples from tissue homogenates or extracts.

Fluorescence detection of enzymatic activity by encapsulation of enzymes within liposome based nano-biosensors was reported to improve enzyme stability against denaturation, unfolding and environmental effects [28].

Among the fluorescence detection methods used to probe enzymatic activity, fluorescence resonance energy transfer (FRET) is used due togenerally provide with improved spatial resolution and sensitivity. FRET based sensors are less sensitive to environmental changes and illumination factors - as a result it is a step forward in analytical performance as compared to intensity based fluorescence sensors. There is a large interest in employing FRET in the design of biological assays. As donors, luminescent quantum dots appear to be a practical alternative to organic fluorophores due to their higher photo and chemical stability, high emission quantum yield, wide excitation range (which enables choosing an excitation wavelength such that to avoid direct excitation of the acceptor) and wavelength tunability [29-31]. Quantum dots conjugated to peptides labeled with molecular acceptors were also used as donor probes in the design of sensors for enzymatic activity [29, 32, and 33].

However Cd-containing quantum dots have a limited applicability in the analysis of cells and tissues due to their potential toxicity.

Therefore, to improve the biocompatibility of quantum dots and lessen toxicity issues, we incorporated quantum dots as donor probes and rhodamine labeled peptides as acceptors in polyelectrolyte multilayers, using layer-by-layer deposition techniques.

Furthermore, we designed a surface sensor for monitoring the proteolytic activity of pancreatic exocrine cells with direct application in studies of tumor invasion and metastasis of malignant tumors.

1.3. Fluorescence and Fluorescent Molecules

Fluorescence is defined as a type of luminescence and involves the absorption of light by a given molecule, propelling it to a singlet excited state, where from the molecule returns to ground state by emission of light. In the excited singlet state the electron is paired to the second electron in ground electronic state. As compared to fluorescence, phosphorescence, which is another type of luminescence, requires emission of a photon from triplet excited state. The electron has the same spin orientation with the one corresponding to the ground state. The outcome of this is that the transition to ground state is not spin-allowed and the emission lifetime is longer (10^3-10^0 s^{-1}) as compared to the emission lifetime in fluorescence (10 ns) [34].

Fluorescent molecules are generally aromatic molecules (example: quinine, fluorescein, rhodamine B, acridin Orange, and i.e.) with planar, rigid structures. Aliphatic molecules with extended π electron systems can also be fluorescent. The electronic transition is a transition of π to π^* low-lying singlet excited state. Potentially fluorescent molecules are also those which contain a lone pairs of electrons which can be promoted in electronic transitions, like nitrogen [35].

Fluorophores can be classified as intensity-based probes and wavelength ratiometric probes.

In intensity based measurements, fluorophores show only changes in intensity in the emission spectra but no spectral shift due to a difference in the quantum yield between free and complexes.

Wavelength ratiometric probes show spectral shifts in the absorption and emission spectra upon interaction with an analyte.

Sensitivity of fluorescence based methods is higher than absorption methods since a single fluorescent molecule could generate thousands of photons.

Typically fluorophores are also characterized by a high rate of photobleaching. This process results in destruction of fluorophores by irradiation and loss of fluorescence.

There are a few characteristics which differentiate fluorescence from scattering (Raman, Rayleigh): emission occurs at longer wavelengths than excitation, two clearly separated peaks for excitation and emission are observed, quantum yield is independent of the excitation wavelength.

1.4. Jablonski Diagram

A Jablonski diagram is the representation of the physical processes which occurs during excitation of a molecule and its emission (Figure 1.1).S_0 represents ground singlet electronic state while S_1 and S_2 represent first and second excited singlet electronic states. 0, 1, 2 represent the vibrational energy levels of each of these electronic states.

Excitation of a fluorophore propels the electron on higher electronic levels like S_1 or S_2.

The surplus of energy from S_2 is subsequently lost through nonradiative vibrational relaxation which brings it to a zero vibrational level of S_2. It is possible then that the molecule relaxes to the lowest vibrational level of S_1 through a nonradiative internal conversion which occurs in 10^{-12} s or less [34, 35]. Internal conversion is complete before the fluorescence emission which occurs in 10^{-8} s.

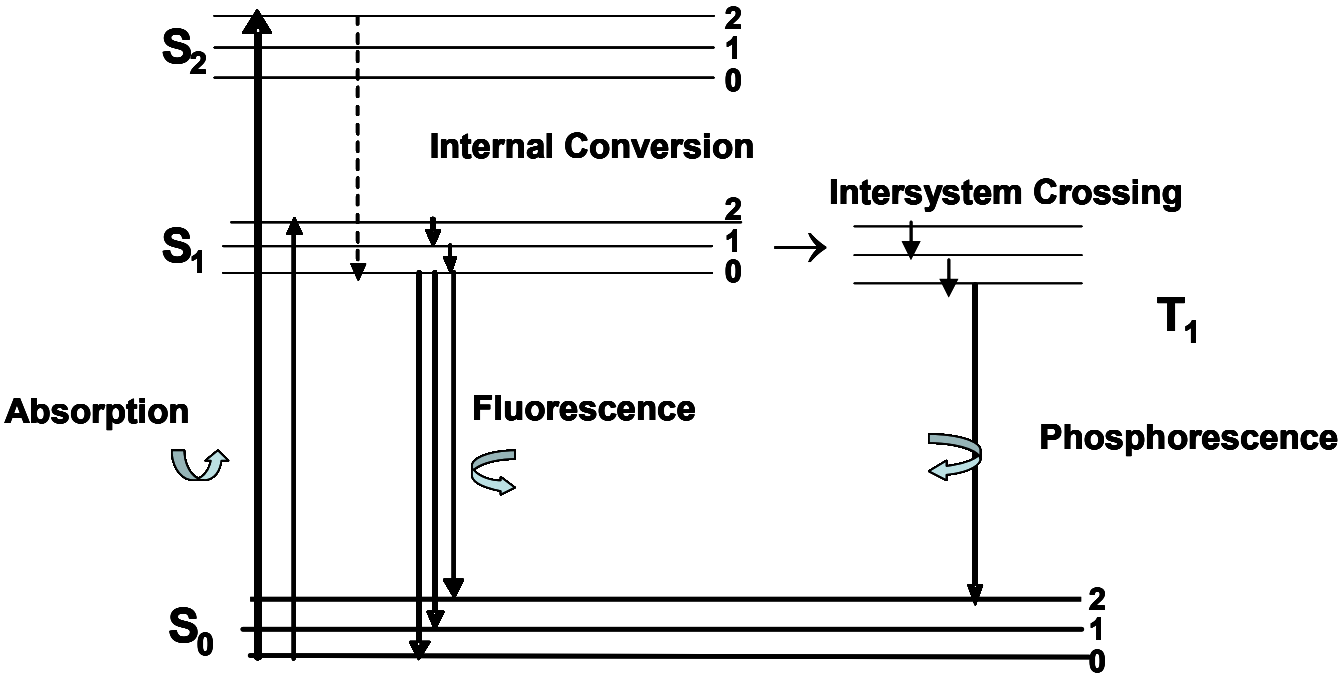

Figure 1.1 Representation of a Jablonsky diagram.

Fluorescence emission returns the molecule to any vibrational ground state level. As a result the emission spectrum is a mirror image of the absorption spectrum ($S_0 \rightarrow S_1$). Because the spacing of vibrational levels in the excited state resembles the ground state, the vibrational structures are similar in the absorption and emission spectra [1].

Typically, the fluorescence spectrum appears at longer wavelengths due to the energy lost during vibrational relaxation (Stokes shift).

In special cases, through a non-radiative intersystem crossing, the molecules could undergo a spin conversion from singlet S1 to triplet state T_1.

The emission of light from triplet state is called phosphorescence and is represented at longer wavelength in the emission spectrum. Heavy atoms like iodine and bromine perturb the electron spins and enhance state mixing which enhance the phosphorescence [34, 35].

The non-radiative deactivations represented in Figure 1.1. are internal conversion, intersystem crossing and vibrational relaxation. The internal conversion is a transition between the same spin states while intersystem crossing involves different spin states. Vibrational relaxation is a fast process and result from collisions between molecules and their quenchers.

1.5. Fluorescence Efficiency and Lifetime

Quantum yield (Φ_f) and fluorescence lifetime are the most important characteristics of fluorescence. Quantum yield is defined as the ratio between the number of emitted photons and number of absorbed photons [35].Considering the rate constants of some of the radiative and nonradiative processes, the fluorescence efficiency can also be represented as:

$$\Phi_f = k_f / (k_f + k_{ic} + k_{is} + \mathbf{kq}) \quad (1.1)$$

Where the subscripts f corresponds to fluorescence, ic stands for internal conversion, is for intersystem crossing, kq is for quenching [35]. The brightest molecules approach unit in their quantum yield.

The fluorescence lifetime (τ) is defined as the first order decay process of a fluorescent molecule which excited by a photon, relaxes from excited state through different radiative and nonradiative processes.

1.6. Mechanism of Sensing of Optochemical Sensors

Fluorescence based sensors show changes in fluorescence quantum yield, wavelength, anisotropy and lifetime upon interaction with specific analytes. The advantages of using intensity based sensors include that they are sensitive, versatile, and only require simple instrumentation.

1.6.1. Photoinduced Electron Transfer

ZnAF2, a fluorescent sensor molecule for Zn^{2+} used in the design of glass cover slip zinc film sensors and antibody zinc sensors, was synthesized from corresponding 6-aminofluorescein [19].The excitation wavelength of this compound is in the visible range, a characteristic which eliminates possible interferences from biological specimens which auto fluoresce in ultraviolet light. The fluorescence quenching of aminofluorescein is explained by manipulation of

photoinduced electron transfer phenomenon (PET). Photoinduced electron transfer is a transfer of a lone pair of electrons of a neighboring amine in presence of the light, into the aromatic ring [1].

Photoinduced electron transfer was largely used to design sensors for metal ions [1, 36, 37].Typically in the absence of zinc ions the dye forms an exciplex complex with amine groups. In the presence of metal ions the exciplex is no longer formed and aminofluorescein becomes fluorescent.

Aminofluorescein itself has low quantum yield fluorescence due to a high HOMO (highest occupied molecular orbital) level of the electron donating group [19]. In the presence of light at a suitable wavelength (Figure 1.2.), fluorescein molecules propel an electron from the HOMO orbital to the LUMO orbital (lowest unoccupied molecular orbital).

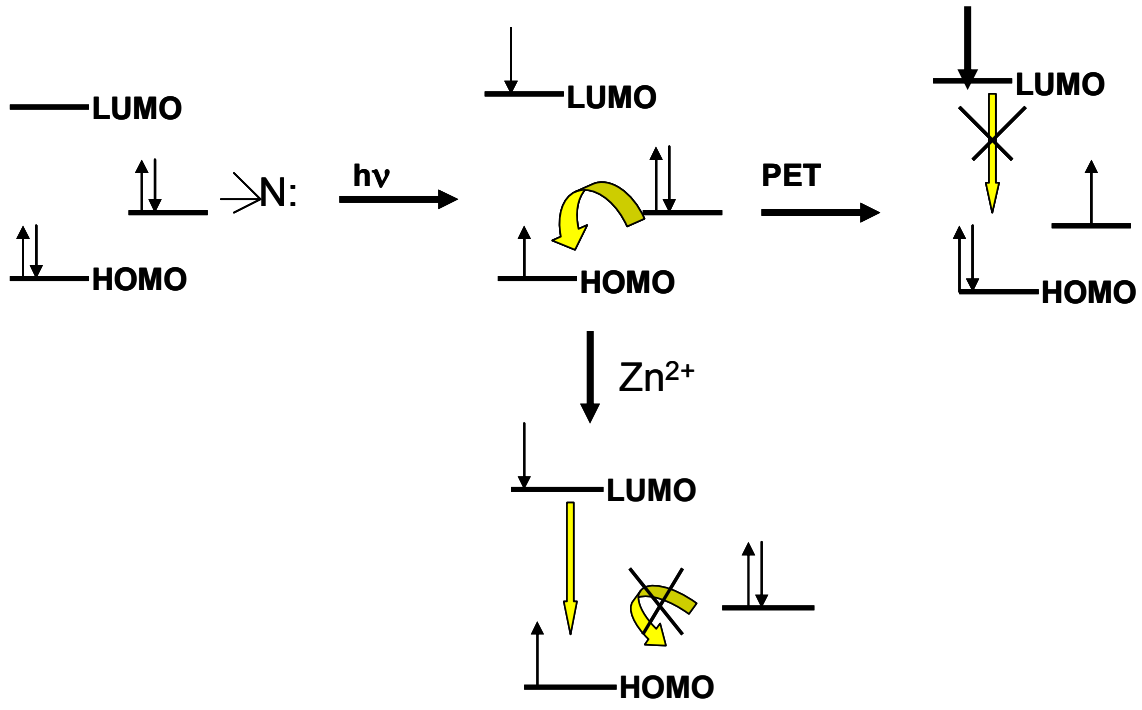

Figure 1.2 Diagram representing the mechanism of photo induced electron transfer

One of the lone pair of electrons of neighboring nitrogen, from the zinc binding site, will occupy HOMO orbital of the excited molecule. The outcome of this configuration consists in blocking the fluorescence pathway (PET). When the electron donation is constrained by a complex formation with zinc ion (Figure 1.3) and involving the lone pair of electrons of nitrogen (which converts it in a less electron donating group) then the fluorescence is highly augmented.

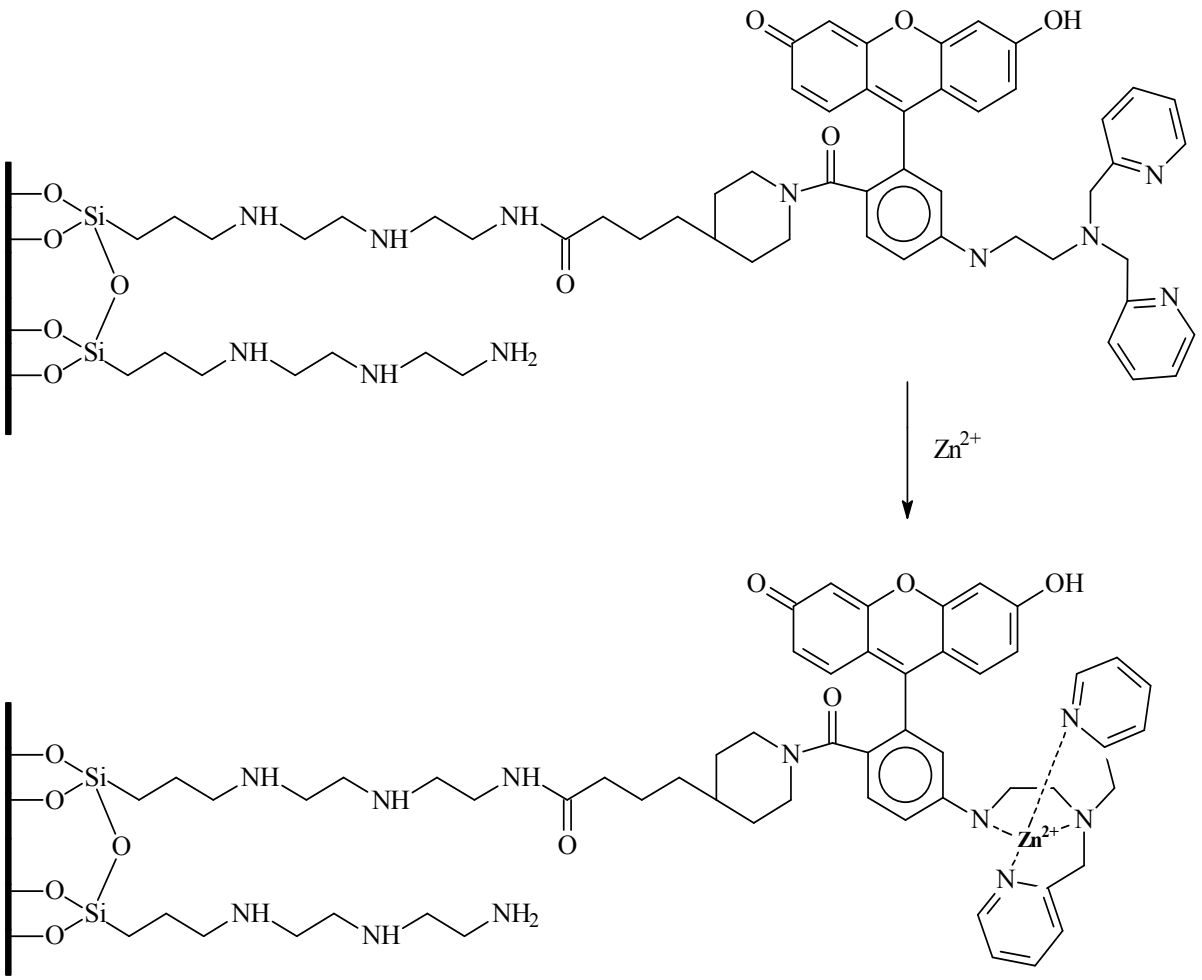

Figure 1.3 Representation of complex formation of glass cover slips zinc film sensor in presence of zinc ions

1.6.2. Fluorescence Resonance Energy Transfer

Fluorescence resonance energy transfer (FRET) is a non-radiative transfer of excited-state energy from a donor (D) to an acceptor (A). Energy transfer occurs when the emission spectrum of a donor molecule overlaps with the absorption spectrum of an acceptor. Förster resonance energy transfer involves a dipole-dipole coupling mechanism followed by a non-radiative transfer of excitation energy to the acceptor. The resonance term is to define a transfer which does not involve photons.

The rate of energy transfer (k_T) is a measure of the relative orientation of donor and acceptor dipoles in the interaction space, distance between them and the degree of spectral overlap of donor emission spectrum and acceptor absorption spectrum(relation 1.3) [38]. τ_D represents the decay time of donor in absence of acceptor, R_0 is the Förster distance and r represents the actual donor-acceptor distance.

The distance at which the energy transfer is 50% efficient is known as Förster distance and covers a range between 2 and 7nm.

$$k_T = 1/\tau_D \, (R_0/r)^6 \qquad (1.3)$$

If R_0 = r, the transfer efficiency is then equal to 50%. The typical application of FRET is in measuring the separation distance between two sites of a molecule. Förster distances ranging from 2 to 9nm are particularly useful in measuring distances of large biological molecules (ex. DNA, protein folding).

The efficiency of resonance energy transfer was shown by Förster to be dependent on the r^6 power distance between donor and acceptor [38]:

$$E= R_0^6 /(R_0^6 +r^6) \quad (1.4)$$

The transfer efficiency approaches unity when the distance between donor and acceptor falls below the Förster distance. For a system where donors and acceptors are randomly distributed in solution, the R_0 is expressed as follows:

$$R_0 = [3000/2 \pi^{3/2} NA_0]^{1/3} \quad (1.5)$$

N represents Avogadro number and A_0 is the concentration of acceptor with a 76% energy transfer [38].

The transfer efficiency is typically calculated (rel.1.6) using the relative fluorescence intensity of donor (F_D) without acceptor and in presence of acceptor (F_{DA}) [38].

$$E= 1- F_{DA}/ F_D \quad (1.6)$$

The orientation factor k^2 is a function of the donor and acceptor transition dipole moments and accounts the angles between dipoles and the vector joining them. The relative orientation of donor and acceptor ranges from 0, when the dipoles are oriented perpendicular to each other, to 4 for collinear dipoles [38].

FRET in PEMs (polyelectrolyte multilayers) was employed to investigate the distribution of donor and acceptors within the matrix and evaluate their average separation (Chapter 5). The distance –dependent fluorescence resonance energy transfer was exploited in the design of the FRET based surface sensor for enzymatic activity. The sensor was developed by incorporating quantum dots as donors and rhodamine labeled neurotensin as acceptors in polyelectrolyte multilayers using layer-by-layer deposition techniques. The changes in FRET signals between quantum dots and immobilized rhodamine on neurotensin, were indicative of the enzymatic activity which hydrolyzes the labeled neurotensin.

References

1. Joseph R. Lakowicz, Principles of Fluorescence Spectroscopy, Chapter 19: Fluorescence Sensing, pg 531-572, Kluwer Academic /Plenum Publishers, 1999
2. Cooper, M.A.; *Nat. Rev. Drug. Discov*. **2002**, 1(7), 515-528
3. Gabriela Blagoi, Fluorescence Resonance Energy Transfer (FRET) Based sensors for Bioanalysis, Dissertation: Chapter 1, 2004
4. Clark, H. A.; Hoyer, M.; Philbert, M. A.; Kopelman, R. *Anal. Chem.* **1999**, *71* (21), 4831-4836.
5. Nguyen, T.; Rosenszweig, Z. *Anal. Bioanal. Chem*. **2002**, *374*, 69-74
6. McNamara, K. P.; Rosenzweig, N.; Rosenzweig, Z. *Mikrochim. Acta* **1999**, *131*, 57-64.
7. Ji, J.; Rosenzweig, N.; Griffin, C.; Rosenzweig, Z. *Anal. Chem*. **2000**, *72*(15), 3497-3503.
8. Ji, J.; Rosenzweig, N.; Jones, I.; Rosenzweig, Z. *Anal. Chem.* **2001**, *73* (15), 3521-3527.
9. Ma, A.; Rosenzweig, Z. *Anal. Chem*.; **2004**; 76(3); 569-575.
10. Tan, S.-Z.; Niu, C.-G.; Jiang, J.-H.; Shen, G.-L.; Yu, R.-Q. *Analytical Sciences* **2005**, 21, 967-971
11. Yoo,D.; Shiratori, S.S.; Rubner, M.F. *Macromolecules* **1998**, 31, 4309-4318
12. Decher, G. *Science* **1997**, 277, 1232
13. Lee, S.-H., Multilayer thin films employing electrostatic layer-by-layer self-assembly for optical device applications , Thesis , Source DAI-B 61/09, p. 4751, Mar 2001
14. Chausmer, A.B.; *Journal of the American College of Nutrition* **1998**, *17,* 109-115
15. Kennedy, R.; Huang, L.; Aspinwall, C. *J Am Chem Soc* **1996**, *118*, 1795-1796
16. Jindal, R.M.; Taylo, R.P.; Gray, D.W.; Esmeraldo, R.; Morris, P.J . *Diabetes* **1992** ,*41*, 1056-1062
17. Qian, W.J.; Aspinwall, C.A.; Battiste, M.A.; Kennedy ,R.T. *Anal Chem* **2000** ,*72*, 711-717
18. Qian, W.J.; Gee, K.R.; Kennedy, R.T. *Anal Chem* **2003,** 75, 3468-3475.
19. Hirano, T.; Kikuchi, K.; Urano, Y.; Higuchi, T.; Nagano, T. *J Am Chem Soc* **2000** , *122*, 12399-12400
20. Uchima, Y.; Sawada, T.; Nishihara, T.; Umekawa, T.; Ohira, M.; Ishikawa, T.; Nishino, H.; Hirakawa, K. *International Journal of Molecular Medicine* **2003**, 12, 871-878
21. Zhefeng, F.; Liming, D.; Xiaotao, J.*CJI* **2001**, 3 (11)
22. Wilharlitz, P.; Dreew, S.; Krismer, R. et al. *Mikrochim Acta*. **1997**, 125: 45
23. el-Yazigi, A.; Al-Saleh, I.; Al-Mefty, O. *Clin.Chem*.**1986**, 32(12): 2187-90
24. Twining, B.S.; Baines, S.B.; Fisher, N.S.; Maser, J.; Vogt, S.; Jacobsen, C.; Tovar-Sanchez, A.; Sanudo-Wilhelmy, S.A. *Anal Chem*. **2003**, 75(15):3806-16
25. Nakae, Y.; Naruse, S.; Shibata, T.; Kitagawa, M.; Kondo, T.; Hayakawa, T.; Kuno, N.; Kurimoto, K. *Rinsho byori* **1994**, 42(2):139-42.
26. Terada, T.; Morita, T.; Hoso, M.; Nakanuma, Y. J. Clin Pathol. 1994, 47(10), 924-927
27. Terada, T.; Yukisato,K.; Keigo,A.; Yoshiko,M.; Masako, K.; Kenichi, H.; Teiichi, M.; Tetsuo, O.; Yasuni, N. *Virchows Arch* **1997**, 431,195–203
28. Vamvakaki, V.; Fournier, D.; Chaniotakis, N. A. Biosensors & bioelectronics 2005, 21, 384-388
29. Shi, L.; Rosenzweig, N.; Rosenzweig, Z. *Anal. Chem*.**2007**, 79,208-214
30. Willard, D. M.; Carillo, L. L.; Jung, J.; Van Orden, A. *Nano Lett.* **2001**, 1, 469-474.

31.Tran, P. T.; Goldman, E. R.; Anderson, G. P.; Mauro, J. M.; Mattoussi, H. *Phys. Status Solidi B* **2002**, *229*, 427-432.
32. Medintz, I. L.; Clapp, A. R.;. Brunel, F. M.; Tiefenbrunn, T.; Uyeda, H. T.;Chang, E. L.; Deschamps, J. R.; Dawson, P. E.; Mattoussi, H. *Nat. Mater.***2006**, *5* (7), 581-589.
33. Clapp, A. R.; Medintz, I. L.; Mattoussi, H. *Chem Phys Chem* **2006**, *7* (1), 47-57
34. Joseph R. Lakowicz, Principles of Fluorescence Spectroscopy, Chapter 1: Introduction to Fluorescence, pg 1-23, Kluwer Academic /Plenum Publishers, 1999
35. Howard A. Strobel; William R. Heineman, Chemical Instrumentation: A Systematic approach: Chapter15.2 Luminescence Spectra: Energy, Intensity, and Lifetime pg.517-522, John Wiley & Sons, 1989
36. Czarnik, A.W. Principle of fluorescent probe design for ion recognition, in Topics in Fluorescence Spectroscopy, Vlume 4: Probe Design and Chemical Sensing, J.R. Lakowicz, Plenum Press, New York, pp. 49-70, 1994
37. Fabrizzi, L.; Poggi, A. *Chem.Soc. Rev*. **1995**, 24, 197-202
38. Joseph R. Lakowicz, Principles of Fluorescence Spectroscopy, Chapter 13: Energy Transfer, pg 367-395, Kluwer Academic /Plenum Publishers, 1999
39. Kerem, E.; Schwartz-Arad, D.; Bartfeld, E.; Ron, N.; Ariel I.; Zajicek, G. *Histochemistry and Cell Biology* **1989,** 91(1), 47-50
40. Callea, F.; Desmet, V. L. *The Histochemical Journal* **1982**, 14(4), 545-552
41. Rhoades, E.; Gussakovsky, E.; Haran, G. *Proc. Natl. Acad. Sci.* **2003**, 100, 3197

CHAPTER 2

EXPERIMENTAL

This chapter describes the methods and chemical instrumentation used in performing the experiments. Specific details about the experimental set-up are provided in chapters 3, 4, and 5.

Instrumental Methods

2.1. Spectrofluorometry Measurements

A spectrofluorometer requires a wavelength isolation module in both excitation and emission, and light collecting optics which couple the wavelength isolation modules with sources of light. For a given substance, the absorption and emission spectrum is depicted versus wavelength. The fluorescence spectrum appears at longer wavelength than the excitation due to the energy lost in the singlet excited state through vibration relaxations. The excitation and emission measurements in this dissertation were performed using a Photon Technology International Spectrofluorometer (QM-1 model). This instrument is equipped with a xenon lamp as light source, two monochromators for wavelength isolation and a photomultiplier tube detector.

2.1.1. Light Source

A 75 watt high-pressure continuous output xenon lamp is the excitation source for the

spectrofluoremeter. The output light ranges from 250-750nm. A fused quartz envelope encloses two tungsten electrodes and xenon gas under high pressure. Light is generated when a high voltage pulse is applied through electrodes and xenon ions are formed. During operation, xenon arc lamps generate ultraviolet radiation that ionizes the surrounding oxygen and causes ozone to form. Heat and ozone generated during operation of the lamp are removed by directing cooled air through the lamp.

2.1.2. Monochromator

A monochromator is an optical system which narrows the spectral band of the incident light. A monochromator contains an entrance slit, a lens which collimates the light, a dispersing device, a lens which focuses the dispersed light and an exit slit. The entrance slit, a rectangular aperture, along with the exit slit is adjustable, playing a role in the performance of the monochromator. Collimated light is dispersed by either a grating or prism. The components of the incident beam are refracted in different angles by prisms. In comparison, gratings provide better resolution and dispersion of incident radiation. The PTI fluoremeter is equipped with two monochromators, one for excitation mode and one for emission mode.

2.1.3. Photomultiplier tube

Photomultiplier tubes are detectors which convert the intensity of light proportionally into current. Sealed in an envelope under vacuum are a photocathode, sets of dynodes as amplifiers and an anode. When an incident photon falls on the surface of the photocathode it causes an

ejection of a photoelectron. The photocathode typically operates at high negative potentials between -1000-2000V. Also, the array of dynodes is kept at negative potentials, which approach zero toward the end of dynode chain. The difference in potential between the photocathode and the dynode causes the photoelectron to be attracted and accelerated toward the first dynode. Additional electrons are produced, a process that continues to propagate down the chain of dynodes, resulting in a current pulse arriving at the anode. Amplification of the signal is directly related to the voltage and number of dynodes.

2.2. Digital Fluorescence Imaging Microscopy System

Fluorescence microscopy, which exploits the properties of fluorescence emission of single molecules upon specific excitation, gives information about their spatial distribution with direct application in biological experiments. Spectroscopic properties of fluorescent molecules change with changes in the parameters of the medium used during imaging: pH, viscosity, refractive index, ionic concentrations, etc.

Fluorescence measurements of fluorescent indicators were performed on an epifluorescent microscope Olympus IX-70.

Fluorescence microscopes are typically equipped with a mercury or xenon lamp (or laser system) as a light source. The output of the lamp passes through collecting optics to a filter cube that contains a set of excitation and emission filters and a dichroic mirror. The fluorescence produced after excitation of the sample is collected by the objective and directed through different paths to the detector and eyepiece. The filter cube, for ZnAF2 imaging and spectral data, contained a 480±30 nm band-pass excitation filter, a 500-nm dichroic mirror, and a 535±40 nm band-pass

emission filter. The filter cube for FRET measurements contained 425±40nm excitation filter, a 460nm dichroic mirror and 475nm long pass emission filters. The images are obtained using a CCD camera (Rupert Scientific, Model 256HB) for recording spectral fluorescence data [1].

This camera is coupled to a 150-mm three-mirror spectrograph (Acton Research Inc.) An exposure time of 0.1 s was used to acquire the fluorescence spectra and images. The Roper Scientific software WinSpec/32 was used for image analysis. Adobe PhotoShop v3.0 and Image J software were used to process the images.

2.2.1. Microscope objective

Microscope objectives are designed to focus excitation light on a sample and to collect emission light from the sample. When excitation and emission light travel through the same objective it is called epifluorescence microscopy. As compared to transmitted fluorescence, epifluorescence more efficiently separates excitation and emission light. The spatial resolution of a microscope [1] is defined as the minimum separation distance between two distinguishable points in a field.

$$R=1.22\lambda/2(NA) \quad (1)$$

$$NA= n \sin\alpha \quad (2)$$

R stands for the separation distance, NA is the numerical aperture of the objective; n in relation (2) is refractive index of the medium surrounding lens; α is angular aperture; λ is the wavelength

of incident light. Using immersion oil instead of air as medium, improves the resolution by a factor of 1.5.

$$F = 10^4 \bullet (NA^2/M)^2 \qquad (3)$$

The light-gathering power of the objective (F) (3), which affects the brightness of the image, is a function of numerical aperture and the square of the magnification of the image.

In fluorescence imaging, as the magnification increases and numerical aperture increases, the spatial resolution increases, but there is a risk of photobleaching the sample.

The fluorescence images and spectra were recorded using a 20× microscope objective with NA = 0.5 and a 40× microscope objective with NA = 0.9. NA values for oil immersion objectives range from 0.1 for low magnification objectives to 1.6 for high magnification objectives. Typically, objectives are composed of three groups of doublets of lenses, a lens triplet group, and three individual internal single-element lenses. A front lens and a meniscus second lens are designed to capture the incident light at high numerical aperture minimizing the spherical aberration.

2.2.2. Filter cube

A dichroic mirror is mounted along with the excitation and emission filter on an optical device called a filter cube. The block mounting provides flexibility to change the filters and dichroic mirror, allowing adaptation for each experiment set-up. Figure 2.1 represents the typical light paths through a filter cube in an inverted fluorescence microscope. Excitation and emission

filters are placed in front and underneath the dichroic mirror, a set-up which allows separation between the excitation and emission light.

2.2.3. Dichroic mirror

A dichroic mirror is a color filter which separates the excitation and emission paths. The surface of the mirror is coated with a thin layer of metal. The thickness and type of coating control the percent of reflectivity and transmission of incident light as well as the wavelength of processed waves. The principle by which these optical devices operate is interference. The values below the transition wavelength are reflected into the objective, while the ones above the value are transmitted. The excitation light reflected by dichroic mirrors is directed through the objective to excite the fluorescent probes.

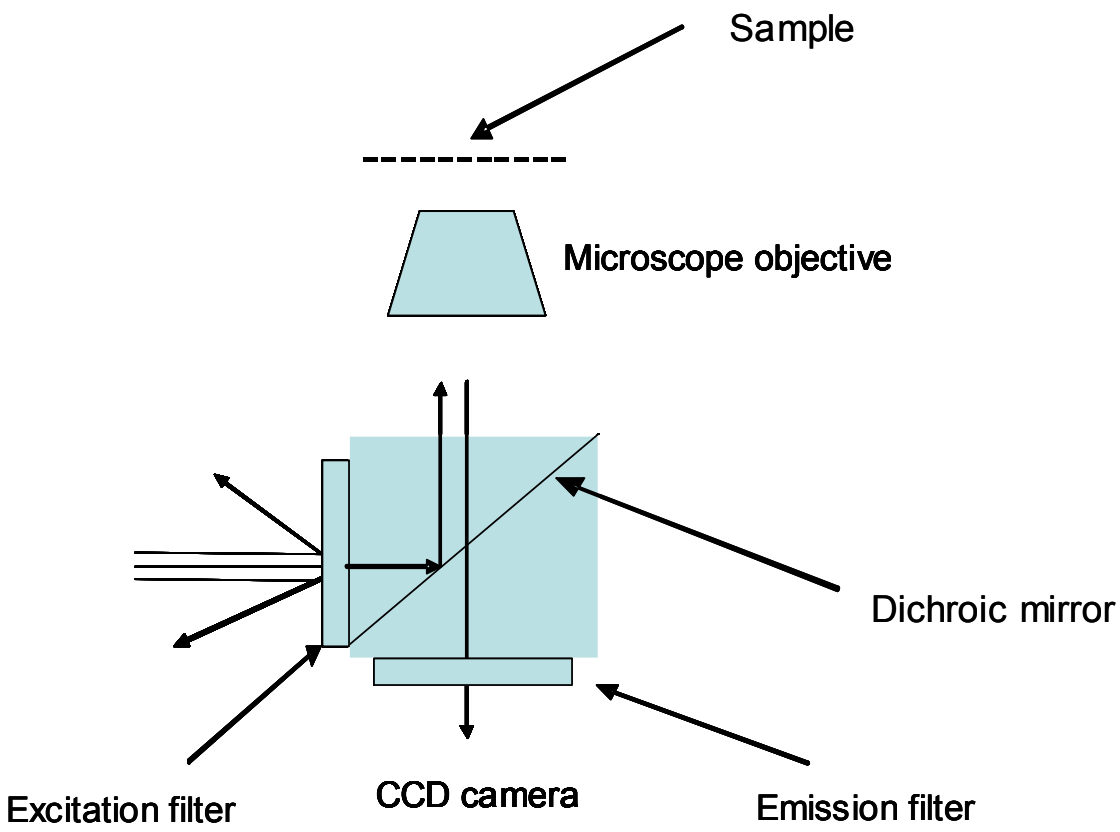

Figure 2.1 Representation of light path through an inverted epifluorescence microscope

The fluorescence light is collected by the objective and transmitted by the dichroic mirror to the emission filters.

2.2.4. Excitation and Emission Filters

To enhance the efficiency of separation between excitation and emission light, excitation and emission filters are used along with the dichroic mirror (figure 2.1.). The excitation filters are located in front of dichroic mirror and select the desired excitation wavelength. Reflection losses take place at the boundary of the excitation filter due to changes in the refractive index. Emission

filters placed underneath the dichroic mirror select the desired emission wavelength which and eliminates residual excitation light.

2.2.5. Spectrograph

Diffraction gratings are used to separate polychromatic radiation into monochromatic. The dispersed radiation is then directed to the CCD camera. Grating selection allows for the selection of desired wavelengths according to each experimental requirement.

2.2.6. Light Source

A 100 watt high-pressure mercury lamp was used as the light source for the fluorescence microscopy system. The reason to use a high intensity light source is to enhance the detection of emission from fluorescent probes that have a low quantum yield. However photobleaching, photochemical destruction of fluorescent molecules due to exposure to intense illumination, could occur and is therefore minimized by using neutral density filters.

A high pressure mercury lamp is a continuous optical source in the visible and UV spectrum. In the discharge spectrum, visible and UV regions are represented unevenly with peaks at 313, 334, 365, 406, 435, 546 and 578 nm. The output intensity at other visible wavelengths is less intense. Fluctuations in the emission of the lamp are caused by changes in internal pressure and temperature.

Two tungsten electrodes are placed in an arc quartz tube. The tube is filled with mercury. The gas is ionized under a DC arc.

The emission intensity of the lamp decreases in time due to accumulation of electrode metals on the lamp [2]. The lifetime of mercury lamp is limited to 200 hours.

2.2.7. Phase Contrast Microscopy

Since imaging of transparent specimens is less efficient in bright field microscopy, this is overcome by using contrast-enhancing optics, which allows visualization of colorless details. The use of phase contrast microscopy introduces considerable improvement for "in vitro" biological experiments, because it allows visualization of cellular details with similar transparency. Phase contrast microscopy was employed in experiments of visualization of beta pancreatic cells labeled with antibody A2B5-ZnAF2 sensor. In high contrast images, cellular details are more distinguishable due to differences in their refractive index. Phase contrast optics allow for better imaging of cellular membranes and adhesions of Min6 cells cultured at confluence. A Zeiss Axiovert 200 system was employed for recording phase contrast images in biological experiments. Enhancement of image contrast is ensured by using phase contrast optical components, to convey changes in amplitudes of electromagnetic waves by changes in phase.

The output of a tungsten-halogen lamp passes through a collector lens and focuses on a condenser. A phase plate in the light path after illumination of the sample separates the undeviated light from the highly refracted light which is retarded in phase. The waves are focused at image plane and phase contrast image is formed. The phase effect of the image in the eyepiece can be enhanced through variation of optical elements.

2.2.8. Charge Coupled Device (CCD Camera)

Nowadays, fluorescence microscopy techniques widely use as charged coupled plasma devices CCD camera as imaging detectors. A CCD camera is an array of coupled light sensitive capacitors. Charge coupled plasma devices are organized in pixels which accumulates charges upon light exposure. CCD chips are silicon based integrated circuits. The layer of silicon is p-type semiconductor doped with boron. Output light from specimens is focused by lens on the capacitor. Interaction of photons with silicon atoms causes ejection of electrons (figure 2.2). Incident light, on the silicon chip, should have high enough energy to create electron-hole pairs. The accumulated charge is directly proportional with the amount of incident light. As a capacitor, the pixel, a subunit of CCD devices, stores charges between plates. When a voltage pulse is applied to the read out gate, the charge packets travel across the chip through registers. The shift registers transport data from a latch in a serial mode [3]. The last pixel in the series transfers the charge to an amplifier which converts it in a voltage [4]. The voltage is then digitized in an intensity value. Two dimensional images are formed by reading charge at each particular pixel. One slice of image is formed by a one-dimensional array of pixels while the whole image is captured by a two-dimensional array.

CCD cameras are also used as detectors in fluorescence spectroscopy. A spectrograph is a monochromator without an exit slit, where the dispersion device, a concave diffraction grating, is typically coupled with a CCD camera. This association allows of detection of low concentration fluorescent probes. CCD cameras have a high signal-to-noise ratio and are more sensitive than a photomultiplier tube [5]. In a photomultiplier tube, there is a background current referred as dark current.

Dark counts are minimized by cooling the tube to -40^0 C [3]. In a CCD camera, cooling to -90^0 C minimizes the dark counts to less than an electron per pixel [5].

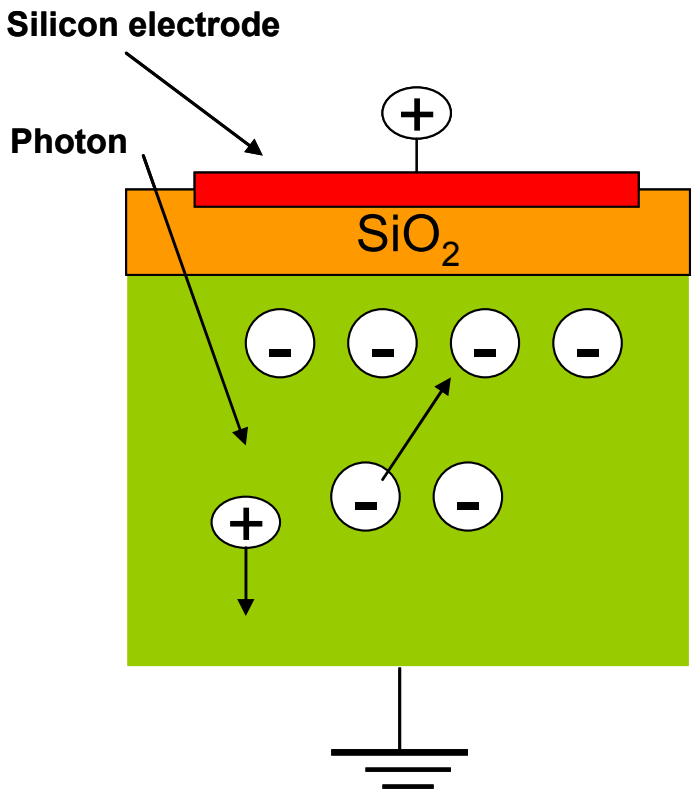

Figure 2.2 Representation of a CCD pixel. The capacitor is formed by deposition of a silicon dioxide layer on top of polysilicon substrate. The electrode is deposited on top of a SiO_2 layer.

2.3. Microplate Readers

The spectroscopic measurements of zinc release events from beta pancreatic cells, cultured at confluence, were performed using a SpectraMax M2 microplate reader (Molecular Devices, Inc.).

Microplate readers are multi-detection systems with a double monochromator, dual-mode cuvette ports and a top reading capability.

The system is equipped with a spectrophotometer for absorbance (UV-Vis) measurements and a spectrofluorometer for fluorescence. The microplate reader was used in spectrum module with a capability to detect 96 wells microplates. SoftMax Pro software was employed.

2.3.1. Double Monochromators

The microplate reader uses two monochromators: an excitation monochromator and an emission monochromator for tuning different wavelength settings. The output of a xenon flash lamp, as light source, is directed to a concave holographic grating for tuning the different excitation wavelengths. In a concave grating the focusing is combined with dispersion. The advantage of using a concave grating is in the elimination of two monochromator mirrors. Holographic gratings are polished glass materials, covered with a photoresist to reduce astigmatism at multiple angles [6]. The selected light travel through 1mm fiber optic bundles to cuvette ports and microplates. In the cuvette mode, the incident light is reflected by an elliptical mirror and directed to the cuvette. The fluorescence emission of fluorescent probes is focused on an elliptical mirror and sent to a concave holographic grating. The desired wavelength is selected

and reaches a photomultiplier tube detector. For microplate mode, the light passes through the second fiber optic to a focusing elliptical mirror. The resulted beam investigates then the top of the microplates. The fluorescence light is collected and directed to the second wavelength isolation module and then to the PMT detector.

2.3.2. Light Source

A xenon flash lamp is a light source with a continuous light output between 250-700nm. Spectral outputs, in the discharge spectrum, show sharp lines near 450 and 800nm. The anode and cathode are sealed in a quartz envelope filled with xenon gas. Directed airflow through the housing of the lamp removes excess heat and ozone produced during operation. The flash is generated by ionization of xenon atoms when a high voltage pulse is applied at the cathode. Collision of xenon atoms with the electrons, which travel across the arc, results in ionization of the gas [7].

2.3.3. Temperature Control (Chamber) Module

When performing biological experiments, one of the drawbacks related to exploring precise biological functions "in vitro" pertains to the requirements for optimum growth conditions (5%CO_2, 37^0C temperature, media, humidity). To address the biological significance of the cell culture requirements, the spectroscopic experiments monitoring zinc release from beta pancreatic cells were performed on a microplate reader, which has a 37^0C temperature control module.

2.4 Absorption Spectrometry

Spectrophotometric techniques explore the properties of molecules of interacting with specific frequencies of radiation. The absorption spectrum of a particular substance is a representation of absorption intensity versus wavelength. Since molecules have discrete energy levels, they absorb those frequencies which propel them from ground state to excited electronic state. The total energy of a molecule could be expressed as sum of translational, rotational, vibrational, electronic and nuclear orientation energy. Absorption of ultraviolet and visible radiation promotes particular transitions of these categories.

Beer's law is used to relate the intensity of absorption with the concentration of absorptive molecules in the light path.

$$A=\varepsilon bc \qquad (1)$$

In expression (1), A is absorbance; b is the path length; ε is defined molar absorptivity and c is concentration.

For absorption measurements a Varian UV-VIS-NIR spectrophotometer system, model CARY 500 Scan was employed. This system is a double beam spectrophotometer.

The advantages of using a double channel consist in compensation for the fluctuations in lamp intensity, detector or electronics. The sample module is doubled with a reference cell. The output of a mercury lamp light source travels through a wavelength isolation device (monochromator), and the resultant beam is split into two beams by a beam chopper before it investigates the sample area. The two beams are rejoined after the sample area and reach a lead sulfide detector.

2.5. Atomic force microscopy

Atomic force microscopy (AFM) belongs to a very high-resolution category of scanning force microscopy. Atomic force microscope is an ideal instrument for studying surfaces, films and coatings with a nanometer resolution. It provides the ability to image the topography of various surfaces like conductive and insulators materials [8], organic films [9, 10], biomaterials like amino acid crystals [11], fibrinogen [12] and obtain information about height, optical absorption, or magnetism.

The principle by which AFM works is by measuring attractive or repulsive forces between a tip and the sample. The sample surface is scanned by a tip mounted to a cantilever spring (Figure 2.3). AFMs measure the forces between the tip and surface of the sample through the vertical deflection of the cantilever. This data is then converted to "force-versus-distance curves" [8].

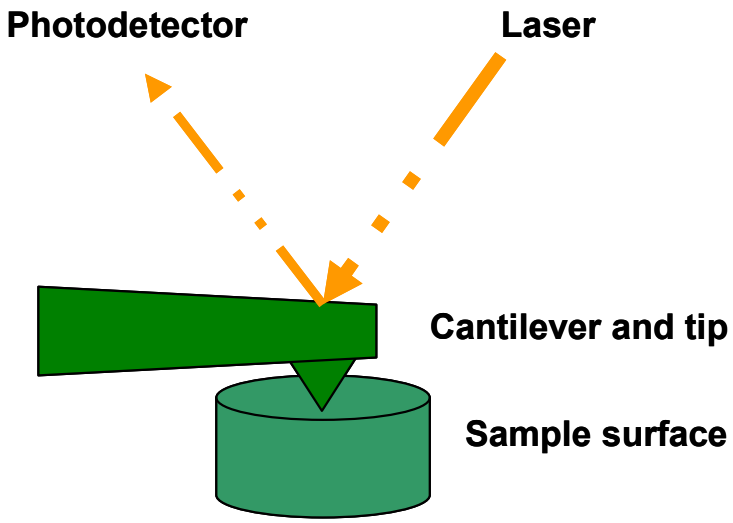

Figure 2.3 Representation of an atomic force microscope set-up

Cantilevers are typically made of silicon or silicon nitride with an oxide layer on the surface. There are differences in the properties of the top and bottom sides. The top side is covered with a gold layer to enhance the reflectivity of the laser beam. The bottom face is exposed to changes in surface stress due to interaction with sample. The shape of the cantilever changes when repulsive forces create a vertical deflection [8].

While scanning the surface, different set-ups make use of moving the sample vertically by a piezoelectric translator mounted near the sample or by moving the cantilever through a voltage applied to an attached piezoelectric translator [8]. Typically a translator is a device which converts a form of energy into another. Piezoelectric ceramics are used to exploit their ability to generate an electric field in a material, in response to a voltage gradient or mechanical stress applied to it [13]. The piezoelectric material contracts or expands in these conditions causing the sample or the tip attached to it to move.

Today optical lever techniques are largely used to measure the deflection of the cantilever [8, 14 and 15]. A laser beam falls on the end of the cantilever and is reflected. Interaction of forces between the cantilever tip and the surface features of the sample, results in different degree of deflection. The laser beam is reflected under an angle twice the value of the angular deflection of the cantilever. The reflected light reaches a position-sensitive detector.

Atomic force microscopy is a versatile techniques, it allows measurement of topography of solid substrates as well as studies of force interaction in air, organic solvents [16-20] gases, vacuum, or aqueous solution [21].

The cantilever tips are attached at the end of the cantilevers. They are made of oxidized silicon nitride or silicon [8, 22 and 23]. The surface of tips is often modified to change the surface

properties for different application. They can be modified with a photopolymerized polymer made of acrylate and epoxy [24] or gold-thiol coatings, silane [25] etc.

When AFM measures the repulsive forces (contact mode) between sample and tip, the tip is kept in contact with sample very lightly, with angstrom lateral and vertical resolution. In attractive (no contact) mode, the tip is typically kept at 100 angstrom distance from the surface of the sample, and the resulting attractive forces are measured (e.g., electrostatic forces [26], Van der Waals [27]). Non-contact mode is non-destructive and used to record topographic images [28].

Another measuring AFM technique is tapping mode, which allows for the -collection of topographic images with high resolution. The cantilever tip oscillates at frequencies close to those of piezoelectric material. As compared to the contact mode, which is influenced by frictional forces and can be destructive to sample, the tapping mode has sufficient amplitude of oscillations against adhesion forces between tip and surface of the sample.

For measurements of thickness of polyelectrolyte films deposited on top of PDMS, we used an atomic force microscope Dimension 5000, Digital Instruments, Santa Barbara, CA. Topographic information about the patterned PEMs was obtained in tapping mode.

References

1. Namara, K. P.; Nguyen, T.; Dumitrascu, G.; Ji, J.; Rosenzweig, N.; Rosenzweig, Z. *Anal. Chem.* **2001**; 73 *(*14); 3240-3246.
2. Howard A. Strobel; William R. Heineman, Chemical Instrumentation: A Systematic approach: Chapter8.2 Continous sources pg.253-258, John Wiley & Sons, 1989
3. Howard A. Strobel; William R. Heineman, Chemical Instrumentation: A Systematic approach: Chapter 5.7 Latches, Registers, and Devices for Bus Communication pg. 151-155, John Wiley & Sons, 1989
4. Gabriela Blagoi, Fluorescence Resonance Energy Transfer (FRET) Based sensors for Bioanalysis, Dissertation: Chapter 2.2.2.6, pg 40-44, 2004
5. Joseph R. Lakowicz, Principles of Fluorescence Spectroscopy, Chapter 2.6G. : CCD Detectors, pg 47, Kluwer Academic /Plenum Publishers, 1999
6. Howard A. Strobel; William R. Heineman, Chemical Instrumentation: A Systematic approach: Chapter9, Monochromators and Polychromators, pg.320, John Wiley & Sons, 1989
7. Joseph R. Lakowicz, Principles of Fluorescence Spectroscopy, Chapter 2.2.A; Arc and Incandescent Lamps, pg.28, Kluwer Academic /Plenum Publishers, 1999
8. Butt, H.-J.; Cappella, B.; Kappl, M. *Surface Science Reports* **2005**, 59, 1–152
9. Cohen, H.S.; Bray, M.T.; Lightbody, M.L. Atomic Force Microscopy/Scanning Tunneling Microscopy Plenum Press, 1994
10. Marti, O.; Ribi, H. O.; Drake, B.; Albrecht, T. R.; Quate, C.F.; Hansma, P.K. *Science* **1988**, 239:50-52
11. Gould, S.; Marti, O.; Drake, B.; Hellemans, L.; Bracker, C.E.; Hansma, P.K.; Keder, N.L.; Eddy, M.M. and Stucky, G. D. *Nature* **1988**, 332:332-334
12. Drake, B.; Prater, C.B.; Weisenhorn, A.L.; Gould, S.A.C.; Albrecht, T. R.; Quate, C.F. ;Channel, D.S.; Hansma, H.G. and Hansma, P. K. *Science* **1989,** 243:1586-1589
13. Gallego-Juarez, J.A**.** *J. Phys. E: Sci. Instrum*. **1989,** 22 , 804-816
14. Meyer, G.; N.M. Amer, *Appl. Phys. Lett***. 1988**, 53, 2400.
15. Alexander, S.; Hellemans, L.; Marti, O.; Schneir, J.; Elings, V.; Hansma, P.K.; Longmire, Gurley, *J. Appl. Phys*. **1989**, 5, 164.
16. Bustamante, Vesenka, J.; Tang, C.L.; Rees, W.; Guthod, M and Keller, R. *Biochemistry* **1992**, 31, 22-26
17. Hansma, H.G.; Sinsheimer, R.L.; Li, M.-Q. and Hansma, P.K. *Nucleic Acids Res.* **1992**, 20, 3585-3590
18. Hansma, H.G.; Vesenka, J.; Siegerist, C.; Kelderman, G.; Morrett, H.; Sinsheimer, P.L.; Elings, V.; Bustamante, C.; Hansma, P.K. *Science* **1992**, 256, 1180-1184
19. Henderson, E.; *Nucleic Acids Res*. **1992**, 20, 445-447
20. Lyubchenko, Y.L; Gall, A.A.; Shlyakhtenko, L.S.; Harrington, R.E. and Lindsay, S.M. *Biophys. J.* **1992**, 61, A149
21. Lyubchenko, Y.L.; Jacobs, B.L. and Lindsay, S.M. *Nucleic Acids Res*. **1992**, 20, 3983-3986
22. Albrecht,T.R.; Akamine, T.E.;Carver, C.F. Quate, *J. Vac. Sci. Technol.* **1990**, A 8 , 3386.

23. Wolter, O.; Bayer, T.; Greschner, J.; *J. Vac. Sci. Technol*. **1991**, B 9, 1353.
24. Kim, J.M.; Muramatsu, H. *Nano Lett*. **2005,** 5, 309.
25. Tsukruk, V.V.; Bliznyuk, V.N. *Langmuir* **1998**, 14, 446.
26. Stern, J.E., Terris, B.D., Mamin, H.J. & Rugar, D. *Appl. Phys. Lett.* **1988**, 2717−2719
27. Martin, Y.; Williams, C.C. and Wickramasinghe, H.K. *J. Appl. Phys*. **1987**, 61, 4723- 4729
28. Albrecht, T.R. et al. *J. Vac. Sci. Technol.* **1990, A8** (4). 3386-3396

CHAPTER 3

A FLUORESCENCE –BASED ZINC ION SENSOR FOR ZINC ION RELEASE FROM PANCREATIC CELLS

Georgeta Crivat[1], Kazuya Kikuchi[2], Tetsuo Nagano[3], Tsvia Priel [4], Israel Seckler [4], Nitsa Rosenzweig[1] and Zeev Rosenzweig[1*]

1. University of New Orleans, Department of Chemistry and the Advanced materials Research Institute, New Orleans, LA 70148, USA
2. Department of Material and Life Science, Graduate School of Engineering, 2-1 Yamada-oka, Suita City, Osaka, Japan
3. Graduate School of Pharmaceutical Sciences, the University of Tokyo, 7-3-1 Hongo, Bunkyo-ku, Tokyo, Japan
4. Department of Cell Physiology, Medical School, Ben Gurion University, Beer Sheva, Israel

3.1. Introduction

This chapter describes the synthesis and characterization of fluorescence–based zinc ion sensing glass cover slips and their application in monitoring zinc ion release from beta pancreatic cells in cell culture. To fabricate the sensor, the zinc ion indicator ZnAF-2 {6-[N- [N', N'-bis (2-pyridinylmethyl)-2-aminoethyl] amino-3', 6'-dihydroxy-spiro [isobenzofuran-1(3H), 9'-[9H] xanthene]-3-one} was modified to include a sufficiently long linking aliphatic chain with a terminal carboxyl functional group. The recently synthesized ZnAF-2 zinc ion indicator provided high zinc ion selectivity in physiological solutions containing millimolar levels of calcium and other possible interfering cations. The carboxyl-modified ZnAF-2 was conjugated to

the activated surface of glass slides, which then served as zinc ion sensors. It was possible to grow pancreatic cells directly on the zinc sensing glass slides or on a polycarbonate membrane placed on these glass slides. The sensors were used to monitor zinc ion release events from glucose-stimulated pancreatic cells.

Zinc is one of the most abundant transition metals in the body. It is an essential element required by all cells with various functions for example, the control of gene transcription and metalloenzyme function [1-7]. In pancreatic islets, which contain large amount of zinc compared to other tissues, zinc is involved in insulin synthesis, storage and secretion [8]. Insulin is stored as a hexamer complexed with two zinc ions. It is found in a crystalline state and stored within vesicles [9]. When pancreatic cells are stimulated by elevated glucose concentration, insulin is co-released with zinc through exocytosis. The dissociation of the insulin–zinc complex occurs due to exposure to the extracellular pH [8, 10]. The dissociation results in the formation of insulin monomers - the biologically active form of insulin [8, 11, and 12]. The role of zinc ions in insulin secretion and in the pathology of diabetes is not entirely understood. However, numerous reports suggested that diabetes affects zinc homeostasis [13]. Abnormally low levels of zinc were found in many diabetes patients, which was typically associated with a poor renal zinc ion reuptake [13]. Zinc sensing glass slides could find application in studies aiming to understand the role of zinc in the pathogenesis and pharmacology of diabetes.

A number of analytical techniques have been used to detect and quantify zinc in biological samples including inductively coupled plasma atomic emission spectroscopy [14,15], atomic absorption spectrophotometry [16,17], X ray fluorescence [18] and radio-isotopes detection [19].

However, none of these techniques can be used for real time zinc ion detection in cellular systems. Fluorescence sensors that were developed in the last two decades provided a new analytical tool for the detection of intracellular ion levels. Most studies concentrated on the fabrication of sensors for pH and calcium ion measurements in cells [20, 21]. This is due to the availability of fluorescent probes for pH and calcium ion level determination. Zinc ion fluorescent indicators that were used for the analysis of zinc ion in cells include ultraviolet excitable quinoline-based dyes like 6-methoxy-8-quinolyl-para-toluenesulfonamide (TSQ) [22], zinquin [23] and visible light excitable fluorophores like Fluozin-3 [24]. A common limitation of these dyes is their limited zinc ion selectivity, particularly in the presence of calcium. In a recent study Chang *et al*. developed a new zinc ion sensitive dye - Zin-naphthopyr 1 (ZNP1) [25]. It is based on a hybrid seminaphthofluorescein platform, affords single-excitation, dual-emission ratiometric imaging of intracellular zinc ions through controllable zinc ion induced switching between a fluorescein and naphthofluorescein tautomeric forms. The tautomeric chemosensor features excitation and emission maxima in the visible range, excellent selectivity for zinc ions over ubiquitous intracellular metal ions such as sodium, potassium, calcium and magnesium, and a dissociation constant (Kd) for zinc ions of $<$1 nM.

Recently, Kikuchi and coworkers synthesized a new zinc sensitive fluorophore {6-[N- [N', N'-bis (2-pyridinylmethyl)-2-aminoethyl] amino-3', 6'-dihydroxy-spiro [isobenzofuran-1(3H), 9'-[9H] xanthene]-3-one} (ZnAF-2) [1]. This fluorophore is structurally and spectroscopically similar to fluorescein. The excitation and emission wavelengths of ZnAF-2 are 492 and 514 nm respectively. The fluorescence intensity of ZnAF-2 increases with increasing zinc ion concentration. This increase is attributed to photo-induced electron transfer (PET) when ZnAF-2 chelates zinc ions [1]. While similar in zinc sensing properties to ZNP1, ZnAF-2 exhibits higher

long-term stability. The cellular permeability of ZNP1, ZnAF-2 and other zinc ion sensitive dyes remaines a problem since it is difficult to measure zinc ion release from cells if the zinc ion sensing dye is cell permeable. Our current study describes a new approach to overcome the cell permeability problem of zinc ion sensitive dyes in order to facilitate their use to measure zinc ion release from cells. Here we make use of a modified form of ZnAF-2 in the fabrication of zinc ion sensing glass slides. The paper describes the analytical properties of the zinc sensitive glass slides and their application in the measurement of glucose stimulated zinc ion release from beta pancreatic cells.

3.2. Specific Experimental and Technical Details

3.2.1. Materials and Reagents

The zinc ion indicator {6-[N- [N',-bis (2-pyridinylmethyl)-2-aminoethyl]amino-3',6'-dihydroxy-spiro[isobenzofuran 1(3H),9'-[9H]xanthene]-3-one} (ZnAF-2) was modified to include a carboxyl terminated aliphatic chain. TPEN (N, N`, N`-Tetrakis(2-pyridylmethyl) ethylenediamine was obtained from Dojindo Laboratories. Trypsin-EDTA was purchased from Gibco. Magnesium chloride, sodium chloride, potassium carbonate, calcium chloride, magnesium sulfate and potassium phosphate were obtained from EM Industries, Inc. Aqueous solutions were prepared using 18 MΩ deionized water that were conditioned using the water purification system Barnstead Nanopure Diamond. Phosphate buffer (PBS, pH=7.2) without calcium chloride and magnesium chloride, Dulbecco' s modified Eagle medium, antibiotic-antimycotic and fetal bovine serum qualified for cell cultures were obtained from Invitrogen Corporation. HEPES buffer, N-Hydroxysulfosuccnimide sodium salt, N- (3-Dimethylaminopropyl)-N`-ethyl-carbodiimide, benzenethiol 99%, and zinc sulfate were obtained from Sigma-Aldrich. Trimethoxysilylpropyl-Diethylenetriamine was

purchased from United Chemical Technologies, Inc. Nitrilotriacetic acid was purchased from Spectrum Chemical MFG.CORP. 22 mm cover glasses were purchased from VWR Scientific. All reagents were used as received.

3.2.2. Fluorescence Spectroscopy and Microscopy

Emission spectra were obtained using a PTI international (model QM1) fluorometer equipped with a 75-W continuous Xe arc lamp as a light source. Fluorescence microscopy measurements were carried out using an inverted fluorescence microscope (Olympus IX-70) equipped with three detection ports. A 100-W mercury lamp was used as the light source for excitation and a 20X microscope objective was used to collect the fluorescence. The fluorescence microscope filter cube consisted of a 480/30 nm bandpass excitation filter, a 500 nm dichroic mirror and a 535/40 nm emission filter. A high-performance charge-coupled device (CCD) camera (Roper Scientific, SpectraPro 2300) was used for digital fluorescence imaging of the samples. The Roper Scientific software WinSpec 32 was used for data acquisition and spectral analysis. A typical exposure time was 0.1 seconds.

3.2.3. Synthesis of ZnAF-2 Modified with Carboxyl Terminated Aliphatic Chain

The synthesis of ZnAF-2 modified with carboxyl-terminated aliphatic chain is described in Figure 3.1, and it was synthesized following Kikuchi's earlier work (1). Compound 1 (70 mg, 92 μmol) was dissolved in 400 μl of DMF with 50 μl of diisopropylethylamine and 50 μl of diisopropylcarbodiimide. 50 mg of *N*-hydroxysuccinamide were then added to the solution. The

reaction mixture was stirred at room temperature for 24 hours. It was then evaporated to dryness and resuspended in 0.1% TFA. The product was separated by HPLC with ODS column, eluent: initial 20% acetonitrile, 0.1% TFA, final 80% acetonitrile 0.1% TFA. The collected fractions were lyophilized and compound 2 was obtained (19 µmol, 21% yield). Compound 2 (16 mg, 19 µmol) was dissolved in 200 µl of DMF with 15 mg of 4-piperidinebutanoic acid. 8.5 µl of triethylamine were then added to the solution. The reaction mixture was stirred at room temperature for 24 hours. Then, the solution was neutralized with 80µl of 2N HCl. The solution was separated by HPLC with ODS column, eluent: initial 20% acetonitrile, 0.1% TFA, final 80% acetonitrile 0.1% TFA. The collected fractions were lyophilized and compound 3 was obtained (13 µmol, 68% yield). Compound 4 was obtained by deprotection of 3, according to the literature [1].

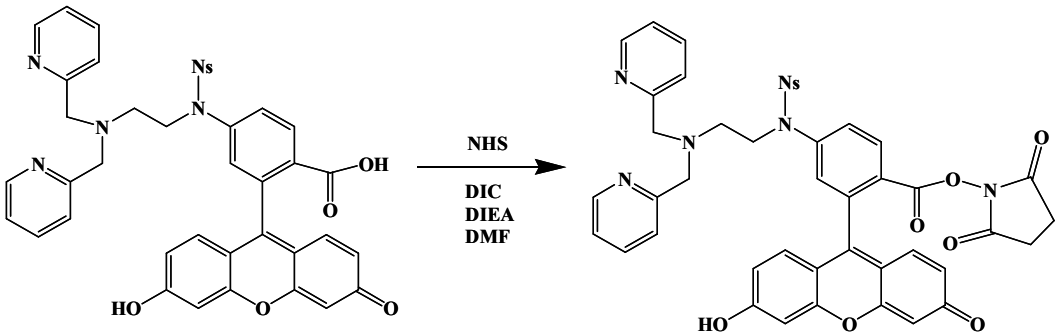

[1] [2]

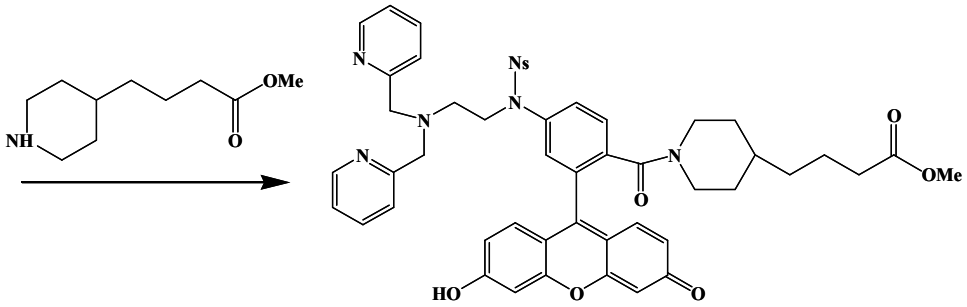

[3]

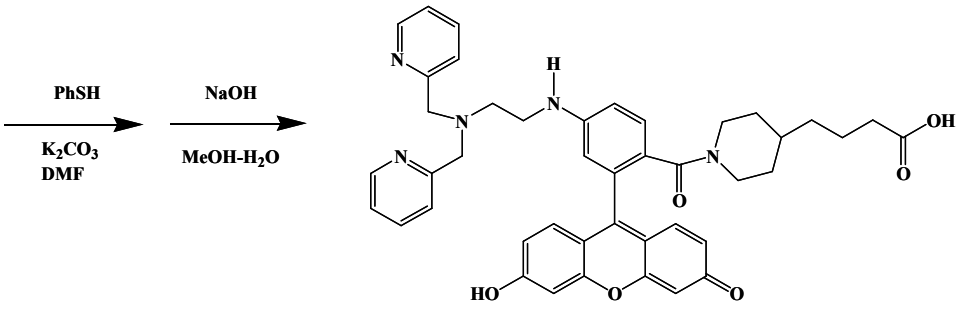

[4]

Figure 3.1 Representation of synthesis of carboxyl modified $ZnAF_2$

3.2.4 Synthesis of Zinc Sensing Glass Slides

Synthesis of the zinc film sensor required investigative techniques to modify and optimize the surface properties. The substrate was a bare white borosilicate glass which was modified by aminosilanization. To provide the film with zinc sensing properties, surface chemistry was used to conjugate the ZnAF2 to the amino modified glass slides.

3.2.4.1. Silanization of Glass Slides

Since the surface of glass slides is covered with chemically inert silanols, methods are commonly employed to silanize the surface with organosilanes bearing various functional groups to confer the surface with neutrophilic or electrophilic reactivity. Typically, mono, di or tri alkoxysilanes with amino or mercapto functional groups such as aminopropyltriethoxysilane [26, 27], trimethoxysilylpropyldiethylenetriamine, amino- ethylaminomethylphenethyltrimethoxysilane [28], aminophenyltrimethoxysilane[29], haloacetamidosilanes[30] are used.

There are different methodologies to deposit the silane films (e.g., aqueous phase [31], vapor phase [32])

3.2.4.1.1. Choice of Silanization Agent

The choice of silanization agent was motivated by the conjugation chemistry which involved an EDC coupling between carboxyl group of ZnAF2 and an amino group from the modified surface. In this respect, APTES and DETA as sources of amine groups are investigated.

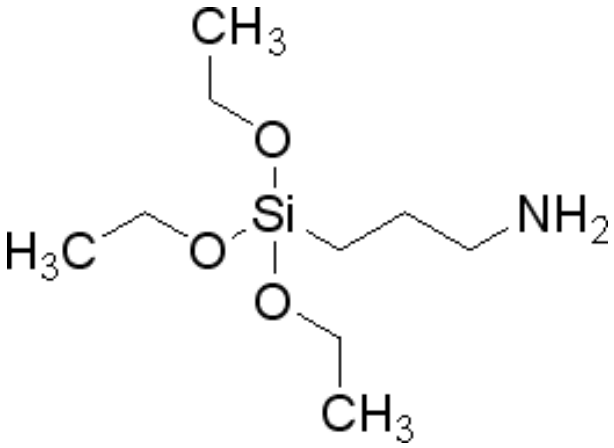

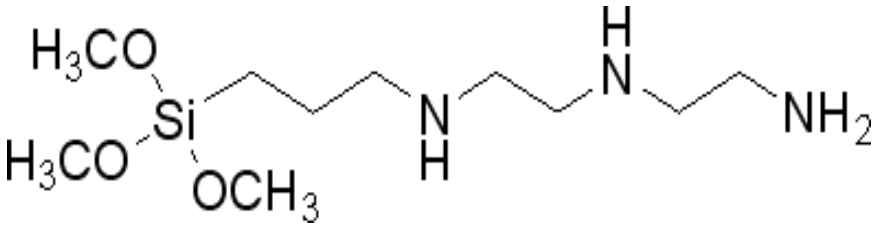

Figure3.2a. APTES
(3-Aminopropyl) triethoxysilane

Figure 3.2 b. DETA
3-Trimethoxysilylpropyl) diethylenetriamine

APTES (Figure 3.2a) is a trialkoxysilane, which requires a hydrolysis reaction to release the alcohol groups. They further condense with the hydroxyl groups of borosilicate substrate. The conjugation chemistry involves two sites of attachment of silanols with the third group free [26, 33].The outcome of this attachment, consists in the possibility of further polymerization of the

free silanols on the surface or in solution before the reaction, which creates heterogeneity in the silanol film.

It was found that increasing the silanization time increases the number of functional groups on the surface of the silica substrate .The concentration of silane and the silanization temperature were less important in controlling the density of functional groups [26]. In spite of their heterogeneity, APTES films found numerous applications in immobilization of biological molecules, such as antibodies, enzymes, DNA and inorganic catalysts. A relatively homogeneous distribution of functional groups was found when low-density coverage was obtained [26]. There are different methods to minimize the polymerization such as postsilanization curing at temperature by cross linking of silanols; silanization in vapor phase [34];or the use of monoalkoxysilanes [26]. Monoalkoxysilanes could drastically reduce the heterogeneity but their limitation is their instability, subject to rapid hydrolysis [26, 35].

Trialkoxysilanes are the most widely used silane agents. Preliminary investigations of aminosilanization agents and procedures revealed that APTES creates a highly heterogeneous silane film and ultimately a highly heterogeneous sensor response to zinc.

Reproducible results of DNA films have been reported when the DETA silanization agent and a heterobifunctional cross-linker SMPB were used to covalently attach the DNA strand through thiol moieties [27]. 3-Trimethoxysilylpropyl) diethylenetriamine (Figure 3.2b) as a silanization agent was further investigated. DETA is a trialkoxysilane with three potentially available amine groups to increase the yield of conjugation reactions between the silanized surface and ZnAF2. Reports suggest that using DETA silane, which was conjugated to DNA oligomers through SMPB crosslinker increased the surface density considerably [27].

Contact angle measurement a surface analysis technique, gives information about the wettability of a specific surface. Comparative studies of sessile drop contact angle measurements of self-assembled monolayer silane films revealed that sessile drop values for EDA (*N*-(2-aminoethyl)-3-aminopropyltrimethoxysilane), DETA (trimethoxysilylpropyldiethylenetriamine) and PEDA ([*m*,*p*-(aminoethyl-aminomethyl)phenethyltrimethoxysilane) were 30, 17 and 42 respectively [27]. It appears that DETA is the least hydrophobic surface, with relevance for the further conjugation chemistry in the aqueous phase.

Optical ellipsometry measurements of DETA film revealed a 6 Å thickness corresponding to one silane monolayer [27, 36].

Prior to silanization, glass microscope cover slips were exposed to acidic treatment to remove particles and impurities. The acid treatment also ensured the release of hydroxyl groups from the borosilicate glass. Preparation of glass slides for silanization consisted of an immersion in 1:1 concentrated HCl: MeOH for 30 min, rinsing with deionized water, treatment with H_2SO_4 for 30 min, and boiling in deionized water for 5 minutes. A solution of 1% silane trimethoxysilyl-propyl-diethylenetriamine (DETA) was hydrolyzed in 1mM acetic acid for 5 min prior to silanization. The silanization reaction (Figure 3.3) was carried out by immersing the treated glass slides in the DETA solution for 30 minutes at room temperature. The silanized slides were thoroughly rinsed with deionized water, dried under N_2 and cured at 110^{o}C for 5 minutes [27].

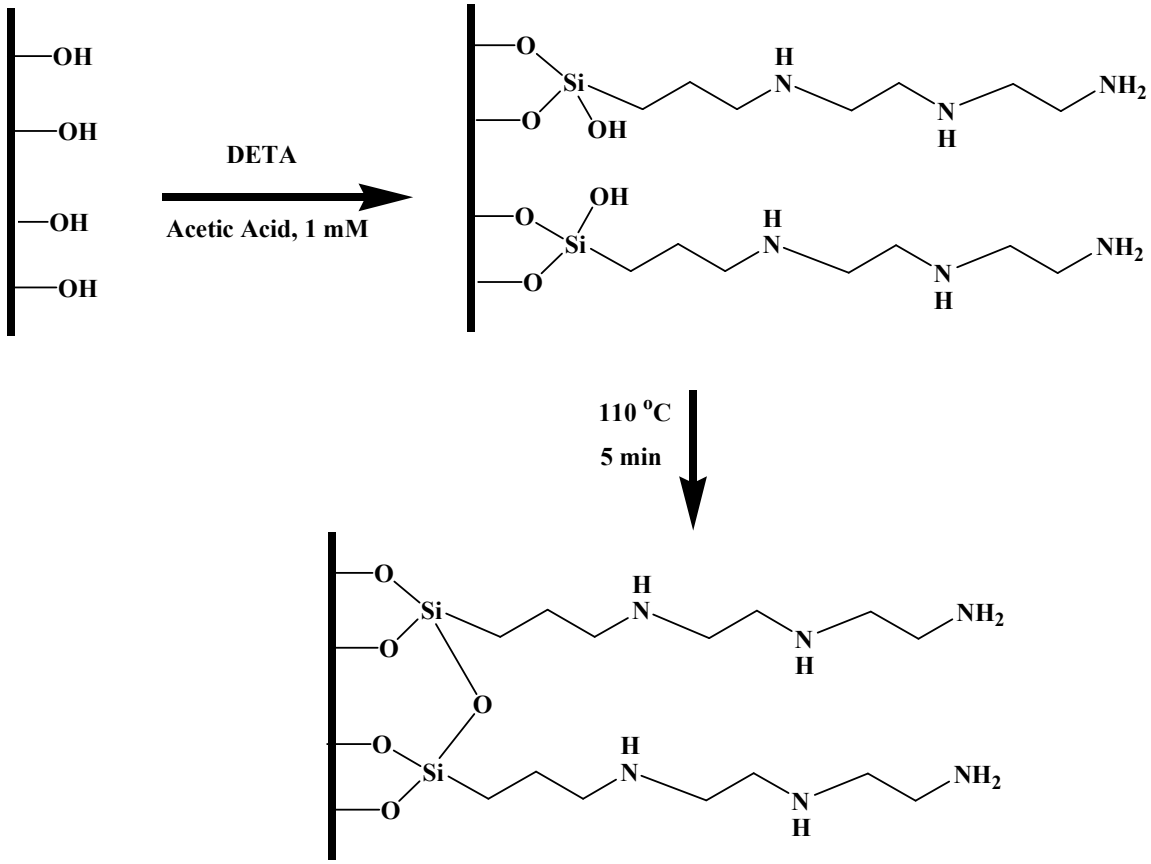

Figure 3.3 Representation of silanization procedure

3.2.4.2. Conjugation of ZnAF-2 to Silanized Glass Coverslips

The conjugation reaction of modified ZnAF2 (Figure 3.4) first requires the activation of aliphatic carboxyl groups in presence of EDC [1-ethyl-3-(3-dimethylaminopropyl) carbodiimide], resulting in the formation of a highly reactive O-acylisourea intermediate.

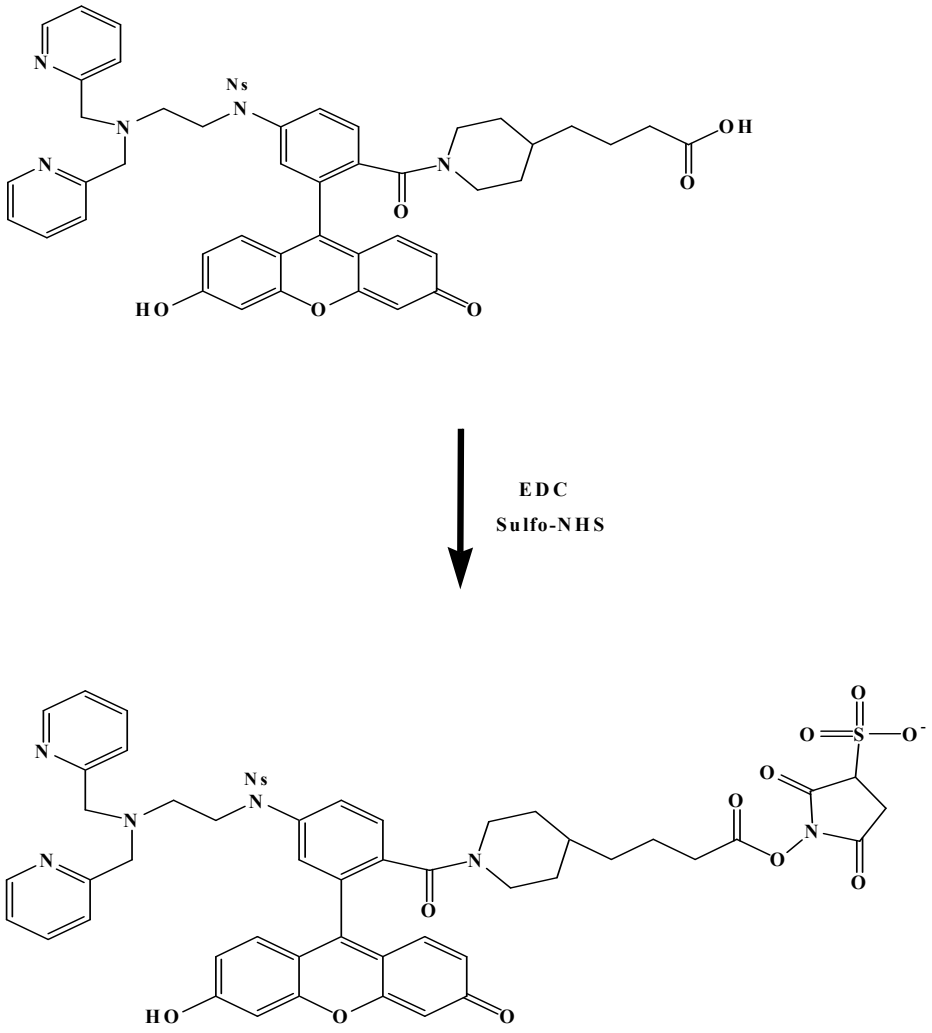

Figure 3.4 Representation of the activation of the carboxyl-modified ZnAF-2 with EDC/sulfo NHS

This complex could easily react with the primary amines of the silanized glass slides to form stable amide bonds. The active ester intermediate (O-acylisourea) is quite unstable in aqueous solution [37] and could easily hydrolyze to regenerate the carboxyl group. Using sulfo-NHS (N-Hydroxysulfosuccinimide) increased the stability of the intermediate by forming longer-lived sulfo-NHS ester intermediates. To activate the modified ZnAF-2 we prepared a 500 μl HEPES buffer solution at pH 7.5 that contained 1 μM of the dye, 20 μM EDC and 50 μM sulfo-NHS. The preparation of ZnAF-2 modified glass slides is shown in Figure 3.5. The glass slides were incubated in the activated ZnAF-2 solution for 6 hours at room temperature. After the coupling reaction the glass slides were thoroughly rinsed with deionized water and sonicated to remove the adsorbed reagents. It should be noted that the secondary amine of ZnAF-2 which is a part of its zinc binding site was protected with nossyl group to preclude the possibility of modifications that would negatively affect the zinc sensing properties of ZnAF-2 during the fabrication of the zinc sensing glass slides. The protecting group was removed from the zinc binding site once ZnAF-2 was covalently bound to the glass surface. The selective deprotection of the nosyl sulfonamide group was carried out in aprotic solvent (DMF), with a 3 molar equivalents of K_2CO_3 salt and 1.5 equivalents of thiolate under argon conditions for 6 hours at room temperature [1, 38].

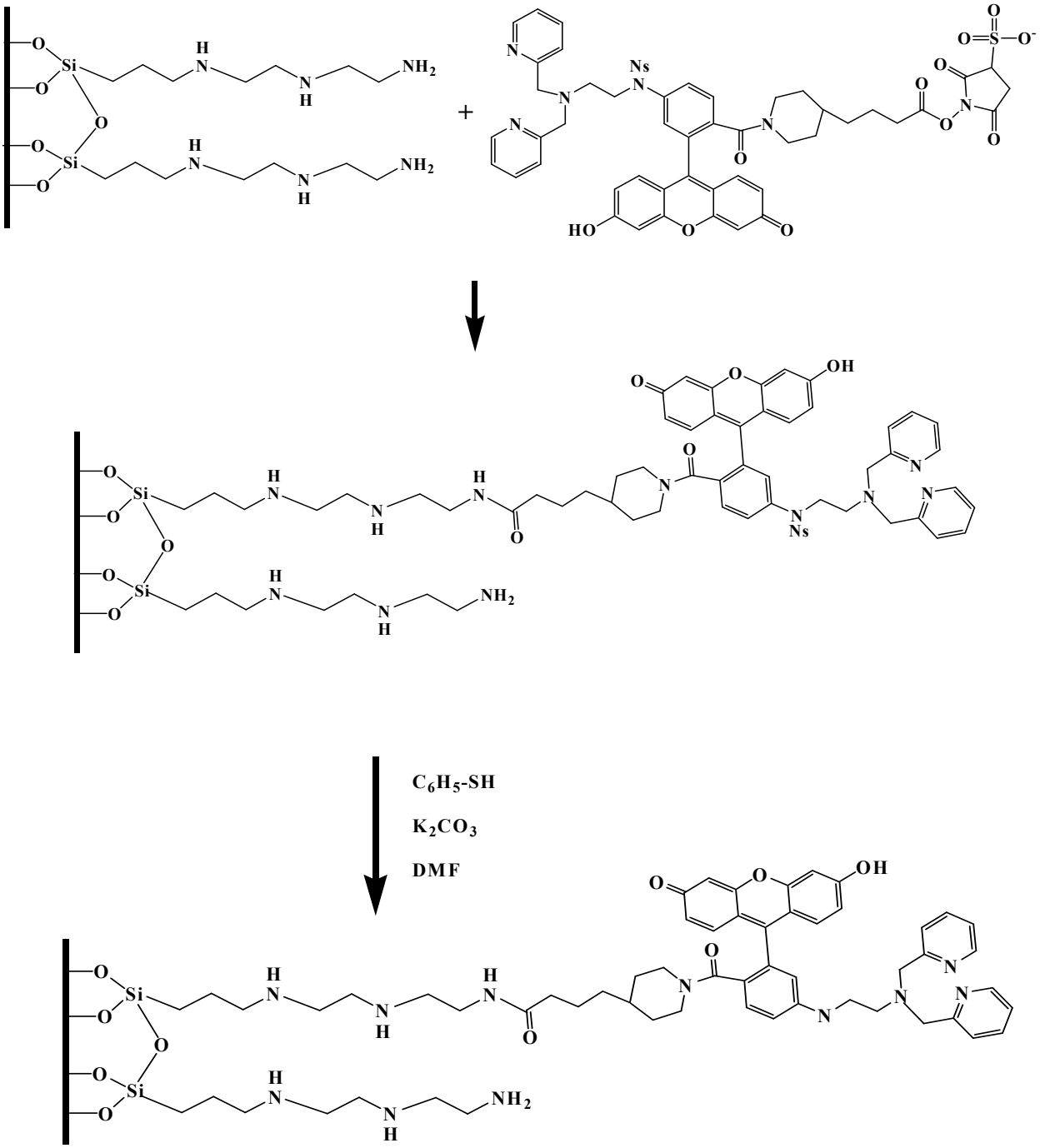

Figure 3.5 Representation of conjugation of ZnAF2 to aminosilanized glass coverslips

3.2.5. Cell Culture and Maintenance

Min-6 cells were kindly provided by Bryan Wolf of Childrens Hospital of Philadelphia. The cells were cultured at 37ºC under 5% CO_2 on polycarbonate membranes of cell culture inserts, allowing media access on both sides of the cells. They were grown in Dullbeco's modified Eagle's medium (DMEM) supplemented with 15% fetal bovine serum (FBS), 1% Antibiotic-antimycotic, 4% L-glutamine and 0.06 mM β-mercaptoethanol.

3.3. Results and Discussion

3.3.1. Zinc Ion Fluorescence Sensing Properties of Modified ZnAF-2

Figure 3.6 shows the zinc ion concentration dependence of the fluorescence intensity of a 5μM solution of the modified ZnAF-2 dye. The excitation and emission wavelengths were 503 nm and 524 nm respectively. It can be seen that the fluorescence intensity increased approximately 7 folds when the concentration of zinc in the solution increased from 0 to 5 μM. The excitation and emission wavelengths were close to the excitation and emission wavelengths of unmodified ZnAF-2 and other fluorescein derivatives. The dynamic range was between 0-2.5 μM.

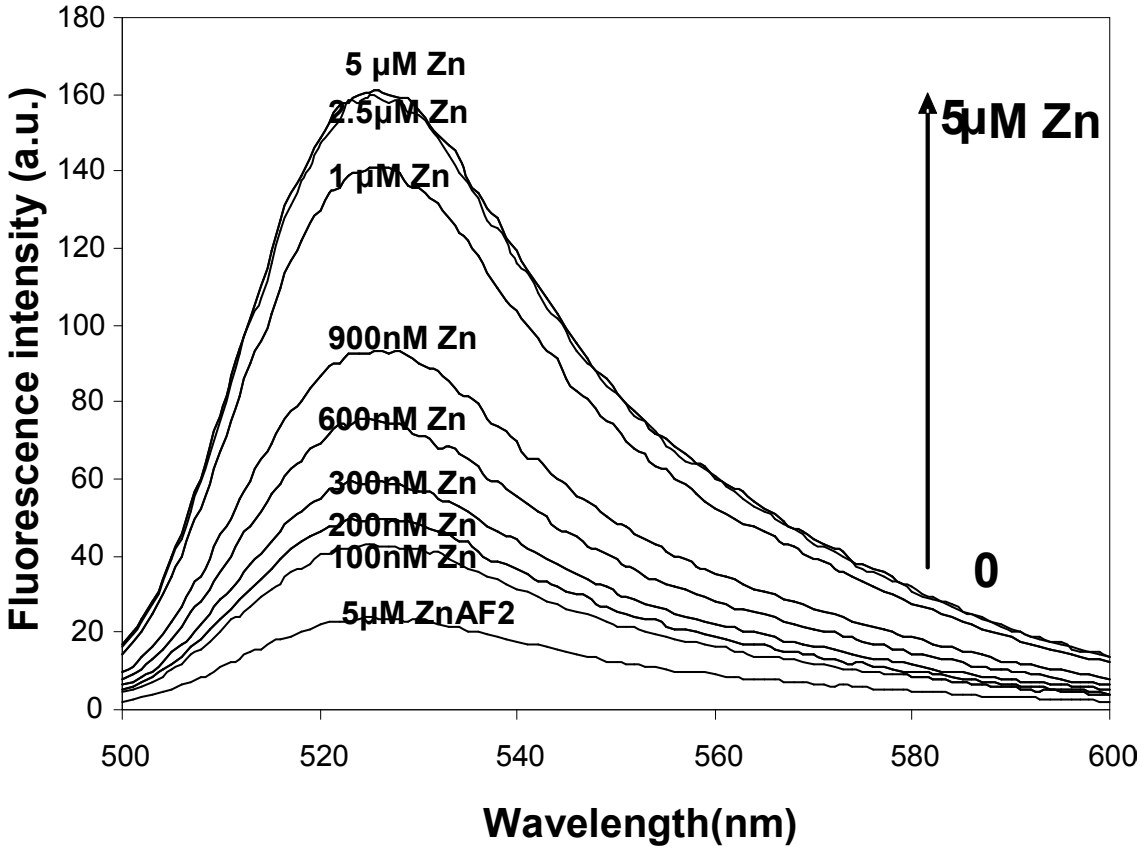

Figure 3.6 Emission spectra of 5uM carboxyl-modified ZnAF-2 at increasing zinc ion concentration between 0 to 5 µM.

3.3.2. Calibration Curve of ZnAF2 Modified Glass Coverslips

Zinc ion sensitive glass slides were fabricated according to the protocol described in the experimental section. It was found that a ZnAF-2 sensor resulted in a maximum response factor of 2.1±0.2. Figure 3.7 represents the emission spectra of zinc sensor in presence of various concentrations of zinc ranging from 0 to 80nM .The fluorescence intensity increased with increasing zinc concentration [40].

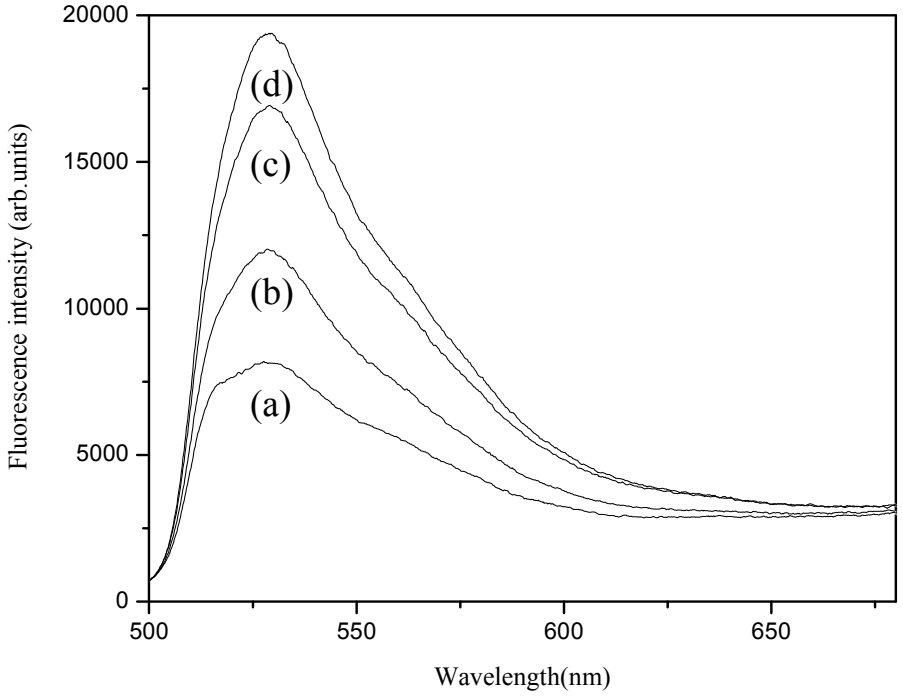

Figure 3.7 Emission spectra of a zinc ion sensing glass slide in solutions of increasing zinc ion concentration (a) 0, (b) 5, (c) 20 and (d) 80 nM.

Figure 3.8 is a representation of analytical curve where each data point is an average measurement .The dynamic range over which the curve is linear is between 1.25nM-20nM.The limit of detection of the film sensor was 1.25nM.This concentration range enables detection of early release events from beta pancreatic cells. The response factor was defined as F_{max}/F_0 where F_{max} was the maximum fluorescence intensity of ZnAF-2-glass slides and F_0 was the fluorescence intensity in the absence of zinc. Fluorescence intensity measurements of the zinc sensing glass slides indicated a large variation of up to 25% between different spots on the glass surface.

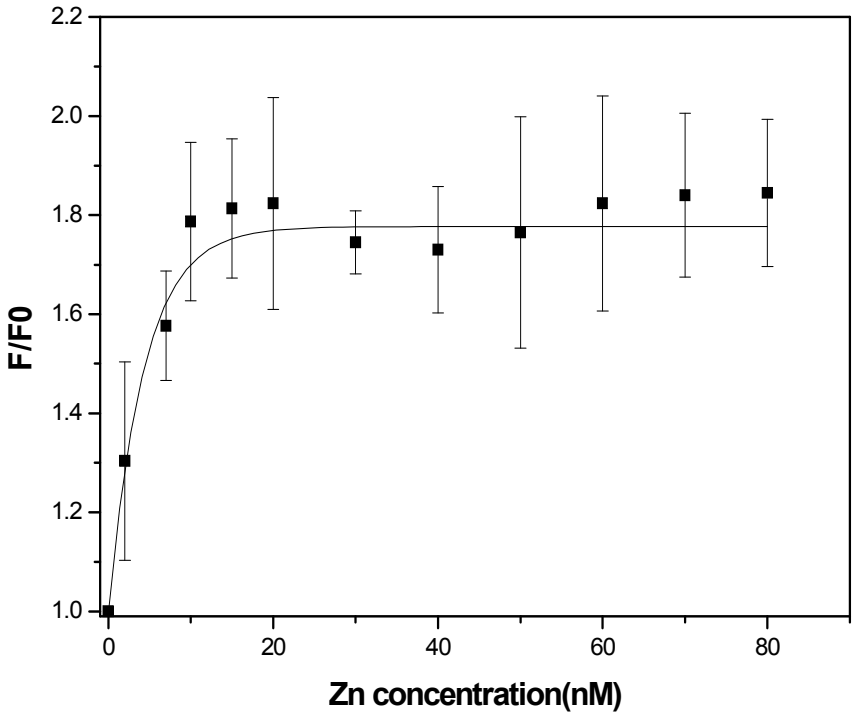

Figure 3.8 Representation of the calibration curve of the response of the Zn sensors to increasing concentrations of zinc1nM-80nM

The relatively high standard deviation in the calibration curve has different contributions to the uncertainty: the physically heterogeneous surface of a borosilicate substrate, the silanization procedure which introduces a non- uniform silane film, the deprotection reaction and degree of availability of the zinc binding site of the sensor after covalent immobilization.

3.3.3. Photo stability of Zinc Sensing Glass Coverslips

Photostability measurements were carried out to optimize the experimental conditions in order to avoid photobleaching during fluorescence microscopy measurements. The zinc ion sensing glass slides exhibited similar photostability properties to glass slides coated with fluorescein. To minimize photobleaching we employed a 20X microscope objective with a numerical aperture of 0.5 and limited the exposure of the glass slides to excitation light by employing an electronic shutter that only opened during the exposure time of the digital camera and by limiting the number of exposures during any given experiments. Under these conditions we could carry out repeated measurements during 30-minute zinc release experiments from cells without significant photodecomposition of the zinc ion sensing indicator.

3.3.4. Selectivity of Zinc Ion Sensing Glass Coverslips

Selectivity studies were carried out to determine whether the covalent immobilization of ZnAF-2 to the glass slides affected the zinc selectivity of ZnAF-2. The selectivity studies (figure 3.9)

showed that the response factor of the glass slide-based zinc sensors were 1.30±0.21 for calcium. The response factor was defined as F_{max}/F_0 where F_{max} was the maximum fluorescence intensity of ZnAF-2-glass slides in presence of various ions and F_0 was the fluorescence intensity in the absence of ions. The response was 1.10±0.2 for magnesium, 1.16± 0.1 for sodium and 1.3±0.3 for iron. The affinity of these cations reached saturation at micro molar concentrations.

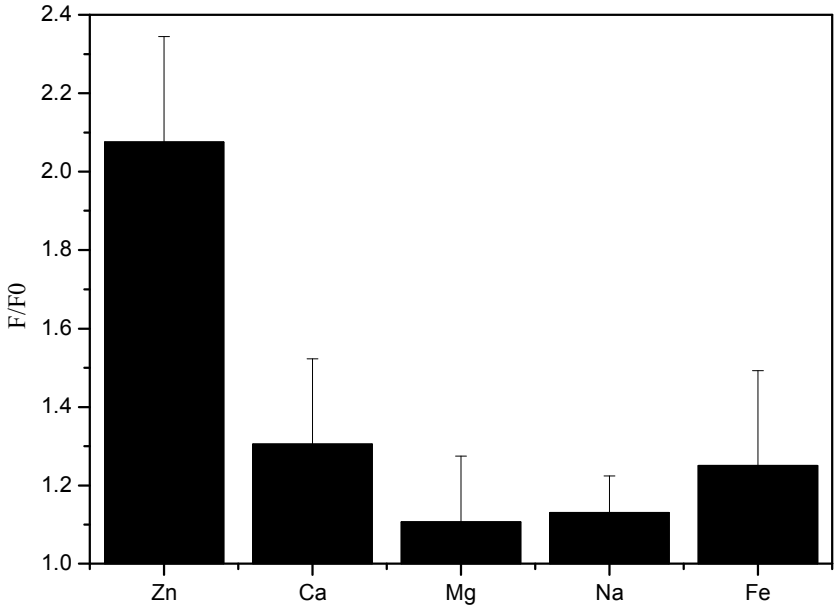

Figure 3.9 Selectivity studies of zinc sensor versus 1 μM of Zn, Ca, Mg, Na, and Fe

Ca^{2+} and Mg^{2+} bind to ZnAF2 to a lesser extent than Zn, because the ZnAF2 binding site contains only four nitrogens to bind to a metal. Ca^{2+} and Mg^{2+} require six nitrogens for coordination.

ZnAF-2 also binds to Fe^{2+} or other transitional metals but it does not significantly affect the fluorescence intensity because it does not bind to the pivotal nitrogen of the fluorescence "switch", the aromatic secondary amine.

3.3.5. Reversibility of Zinc Ion Sensor

Reversibility measurements were performed to demonstrate the capability of the zinc sensing glass slides to detect multiple exocytotic events. The glass slide based sensors were first treated with 1μM zinc solution and the fluorescence increase was recorded instantly. Figure 3.10 represents the fluorescence intensity in arbitrary units versus Zn and TPEN. We observed a decrease to the basal level of the fluorescence intensity of the film sensor when 1mM TPEN solution was added to the glass slides. TPEN is an effective zinc ion chelator.

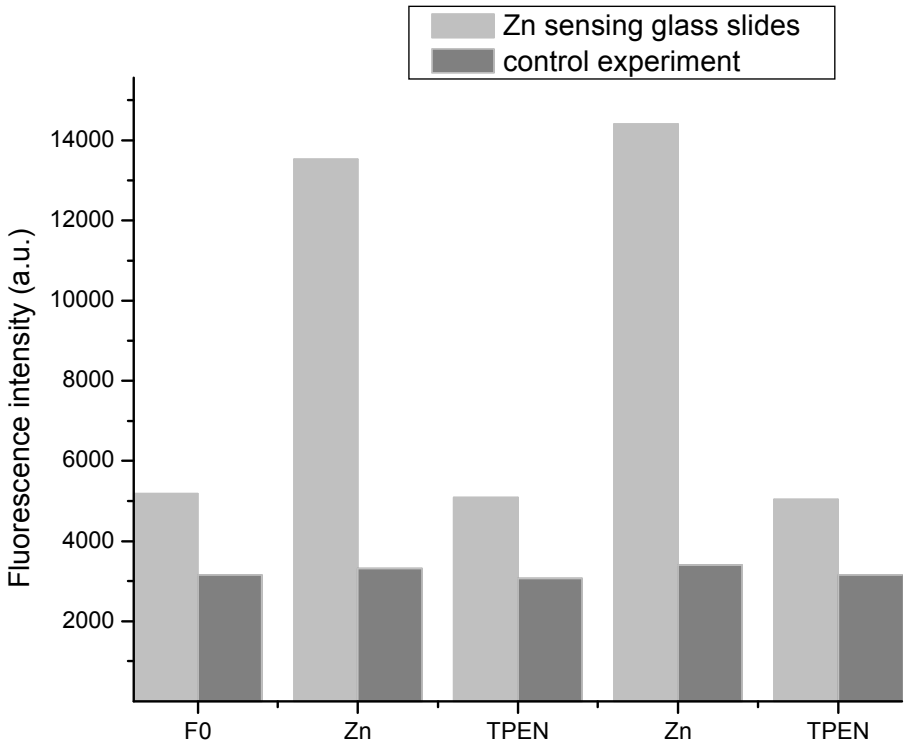

Figure 3.10 Reversibility experiment shows exposure alternately to 1 μM of Zn, followed by 1mM TPEN treatment

At millimolar concentrations, TPEN displaced the zinc ions from the glass slides, which resulted in a fluorescence decrease of the sensor. The sample was thoroughly rinsed with a 100mM HEPES buffer to remove the TPEN and zinc ions from the sensors. Then, the glass slide based sensors were exposed again to a zinc containing solution. As expected, a fluorescence increase of the sensor was observed. The response factor decreased gradually with the number of repeated zinc ion exposures indicating that some of the binding sites were permanently blocked or that the sensing dyes were photobleached. It was possible to run 5 repeated exposures without a significant loss of zinc ion sensitivity.

Control experiments on bare aminosilanized glass slides show no changes in fluorescence intensity with addition alternately of zinc solutions or TPEN solutions. The signal was a source of background.

3.3.6. Time Dependence Measurements

Time dependent fluorescence measurements of the sensors at 524 nm (λex = 503 nm) were carried out to determine the response time of the zinc ion sensing glass slides (Figure 3.11). The fluorescence intensity was measured 10 seconds prior to adding 80 μL of 1 μM zinc ion to the sensor while recording the fluorescence intensity for another 10 seconds. The fluorescence intensity of the sensor increased due to the addition of zinc in less than 1 second. The sensor has the capacity to detect zinc release events in seconds time scale.

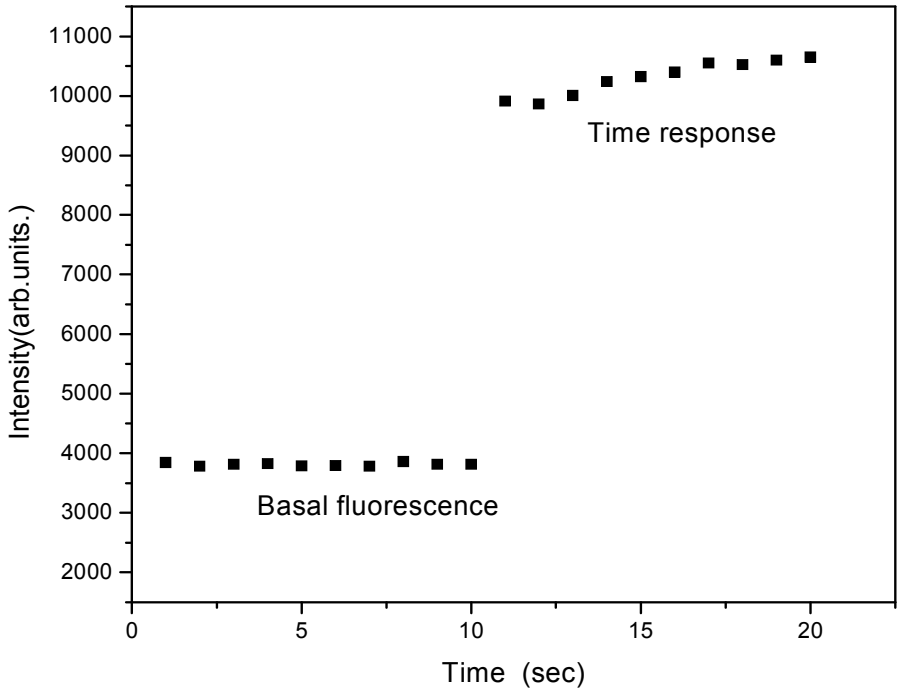

Figure 3.11 Response time measurements of zinc ion sensing glass slides

3.3.7 Application of the Zinc Sensors for the Measurement of Zinc Release from Pancreatic Cells

Min-6 cells were chosen for these experiments since they retain the characteristics of the glucose transport system and glucose metabolism of normal pancreatic beta cells and secrete insulin in response to chemical stimulation by glucose or potassium [39]. 500,000 cells/mL were used in our cell experiments. A polycarbonate membrane, on which Min-6 cells were grown to 50-80% confluence, was placed over the zinc sensing glass slides. The membrane and glass slides were washed with a solution of Krebs-Ringer buffer at pH 7.4 that contained 500 nM TPEN to complex and remove free zinc ions from the solution. The glass slides and membrane were then washed and placed in a Krebs-Ringer buffer free of TPEN. Fluorescence measurements of the zinc sensing glass slide under zinc free conditions were obtained. The cells were then treated with 20mM glucose to induce zinc release.

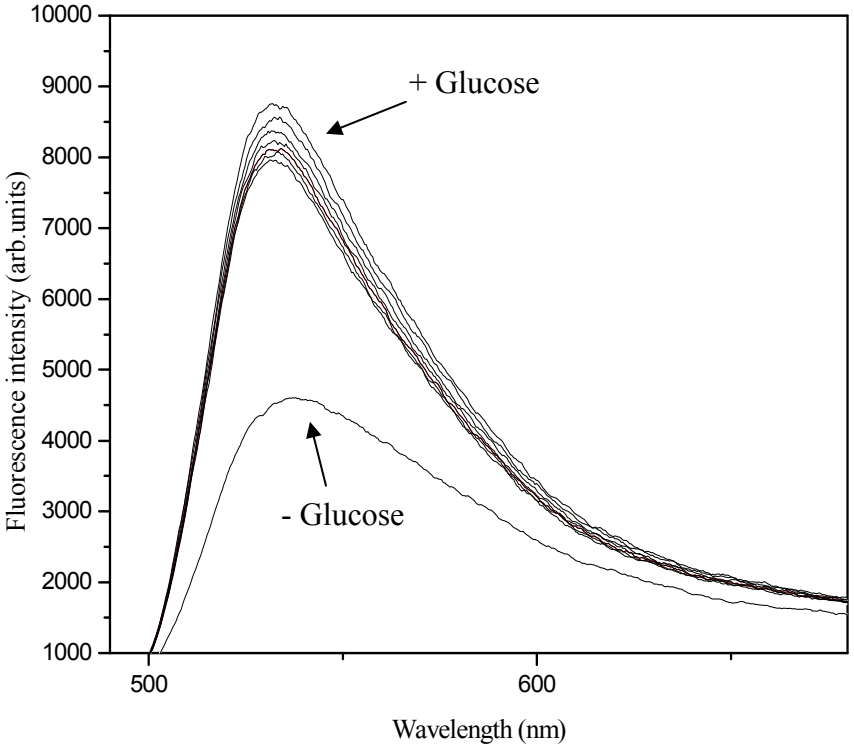

Figure 3.12 Emission spectra of a zinc ion sensing glass slide prior to and following 20mM glucose-stimulated zinc release from Min-6 cells. The spectra were taken at 1 second time intervals.

An instant increase in the fluorescence of the solution by approximately 90% is clearly seen (Figure 3.12) following stimulation with glucose. The increase in fluorescence intensity was attributed to immediate transient release of insulin and zinc following chemical stimulation. Consecutive recordings at 1 sec of fluorescence intensity indicate a saturation of the zinc sensor with up to 20 nanomolar zinc concentrations. Control experiments were done by exposing the sensor to 20mM glucose solutions and we observed a decrease in fluorescence intensity .We also employed fluorescence microscopy imaging measurements to monitor the release of zinc ions from Min-6 cells. In these experiments, suspended Min-6 cells were placed directly on a zinc

ion sensing glass slide. Figure 3.13a shows a transmission image of the cells when placed on the slide. Figure 3.13b shows the fluorescence image of the cells prior to stimulation with glucose. Only a residual fluorescence is seen. Figure 3.13c shows the fluorescence image of the glass slide that was taken immediately following stimulation of the cells with 20 mM glucose. A large increase in the fluorescence intensity of the glass slide is observed, which was attributed to zinc release. The fluorescence increase varied greatly among cells. Some cells did not register a fluorescence increase when stimulated, while others showed a fluorescence intensity increase in response to stimulation. This is indicative of a large cell-to-cell variation in the response to stimulation. Furthermore, it should be noted that binding of released zinc to free insulin competes with the binding efficiency of zinc ions to the surface bound ZnAF-2 molecules. This complicates the quantitative analysis of free zinc released from the Min-6 cells [40].

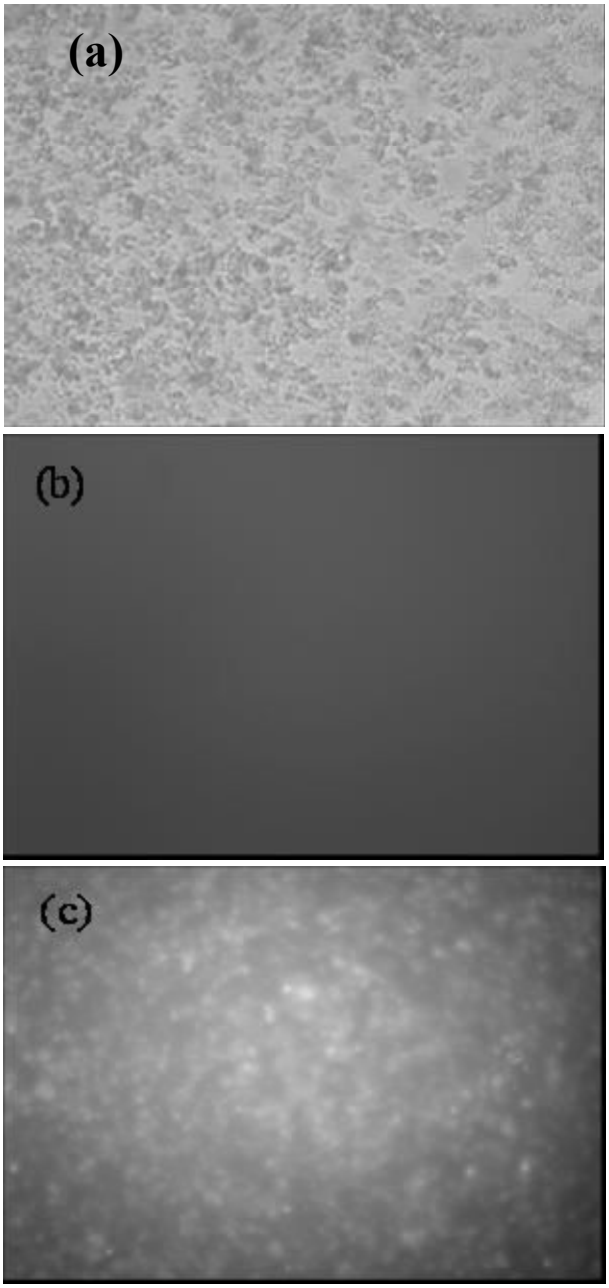

Figure 3.13 a) A 10X transmission image of Min-6 cells in suspension, b) A fluorescence image of a zinc ion sensing glass slide prior to stimulation with glucose, c) A fluorescence image of the same zinc ion sensing glass slide following the stimulation and zinc ion release from beta cells deposited on the glass slide.

3.4 Summary and Conclusions

Zinc ion sensors were fabricated by the covalent attachment of ZnAF-2, a newly synthesized zinc ion fluorescence indicator, to amino modified glass slides. Covalent immobilization of the sensing molecule to the substrate prevents the dye from leaking into the medium or permeating through cell membranes.

Detailed characterization studies indicated that the glass slide-based zinc sensors have high sensitivity, selectivity and the fast response time needed to measure zinc ion release events from pancreatic cells. The sensor was used to measure the release of zinc from Min-6 cells when stimulated by elevated glucose levels. Cells deposited on top of the film sensor maintained their physiological state and responded to glucose stimulation

The study reveals large variations in zinc ion release between individual cells. The analytical properties of the newly developed sensors could be further improved by decreasing the heterogeneity of dye distribution on the silanized glass slides. The limitations of the glass coverslip zinc film sensor relate to a relatively high standard deviation which impedes the reproducibility of measurements. Also, the dynamic range is in low nanomolar concentrations for detection of micromolar release events. However, it is possible to conclude that glass coverslip film sensor could be used to confirm the zinc release events from a biological system. In the future, we will explore alternative approaches to silanization in order to fabricate more homogeneous sensors and extend the dynamic range.

Unlike previously used analytical techniques (atomic absorption spectrophotometry, X ray fluorescence, radio-isotopes detection), fluorescence detection of zinc ions in biological systems provides valuable information about zinc physiology in real time. Additionally, fluorescence

detection of zinc ions released from cultured cells does not require methods that are destructive to the specimens.

References

1. Hirano, T.; Kikuchi, K.; Urano, Y.; Higuchi, T.; Nagano, T. *J Am Chem Soc* **2000** , *122*, 12399-12400.
2. Dudek, E. *Epilepsy Curr.* **2001,** *1*: 66
3. Cohen-Kfir, E.; Lee, W.; Eskandari, S.; Nelson, N. *Proc Natl Acad Sci* **2005 ,** *102* , 6154–6159
4. Ruiz, A .; Walker, M.C.; Fabian-Fine, R.; Kullmann, D.M. *J Neurophysiol* **2004 ,** *91*, 1091–109
5. Minami, A.; Sakurada, N.; Fuke, S.; Kikuchi , K.; Nagano, T.; Oku, N.; Takeda, A. *Journal of Neuroscience Research* **2006**, *83*, 167–176
6.Takeda, A.; Minami, A.; Seki, Y.; Oku, N. *Journal of Neuroscience Research* **2004,** *75*, 225–229
7. Lin, D.L.; Cohen, A.S.; Coulter, D.A. *J Neurophysiol* **2001**, *85*, 1185-1196
8. Chausmer, A.B.; *Journal of the American College of Nutrition* **1998**, *17,* 109-115
9. Kennedy, R.; Huang, L.; Aspinwall, C. *J Am Chem Soc* **1996**, *118*, 1795-1796
10. Dodson, G.; Steiner, D. *Curr Opin Struct Biol* **1998**, *8,* 189-194.
11. Berson, S.A.; Yalow, R.S. *Am J Med* **1966**, *40*, 67-69
12. Helmerhorst, E.; Stokes, G. B. *Arch. Biochem Biophys* **1986**, *245*, 238-242
13. Rabinovitch, A.; Suarez-Pinzon, W.; Strynadka, K.; Lakey, J.; Rajotte, R. *J Clin Endocrinol Metabol* **1996** *, 81*, 3197-3202
14. Zhefeng, F.; Liming, D.; Xiaotao, J. *CJI* **2001** , *3*: 53
15. Wilharlitz, P.; Dreew, S.; Krismer, R. et al *Mikrochim Acta* **1997** , *125*:45
16. El-Yazigi, A.; Al-Saleh, I.; Al-Mefty, O. *Clin Chem* **1984**, *30*, 1358-1366
17. el-Yazigi, A.; Al-Saleh, I.;Al-Mefty, O. *Clin Chem* **1986**, *32*, 2187-2190.
18. Cesareo, R. *Eur J Nucl Med* **1976**, *1*, 49-56
19. Mazen, A.; Gradwohl, G.; de Murcia G *Anal Biochem* **1998**, *172*, 39-42
20. Nguyen, T.; Rosenzweig, Z. *Anal and Bioanal. Chem*. **2002**, *374*, 69-74
21. Nguyen, T.; Dumitrascu, G.; McNamara, K.P.; Rosenzweig, N .; Rosenzweig, Z. *Anal. Chem* **2001***, 73*, 240-3246.
22. Jindal, R.M.; Taylo, R.P.; Gray, D.W.; Esmeraldo, R.; Morris, P.J . *Diabetes* **1992** ,*41*, 1056-1062
23. Qian, W.J.; Aspinwall, C.A.; Battiste, M.A.; Kennedy ,R.T. *Anal Chem* **2000** ,*72*, 711-717
24. Qian, W.J.; Gee, K.R.; Kennedy, R.T. *Anal Chem* **2003,** 75, 3468-3475.
25. Chang, C.J.; Jaworski, J.; Nolan, E.M.; Sheng, M.; Lippard, S.J. *PNAS* **2004**, *101(5)*, 1129-1134
26. Catherine, M.H.; Cass, A.E.G. *Anal Chem* **2001***, 73*, 2476-2483
27. Chrisey, L.A.; Lee, G.U.; O'Ferrall, C.E. *Nucleic Acids Res* **1996**, *24*(15), 3031-3039
28. Chrisey, L.A.; Lee, G.U.; O'Ferrall, C.E. *Nucleic Acids Res* **1996**, *24*, 3040-3047
29. Joos, B.; Kuster, H.; Cone, R. *Anal.Biochem.***1997**, 247, 96-101
30. Pirrung, M.C.; Davis, J.D.; Odenbaugh, A.L. *Langmuir* **2000**, 16, 2185-2191
31. Yuan, W.; Van Ooij, W. J. *J colloid Interface Sci.***1997**, 185(1), 197-209
32. Jonsson, U.; Malmqvist, M.; Olofsson,G.; Ronnberg, I. *Methods Enzymol*. **1998**, 137, 381-388
33. Pirrung, M. C.; Davis, J. D.; Odenbaugh, A. L. *Langmuir* **2000**, *16*, 2185- 2191.

34. Vandenberg, E.; Elwing, H.; Askendal, A.; Lundstrom, I. *J. Colloid InterfaceSci.* **1991**, *147* (1), 103-118.
35. Pohl, E. R.; Osterholtz, F. D. In *Silanes, Surfaces and Interfaces*; Leyden, D. E., Ed.; Gordon and Breach: New York, 1986; pp 481-500.
36. Stenger, D.A., Pike, C. J., Hickman, J. J. and Cotman, C. W. (1993) *Brain Res*.,**630**, 136–147.
37. Hermanson, G.T. *Bioconjugate techniques* :Carbodiimides ; Academic Press :Rockford,Illinois, **1996** ,pp 169-176
38. Stapper, C. and Blechert, S. *J.Org. Chem*. **2002**, *67*, 6456-6460
39. Ishihara, H.; Asano, T. ; Tsukuda, K. ; Katagiri , H. ; Inukai, K. ; Anai, M. ; Kikuchi , M. ; Yazaki, Y. ; Miyazaki , J-I. ; Oka, Y . *Diabetologia* **1993** ,36, 1139–1145
40. Crivat, G.; Kikuchi, K.; Nagano, T.; Priel, T.; Hershfinkel, M.; Sekler, I.; Rosenzweig, N.; Rosenzweig, Z. *Anal. Chem.* **2006**; *78*(16); 5799-5804

CHAPTER 4

TARGETED FLUORESCENCE DETECTION OF ZINC ION RELEASE FROM BETA PANCREATIC CELLS

Georgeta Crivat[1], Kazuya Kikuchi[2], Tetsuo Nagano[3], Nitsa Rosenzweig[1], and Zeev Rosenzweig[1]

1. University of New Orleans, Department of Chemistry, New Orleans, LA 70148
2. Department of Material and Life Science, Graduate School of Engineering, Osaka University, 2-1 Yamada-oka, Suita City, Osaka
3. Graduate School of Pharmaceutical Sciences, the University of Tokyo, 7-3-1 Hongo, Bunkyo-ku

4.1 Introduction

This chapter describes the preparation of antibody A2B5–ZnAF-2 bioconjugate for the targeted measurement of zinc ion release from pancreatic β cells. The sensor was prepared by conjugating mouse A2B5 monoclonal antibody to ZnAF-2, a zinc ion fluorescent indicator. ZnAF-2 {6-[N- [N', N'-bis (2-pyridinylmethyl)-2-aminoethyl] amino-3', 6'-dihydroxy-spiro [isobenzofuran-1(3H), 9'-[9H]xanthene]-3-one} was modified with a carboxyl-terminated linking aliphatic chain. The modified ZnAF-2 was successfully conjugated to the free amino groups of the A2B5 antibody molecules. The zinc ion sensitivity, selectivity and the binding activity of the newly prepared conjugate was not significantly altered compared to the zinc ion sensing properties of free ZnAF-2 and the binding affinity of free A2B5 antibody molecules.

The A2B5-ZnAF-2 bioconjugate attached to β-cells in culture and was used for targeted measurements of zinc ion release from β cells in culture.

There is a growing interest in exploring the biology of β pancreatic cells [1-7]. In pancreatic β cells, zinc, one of the most abundant transition metals in the body is involved in insulin synthesis, storage and secretion. Insulin is co-stored as a hexamer complex with two zinc ions in secretory vesicles located preferentially near the plasma membranes. Exposure to insulin secretagogues induces fusion of vesicles with the plasma membrane and release of zinc-insulin hexamers into the extra-cellular space, where the complex dissociates into zinc ions and insulin monomers. The function of zinc ions following insulin secretion is not well understood. It is suggested that free zinc could have paracrine effects on cells promoting islet death [7]. Zinc deficiency may be associated with low efficiency of insulin production and secretion observed in diabetes I and with complications in diabetes II. [5] Given the importance of zinc ions in this cellular system it is not surprising that many research groups have focused their effort on developing new and improved zinc ion indicators.

Zinc ion fluorescent indicators were previously used for the analysis of zinc ions release from β-cells. These include the ultraviolet excitable quinoline-based dyes like Zinquin [8], and the visible light excitable fluorophores like FluoZin-3 [9, 10]. One of problems in detecting and monitoring extracellular zinc events from β-cells using fluorescence detection was the permeation and diffusion of free fluorescent dyes from the exocytose site. Additionally, zinc ion sensitive fluorophores suffered from interferences, particularly from calcium ions. A new zinc ion sensitive fluorophore {6-[N- [N', N'-bis (2-pyridinylmethyl)-2-aminoethyl] amino-3',6'-dihydroxy-spiro[isobenzofuran-1(3H),9'-[9H]xanthene]-3-one} or ZnAF-2 [11], was

synthesized by Kikuchi and coworkers. The ZnAF-2 has a high sensitivity and selectivity for zinc ions. For example, the response of ZnAF-2 to zinc was almost 50 folds higher than its response to calcium ions at similar concentration. To avoid diffusion and permeability of free dye, we conjugated the dye to various supports [12].Here we present a different approach of conjugation of the dye to an A2B5 monoclonal antibody. It must be noted that labeling protein molecules with fluorophores like fluorescein isothiocyanate (FITC) and tetramethylrhodamine isothiocyanate (TRITC) and Alexa dyes is very common. It enables tracking of antibody molecules when applied as biological probes in cells, tissues or organs or in bioassay development [13-16]. However, the conjugation of ion sensing dyes to antibody molecules for the purpose of targeted ion sensing has not yet been reported.

A2B5 antibody molecules recognize specific sialogangliosides on the surface of neurons, and glial cells, thymus epithelia and endocrine cells like β-cells. Expression of antigens to the A2B5 antibody was shown to be directly related to the physiological state of β-cells [17]. The binding affinity of A2B5 antibody to β-cells, specifically to the ganglioside GT3 is higher in type 1 diabetes which suggests that gangliosides could be involved in the immunopathology of type I diabetes [18].

In our experiments, we used cells derived from a Min-6 mouse insulinoma cell line. Similarly to normal pancreatic cells, Min-6 cells secret insulin in response to stimulation by elevated glucose levels [19, 20]. Antibody A2B5 was reported to bind to islet cell membranes of chicken, mouse, rat, and human [21]. Successful labeling with antibody A2B5 was described in literature using rat insulinoma cell lines RINm5F (90% positive), INS-1 and human insulinoma cell line [21-23].

The analytical properties of the A2B5–ZnAF-2 bioconjugate and its application in detection zinc ion release from Min-6 β-cells are further discussed. In addition to targeted measurement of zinc ion release, this sensor address a solution to the permeation problem observed when free dyes are used for zinc ion release measurements from cells.

4.2. Specific Experimental and Technical Details

4.2.1. Materials and Reagents

Materials and methods - The newly developed zinc ion indicator {6-[N- [N',-bis(2-pyridinylmethyl)-2-aminoethyl]amino-3',6'-dihydroxy-spiro[isobenzofuran 1(3H),9'-[9H]xanthene]-3-one} (ZnAF-2) was modified to include a carboxyl terminated aliphatic chain(kindly provided by Prof.Kazuya Kikuchi, University of Japan; TEF LABS from Austin, TX). TPEN (N, N`, N`-Tetrakis (2-pyridylmethyl) ethylenediamine was obtained from Dojindo Laboratories. Trypsin-EDTA was purchased from Gibco. Mouse A2B5 monoclonal antibody was purchased from Chemicon International. Magnesium chloride, sodium chloride, potassium carbonate, calcium chloride, magnesium sulfate and potassium phosphate were obtained from EM Industries, Inc. Aqueous solutions were prepared using 18 MΩ deionized water that were conditioned using the water purification system Barnstead Nanopure Diamond. Phosphate buffer (PBS, pH=7.2) without calcium chloride and magnesium chloride , Dulbecco' s modified Eagle medium, antibiotic-antimycotic and fetal bovine serum qualified for cell cultures were obtained from Invitrogen Corporation. HEPES buffer, N-Hydroxysulfosuccnimide sodium salt, N- (3-Dimethylaminopropyl)-N`-ethyl-carbodiimide, benzenethiol 99%, and zinc sulfate were obtained from Sigma-Aldrich. Microcon centrifugal filter devices YM-100 were purchased from Millipore. All reagents were used as received without further purification.

4.2.2. Fluorescence Microscopy and Spectroscopy Measurements

Excitation and emission spectra were obtained using Varian Cary Eclipse spectrofluorometer. SpectraMax M2 microplate reader (Molecular Devices, Inc.) was used for detection of zinc release from Min6 cells labeled with antibody sensor. The multi-detection microplate reader consists of a 50-Watt xenon flash lamp as a light source, dual monochromators and a photodetector. Detection modalities include absorbance (UV-VIS) and fluorescence. The instrument is equipped with a controlled temperature feature, which enabled zinc release measurements at constant temperature.

Digital fluorescence microscopy system consisted of an inverted fluorescence microscope (Olympus IX-70) equipped with three detection ports. A 100-W mercury lamp was used as the light source for excitation. A 20X microscope objective (NA = 0.5) was used to collect the fluorescence. A filter cube consisting of a 480/30x bandpass excitation filter, a 500 nm dichroic mirror and a 535/40x bandpass emission filter were used to ensure spectral purity. A high-performance charge-coupled device (CCD) camera (SpectraPro, model 2300i) was used for obtaining spectra from the samples. The Roper Scientific software WinSpec 32 was used for data analysis. The exposure time was 0.1 seconds. A second fluorescence imaging system consists in an inverted fluorescence microscope (Olympus IX51), similar objective and filter cube and a high resolution CCD camera (CCD) (Andor Technology, DV434-BV) was used to obtain digital fluorescence images of the cells. To visualize zinc release from beta pancreatic cells, images were recorded with a Zeiss fluorescence microscope with a heated stage to 37^{o} C and CO_2 control. AxioVision Rel.4.5 software was used for recording the images.

4.2.3. Maintenance of Min-6 Cell Line in Culture

Min-6 cells were a gift from Bryan Wolf of Childrens Hospital of Philadelphia. The cells were cultured at 37ºC under 5% CO_2. They were grown in Dullbeco's modified Eagle's medium (DMEM) supplemented with 15% fetal bovine serum (FBS), 1% Antibiotic-antimycotic, 4% L-glutamine and 0.06 mM β-mercaptoethanol. When preparing subcultures, the cell medium was removed from the cell culture flask and 5 mL trypsin was added. The cells are incubated for 5 minutes in trypsin solution and neutralized with DMEM medium. 250,000 cells/mL were distributed into 96-well plates and were allowed to grow until reaching confluence.

4.2.4. Synthesis of the A2B5-ZnAF-2 Bioconjugate

The EDC-based conjugation of ZnAF-2 to A2B5 monoclonal antibody molecules is shown in figure 4.1. A solution containing 10 μM modified ZnAF-2 and 1 mM zinc sulfate was used in the conjugation reaction. The zinc ions are to prevent the attachment of NHS ester intermediates formed during the EDC coupling reaction to the secondary amines of the zinc ion binding site. Also other source of interferences is binding at the binding site of sodium or other cations present in working buffers. The modified ZnAF2 was then activated at the free carboxyl group in the presence of 100 μM EDC. This step in the EDC coupling reaction leads to the formation of the highly reactive O-acylisourea intermediate. To stabilize the intermediate, the reaction took place in the presence of 250 μM sulfo-NHS. The activated dye was then reacted with 0.25 mg/ml A2B5 antibody molecules under continuous stirring at room temperature for 2 hours. The bioconjugate was separated from excess dye and reaction by products using spin dialysis at

14,000g for 10 minutes. The cutoff of the spin dialysis membrane was 100,000Da. The zinc ion-binding site of ZnAF-2 was freed by adding 2 mM TPEN, a strong zinc ion chelator. The bioconjugate was then separated from the TPEN-zinc complex by spin dialysis at 14,000g for 10 minutes. In a similar matter 0.25 mg/ml A2B5 antibody was labeled with 10 μM FITC [25].

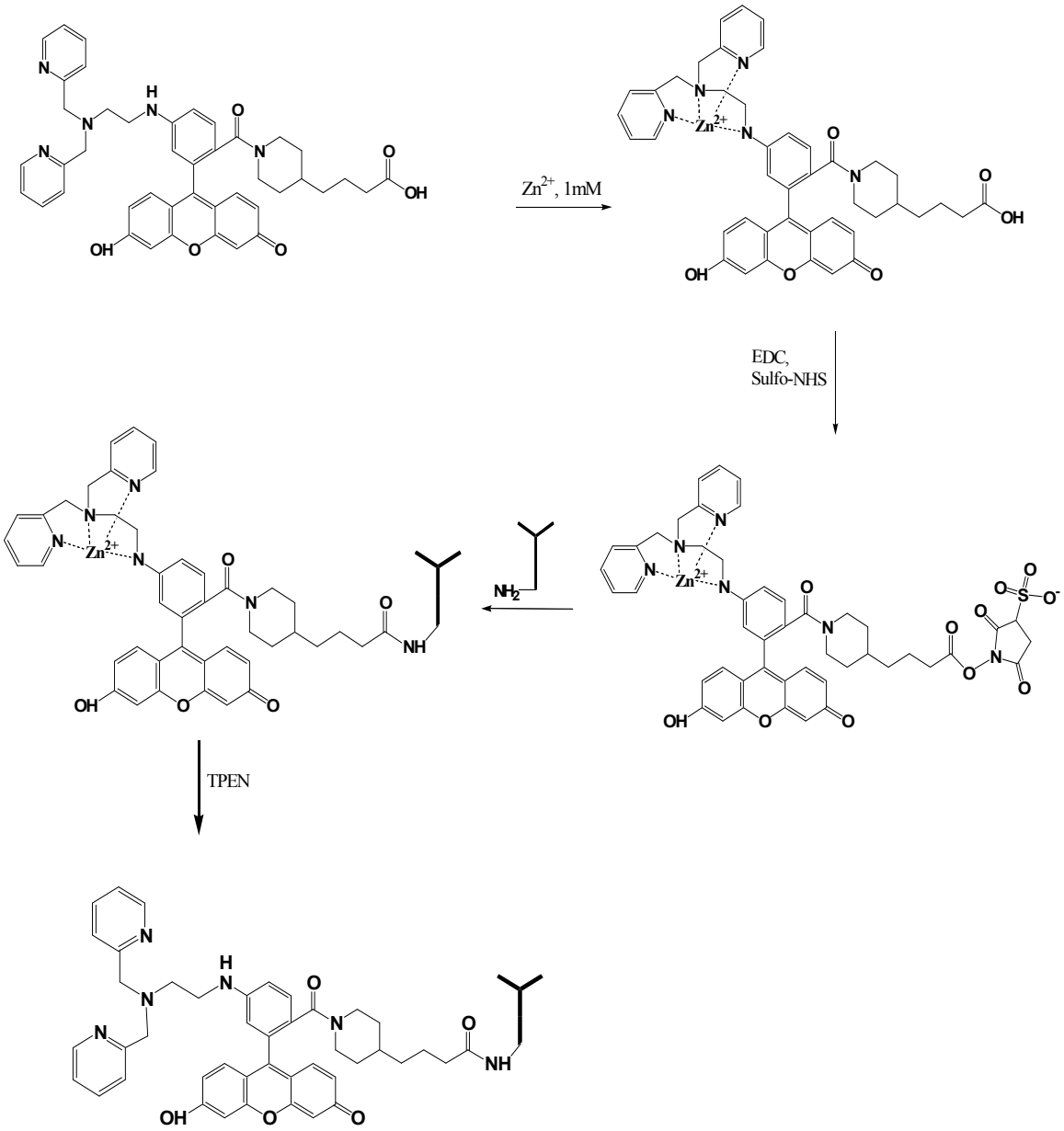

Figure 4.1 A schematic diagram describing the synthesis of the A2B5- ZnAF-2 bioconjugate

4.3. Results and Discussion
4.3.1. Synthesis of the A2B5-ZnAF-2 Bioconjugate

The conjugation chemistry used to bind fluorophores to antibodies should minimize physical blocking of the binding site of the antibody to its corresponding antigen. Previous studies showed that the activity of antibodies is retained when fluorophores are attached to sulfhydrils groups following the reduction of disulfides in the hinge region of antibody molecules. The labeling efficiency of this technique is limited due to the low abundance of sulfhydrils groups in antibody molecules. Another common strategy is to bind the labeling flurophores to glycosydic groups of polysaccharides, which are attached to the Fc region of antibody molecules. This method is limited mostly to polyclonal antibodies that contain polysaccharides in their Fc region [13]. Another common technique is to couple the labeling fluorophores to primary amines or carboxylate groups, which are uniformly distributed on the surface of the antibody molecules. Since it is possible that the dye molecules could bind to amino groups in the antibody-binding site, which would result in decreased antibody activity, the resulting bioconjugate must be tested to ensure retention of antibody activity. In this respect, the modified ZnAF-2 was conjugated to A2B5 monoclonal antibody molecules by forming amide bonds between the carboxyl group of the modified ZnAF-2 and the ϵ-amino or N-terminal α–amino groups of lysine residues of the A2B5 monoclonal antibody molecules. Figure 4.1 describes the preparation scheme of the A2B5–ZnAF-2 bioconjugate. To prevent binding of sulfo-NHS ester intermediate to the secondary amines of ZnAF-2, which is a part of its zinc ion-binding site, the binding sites was saturated with 1 mM zinc sulphate prior to the conjugation reaction. The free carboxylate group of the modified ZnAF-2 was first activated with N- (3-Dimethylaminopropyl)-N`-ethyl-carbodiimide to give a short-lived active O-acylisourea intermediate which was stabilized by

sulfo-NHS. The active intermediate reacted with the amine groups of the A2B5 antibody molecules. Using EDC along with sulfo-NHS was shown before to increase the yield of the conjugation reaction. As previously mentioned, the binding site of bioconjugate was later freed using TPEN to remove the zinc ions bound to the ZnAF-2 zinc ion binding site.

4.3.2. Analytical Properties of the A2B5-ZnAF-2 Bioconjugate

The spectral properties of the A2B5-ZnAF-2 bioconjugate were measured to study the effect of the conjugation on the spectral properties of ZnAF-2. Excitation and emission spectra of A2B5-ZnAF-2 bioconjugate, in 50 mM HEPES buffer solutions at pH 7.4, show excitation and emission peak maxima at 504nm and 525 nm respectively. The spectra of the A2B5-ZnAF-2 bioconjugate show a very slight shift in the excitation and emission peak, as compared with the excitation peak of the modified free dye at 504nm and emission at 524nm, which could be attributed to slight changes in the chemical environment of the dye due to conjugation to the antibody molecules. The minimal spectral changes are in agreement with previous studies that mentioned the effect of conjugating fluorophores to biomolecules on their fluorescence properties. For example, red shifts in excitation spectra were observed when fluorophores were conjugated to proteins. The extent of these red shifts is often a function of the rate of spectral relaxation, which depends on the specific biomolecule of the bioconjugate [24].

Zinc ion response of the A2B5-ZnAF-2 bioconjugate in aqueous solution**.** Zinc ion measurements using the A2B5-ZnAF-2 bioconjugate were carried out in Hepes solution. Figure 4.2 describes the calibration curve of bioconjugate in presence of zinc concentration ranging from 1 μM to 10μM, where the fluorescence intensity increased with the concentration of zinc

ion. The zinc ion limit of detection of the A2B5-ZnAF-2 bioconjugate was 0.1 μM and the linear dynamic range was between 0.1 and 1 μM zinc.

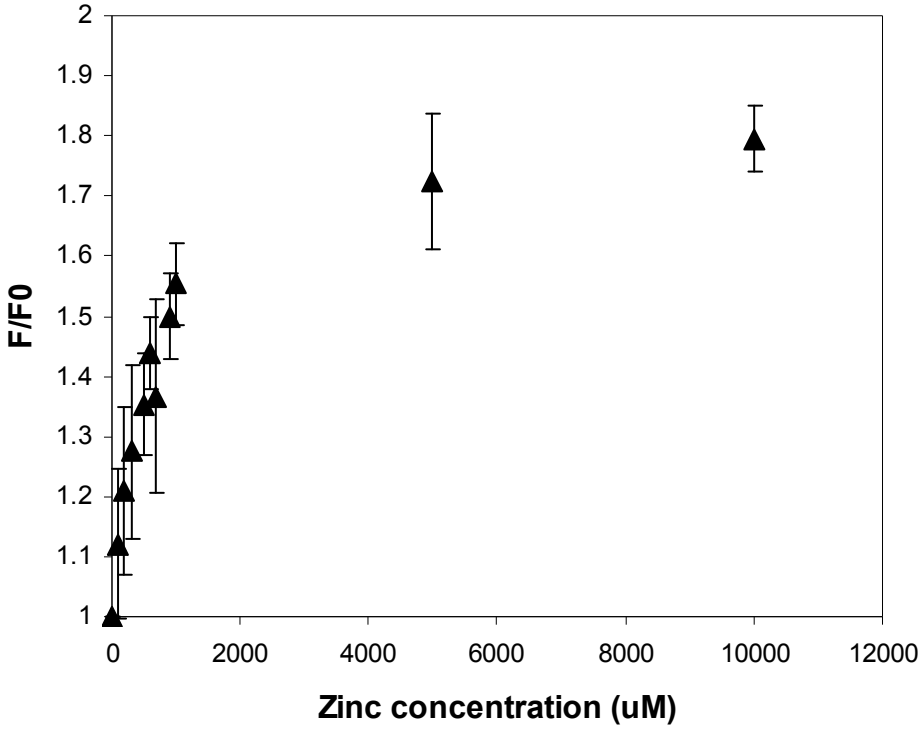

Figure 4.2 Representation of calibration curve describing the fluorescence intensity of A2B5-ZnAF-2 versus zinc ion concentrations ranging from 0 to 10μM. The linear response was between 0 and 1μM zinc ion concentration.

The reduced dynamic range compared to the original free ZnAF2 dye [12] are attributed to partial blockage of the zinc ion binding sites of ZnAF-2 by the antibody molecule. However, the limit of detection and dynamic range of the bioconjugate are still adequate for the expected level of zinc ion level released from β-cells.

4.3.3. Targeted Attachment of A2B5-ZnAF-2 Bioconjugate to Min-6 Cells

Min-6 β-cells were grown in 96 well plates to confluence. The cells were then washed with a solution of 500 nM TPEN to complex and remove free zinc ions and were incubated with 50 μL A2B5–ZnAF-2 bioconjugate for 2 hours at 37°C under 5% CO_2 atmosphere. To remove the unbound bioconjugate, the cells were washed with a PBS buffer solution at pH 7.4 and resuspended in a Krebs-Ringer buffer. The binding affinity of the bioconjugate towards Min-6 cells was tested using fluorescence imaging microscopy. The Min-6 cells are grown to a confluence to the surface of well plates, where the bioconjugate attached to the cells creating a net-like structure (Figure 4.3).

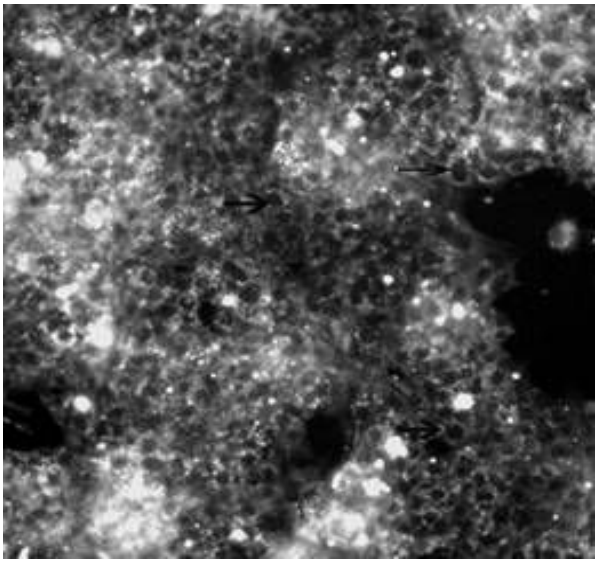

Figure 4.3 Digital fluorescence image of confluent Min-6 cells labeled with the A2B5-ZnAF2 bioconjugate that are attached to the surface of a well.

The signal to background ratio in images of confluent cells was reduced due to background fluorescence of the plastic surface of the well plate and non specific absorption of the bioconjugate to the extracellular matrix. Control experiments were performed using FITC-A2B5 and FITC-AntiGFAP bioconjugates and other non-pancreatic cell types in our laboratory like H9C2. Incubation of the MIN6 cells with FITC-A2B5 bioconjugate resulted in the same level of labeling as with the ZnAF2-A2B5 [25] (Figure 4.4a and b).

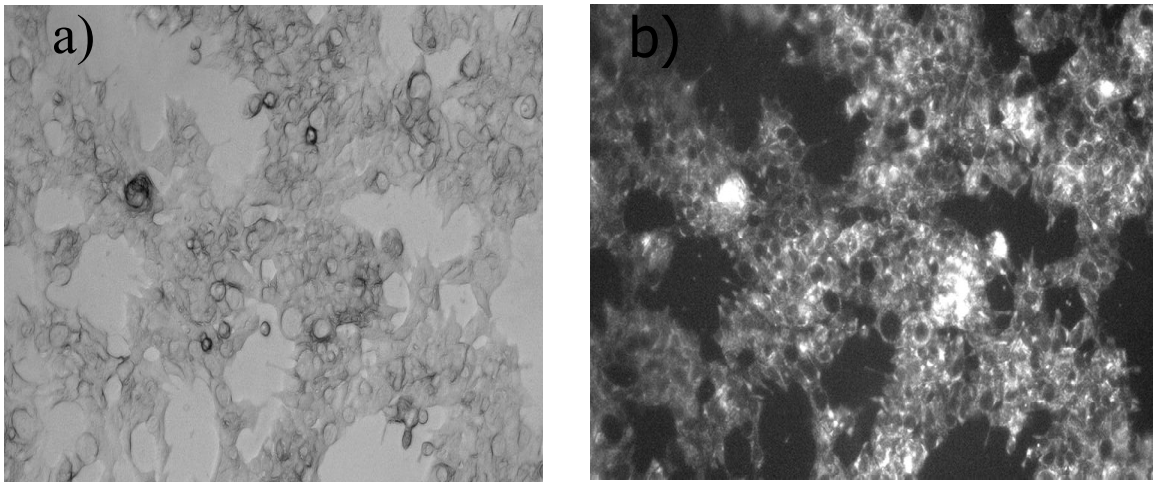

Figure 4.4 Phase contrast image (a) and fluorescence image (b) of MIN6 cells incubated with A2B5-FITC

The fluorescence microscopy imaging of the H9C2 cells incubated with A2B5-FITC bioconjugate, showed only negligible non-specific binding, as well as when MIN6 were

incubated with antibody anti GFAP labeled with FITC, because these cells do not express gangliosidic antigens (Figure 4.5c,d) or they do not express GFAP (Figure 4.5 e, f). The level of non-specific binding was reduced through incubation step of the cells with 1% bovine serum albumin (BSA) prior to incubation of the cells with the bioconjugate [25].

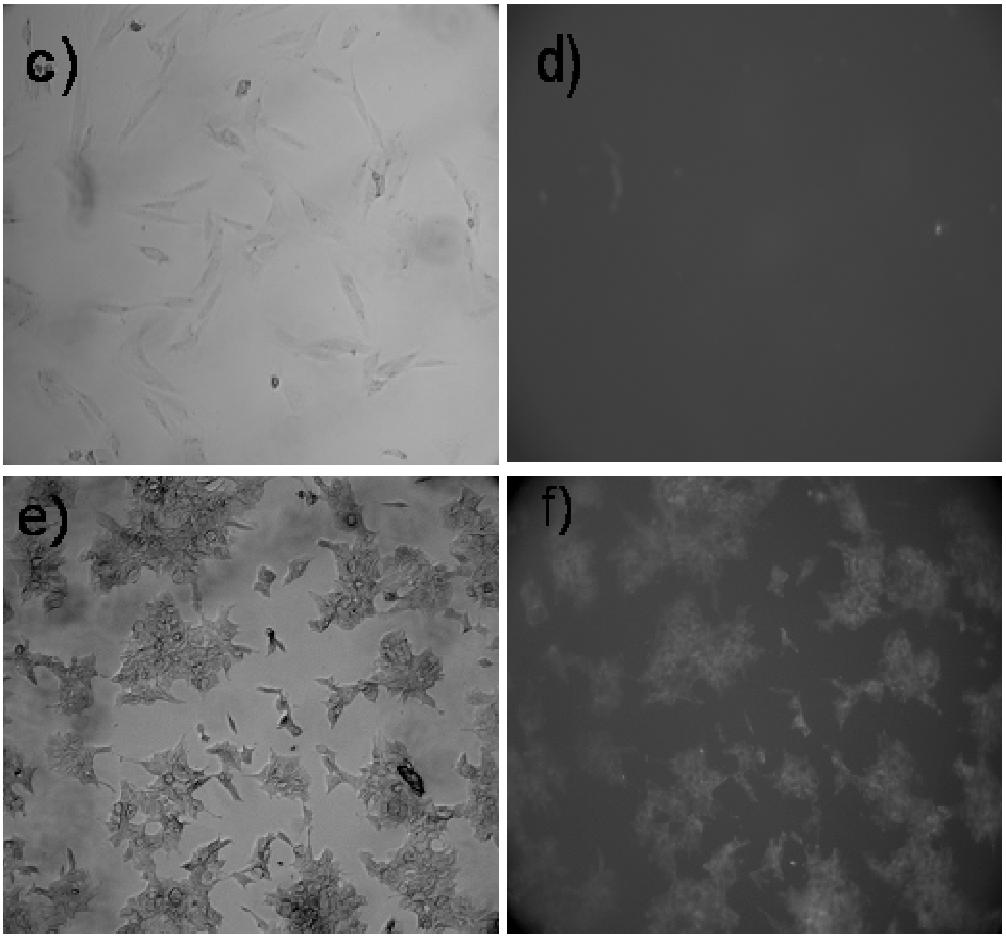

Figure 4.5 c) Phase contrast image and d) fluorescence image of H9C2 cells incubated with A2B5-FITC; phase contrast (e) and fluorescence image (f) of Min 6 cells incubated with anti-GFAP-FITC

4.3.4. Zinc Ion Release Measurements of A2B5-ZnAF-2 Bioconjugate Attached to Min-6 Cells

Zinc ion release from Min-6 b-cells was stimulated by exposing the cells to an elevated 20 mM glucose level. This chemical stimulation was previously shown to induce rapid release of insulin and zinc ions from β-cells. Figure 4.6 shows the average experiments where fluorescence spectra of Min-6 cells labeled with the A2B5-ZnAF-2 bioconjugate prior to and following stimulation with glucose are recorded.

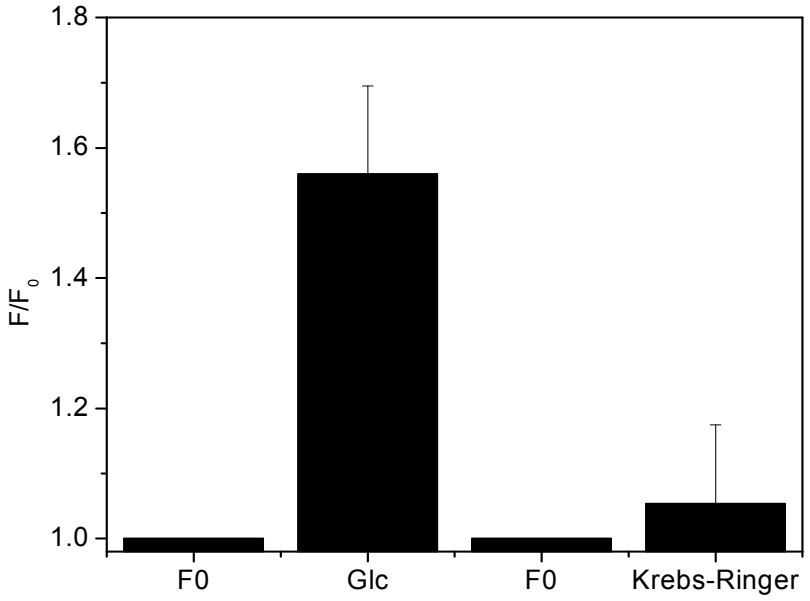

Figure 4.6 Representation of the average intensity of fluorescence transients of 1.56±0.13 in cell experiments and control experiment when cells labeled with antibody sensor were treated with Krebs-Ringer buffer

A clear and rapid increase in the fluorescence intensity by about 70% is observed. Control experiments in which the cells were treated with glucose free Krebs–Ringer buffer solution showed only a small fluorescence increase, which was attributed to adding other divalent ions like calcium to the solution. To visualize the zinc release from MIN6 cells, basal fluorescence images are recorded (image 4.7A) and exposure to 20mM glucose resulted in increase in fluorescence intensity successively (B,C,B) due to immediate release of insulin-zinc. There is heterogeneity in the zinc release response among MIN6 cell population, as there is a difference in their reactivity and loading with secretory vesicles.

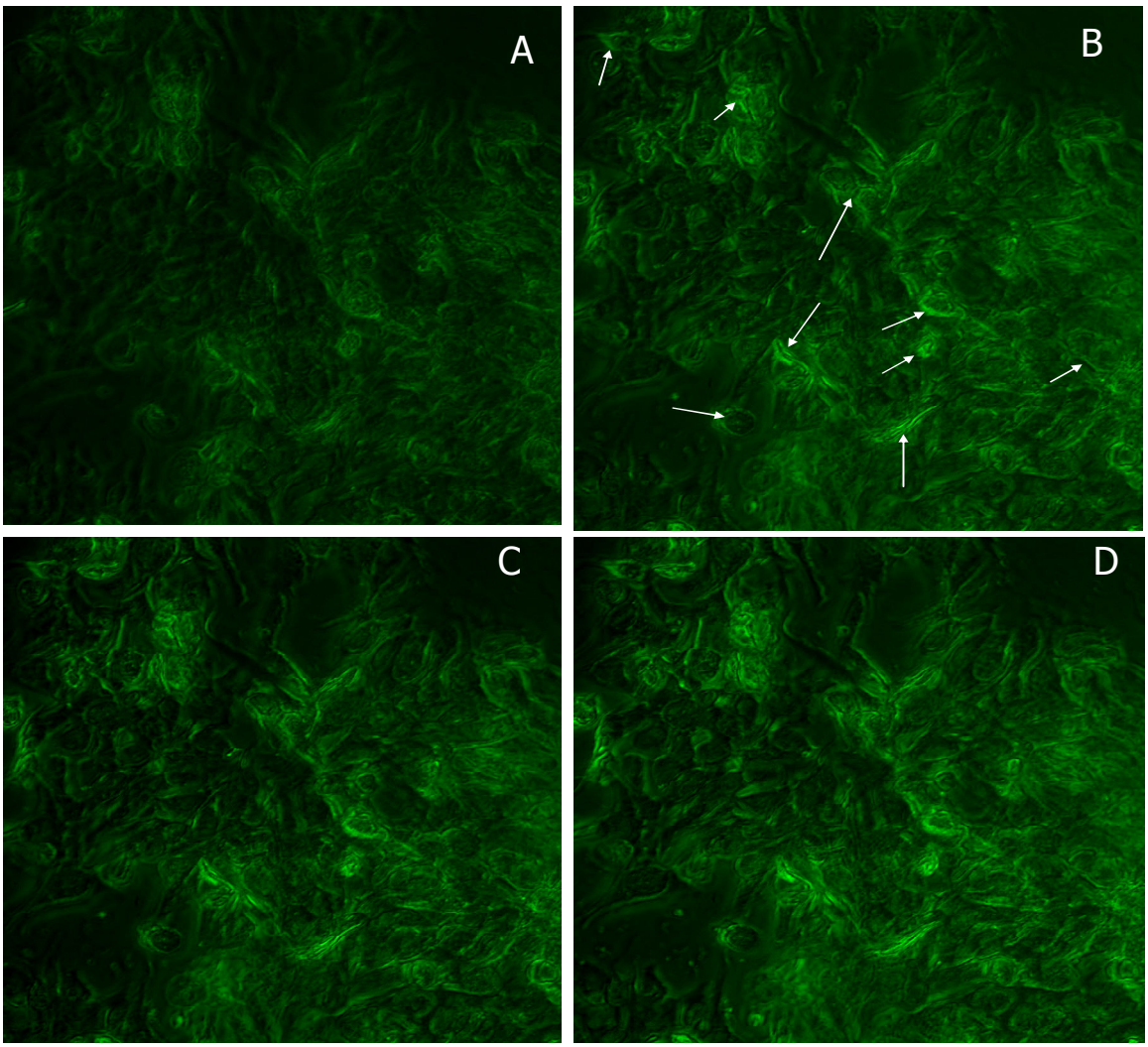

Figure 4.7 A is the basal fluorescence image of MIN6 cells at confluence labeled with A2B5-ZnAF2 bioconjugate; B,C,D successive fluorescence images after 20mM glucose .39% increase in the overall fluorescence intensity was observed. The arrows are pointing to the most active zinc-insulin release areas.

4.4. Summary and Conclusions

This chapter describes the development of a new bioconjugate, consisting of a monoclonal antibody, with the capability to selectively recognize β-cells, and a zinc ion sensing fluorophore, with the capability to measure zinc ion release from β-cells. The monoclonal antibody A2B5 was coupled to the zinc ion indicator ZnAF-2 to form the new bioconjugate. To facilitate its conjugation to the antibody molecules using an EDC coupling reaction, ZnAF-2 was modified with a piperidine carboxylic acid [12]. Our study shows that fluorescence properties, zinc ion sensitivity, and binding activity of the bioconjugate were not significantly altered due to the conjugation reaction. MIN6 cells were stained with labeled A2B5 antibody at a proportionally lower level compared to rat insulinoma cell lines which suggest a less expression of gangliosidic surface antigens. Also we observed that the antibody bioconjugate attached on the surface of cells at a variable level due to difference in the expression of surface antigens between cells and also the confluence stage. Howevever, the antibody A2B5 - ZnAF2 bioconjugate was effectively used to target and detect the zinc release from targeted areas of MIN6 insulinoma cells.

The newly synthesized sensor manifests biocompatibility with beta cells: coated cells retained the properties of insulin release upon glucose stimulation.

A limitation of this sensor consists in the fact that the fluorescence microscopy imaging experiments showed that the bioconjugate attached and responded to glucose stimulation to the surface of the cells at a variable level, suggesting difference in reactivity and loading of secretory granule between the cells. Antibody bioconjugate showed negligible binding to other non-pancreatic cell types. When attached to Min-6 cells, the bioconjugate responded to stimulation of the cells by elevation of glucose level in the cell medium, which induced rapid release of

insulin and zinc from the cells. The newly developed bioconjugate could be used in the future for real time monitoring of zinc release in response to chemical stimulation.

The A2B5-ZnAF2 sensor, as compared to glass cover slip zinc film sensor, is a step forward in the detection of zinc release in biological systems, because due to a higher dynamic range (0-1μM), the antibody sensor can be used to quantitate physiologically relevant zinc level in the micromolar range. On the other hand, this coating allows of detecting exocytotic events in immediate proximity with the region of interest.

Future work is to investigate cell-to-cell signaling mechanisms during insulin-zinc release from beta cells using microinjection delivery of secretagogues to the single cells.

References

1. Qian, W.J.; Gee, K.R.; Kennedy, R.T. *Anal Chem*. **2003,** *75(14)*: 3468-75.
2. Zalewski, P.D.; Millard, S.H.; Forbes, I.J.; Kapaniris, O.; Slavotinek, A.; Betts, W.H.; Ward, A.D.; Lincoln, S.F.; Mahadevan, I. *J Histochem Cytochem* **1994**, *42(7)*: 877-84
3. Jindal, R.M.; Gray, D.W.R.; Shane, P.M.; Morris, P.J. *Biotech. Histochem.* **1993,** *68 (4),* 196-205.
4. Bouckenooghe, T.; Vandewalle, B.; Lukowiak, B.; Kerr-Conte, J.; Belaïch, S.; Gmyr, V.; Dubois, M.; Riachy, R.; Pattou, F. *Cell Transplantation* **2003**, *12(7),* 799-807(9)
5. Chausmer, A.B. *Journal of the American College of Nutrition*, **1998,** *17(2)*, 109-115
6. Ohara-Imaizumi, M.; Nakamichi,Y.; Tanaka,T.; Ishida, H.; Nagamatsu, S. *The Journal of Biological Chemistry*, **2002**, *277(6)*, 3805-3808
7.Kim, B.J.; Kim, Y.H.; Kim, J.W.; Koh, J.Y.; Oh, S.H.; Lee, M. K.; Kim, K.W.; Lee, M.S. *Diabetes* 2000, *49(3)*: 367-72.
8. Qian, W.J.; Aspinwall, C.A.; Battiste, M.A.; Kennedy, R.T. *Anal.Chem*. **2000**, *72*,711-717
9. Gee, K.R.; Zhou, Z.L.; Qian, W.J.; Kennedy, R.T. *J.Am.Chem.Soc* **2002**, *124(5),* 776-778
10. Qian, W.J.; Gee, K.R.; Kennedy, R.T. *Anal Chem*. **2003,** *75,* 3468-75
11. Hirano,T.; Kikuchi,K.; Urano,Y.; Higuchi,T. and Nagano,T., *J. Am.Chem.Soc*. **2000**, *122,* 12399-124002.
12.Crivat, G.; Kikuchi, K.; Nagano, T.; Priel, T.; Hershfinkel, M.; Sekler, I.; Rosenzweig, N.; Rosenzweig, Z. *Anal. Chem.;* **2006**; 78*(16);* 5799-5804
13. Greg T. Hermanson, *Bioconjugate techniques*, **1996**
14. Roitt I., Essential Immunology, **1977**
15. Goding J.W., Monoclonal antibodies: Principles and Practice, **1986a**
16. Nataliya Panchuk–Voloshina, Rosaria P. Haugland, Janell Bishop–Stewart, Mahesh K. Bhalgat, Paul J. Millard, Fei Mao, Wai-Yee Leung, and Richard P. Haugland, *Journal of Histochemistry and Cytochemistry*, **1999**, *47*, 1179-1188
17. Aaen K, Rygaard J, Josefsen K, Petersen H, Brogren CH, Horn T, Buschard K, *Diabetes*. **1990**, *39(6):* 697-701
18. Gillard BK, Thomas JW, Nell LJ, Marcus DM, *J Immunol*.**1989**, *142(11):* 3826-32
19. Kawakami Y, Inoue K, Hayashi H, Wang WJ, Setoyama H, Gu YJ, Imamura M, Iwata H, Ikada Y, Nozawa M, Miyazaki J., Cell *Transplant*. **1997**, *6(5)*: 541-5
20. Hayashi, H., Inoue, K., Aung, T., Tun, T., Yuanjun, G., Wenjing, W., Shinohara, S., Kaji, H., Doi, R., Setoyama, H., Kato, M., Imamura, M., Maetani, S., Morikawa, N., Iwata, H., Ikada, Y., and Miyazaki, J., *Cell Transplant*. **1996**, 5(5 Suppl 1):S65-9
21. Eisenbarth, G. S.; Shimizu, K.; Bowring, M.A.; Wells,S. *Proc. Natl Acad. Sci. USA* **1982**, *79*, 5066-5070
22. Asfari, M.; Janjic, D.; Meda, P.; Li, G.; Halban, P.A.; Wollheim, C.B. *Endocrinology* **1992,** *130*, 167-178
23. Cavallo, M.G.; Dotta, F.;Monetini, L.; Dionisi, S.;Previti, M.;Valente, L.; Toto, A.;U Di Mario, U Di Mario and Pozzilli, P. *Journal of Endocrinology* **1996**, *150(1)*, 113-120
24. Joseph R. Lakowicz, Principles of fluorescence microscopy
25. Rosenzweig, Z.; Rosenzweig, N.; Crivat, G. "Advances in zinc sensors for studying zinc release events from pancreatic cells." *Proceedings of SPIE*; **2006,** 6380

CHAPTER 5

FRET-BASED SURFACE NANO-SENSOR IN MICROFLUIDIC SYSTEMS FOR DETECTING PANCREATIC ENZYMATIC ACTIVITY

Georgeta Crivat[1], Darwin R. Reyes[2], Laurie Locascio[2], Michael Gaitan[2], Nitsa Rosenzweig[1] and Zeev Rosenzweig[1]

1) AMRI, Chemistry Department, University of New Orleans, New Orleans, LA 70148

2) NIST, MD 20899-8120

5.1 Introduction

This chapter describes, for the first time, the preparation of a FRET-based quantum dot sensor, using layer-by-layer deposition techniques, in microfluidic systems, for monitoring enzymatic activity. FRET between Cd-Se quantum dots and rhodamine-labeled polyelectrolyte was investigated. The results suggest that an energy transfer between quantum dots and rhodamine occurs when the fluorescence intensity of quantum dots decreases while the fluorescence intensity of rhodamine increases.

5.1.1 Polyelectrolite Multilayers and Electrostatic Self-Assembly (ESA)

Polyelectrolytes are polymers with large molecular weight, bearing repeating ionic groups. A common application of polyelectrolytes is in the development of thin films using layer-by-layer deposition technique. The layer by layer technique, consisting of the alternating deposition of cationic and anionic polyelectrolytes, has been widely used due to the facile preparation and effectiveness in forming polyelectrolyte multilayer films (PEMs) [1-3].

PEMs found various applications in light emitting devices [4, 5], bioactive material coatings [6, 7], electrically conductive polymers [8], and hollow polyelectrolyte capsules with biomedical and pharmaceutical applications [9-11].

Layer –by –layer deposition is based on the principle of electrostatic interaction between oppositely charged organic polymers. As compared to the Langmuir-Blodgett technique, the adsorption of electrolytes is independent of substrate size and topology [1, 12]. Typically, a substrate with a positive charge is initially immersed in a negative polyelectrolyte resulting in the adsorption of the anionic layer [1, 13]. The high concentration of the polyelectrolyte solution results in a reversal of surface charge. The substrate is then washed with water to remove impurities and non-absorbed polymers (figure 5.1).Immersion in a positive polyelectrolyte results in an adsorption of polycation layer and initial surface charge is restored [1, 14].

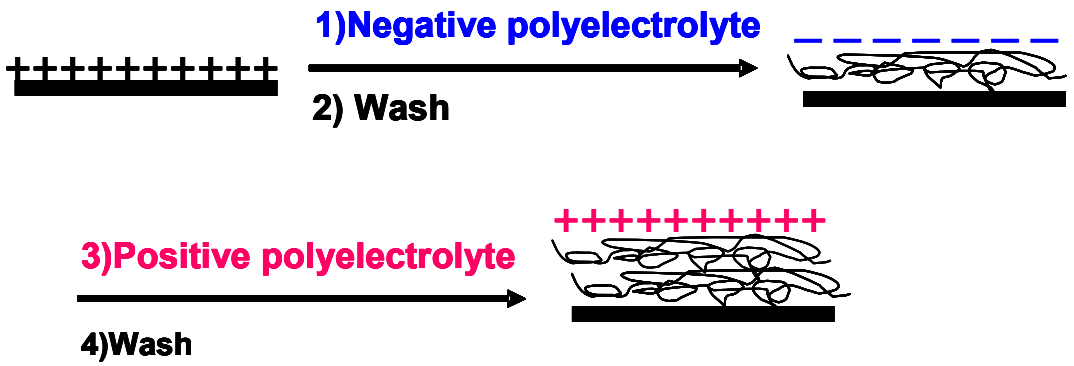

Figure 5.1 Schematic representation of layer-by-layer assembly (LbL)

It is possible to tune the thickness of PEMs film in Angstroms range by a proper choice of deposition parameters [13]. It was shown previously that the thickness of the films increases proportionally with the number of deposited polyelectrolyte layers [1, 14].

The ionic strength of the polyelectrolyte solutions was shown to influence the thickness and smoothness of polymer surfaces. At high salt concentration it was described increased thickness and roughness of PEMs film [1, 4].

Ionic strength and solvent selection (alcohols, mixture of alcohol and water) influences the structure and permeability of PEMs films [15, 16]. The strength of electrostatic forces between polymers increases with decrease in the dielectric force of the medium. Increases in the alcohol

volume causes increases in the attractive forces, resulting in the contraction of polymer chains and “hole” creation [15].

Ionic strength and pH influences the permeability of PEMs. The permeability of PEMs depends on the ionic strength of the solutions from which the films are formed. Generally, the higher the salt concentration the higher the permeability [6]. Influence of pH refers to changes of charge densities on the polyelectrolyte pairs. Thus, the lower pH values induce positive charges in the film which changes the morphology and adds defects to the polymer lattice. For instance PAH (Poly (allylamine hydrochloride)/PSS (Polystyrenesulfonate) capsule at a pH 3 shows stretching of the PAH molecule due to increase in steric energy with shifting pH. These steric energies are a function of energies of bond stretching, angle bending, van der Waals and electrostatic interactions [13].

The porosity of polyelectrolyte multilayers originates from a decrease in contacts between polyelectrolytes with different charge, which results in loosening the lattice structure. Studies of permeability of polyelectrolyte multilayer PAH/ PSS capsules, reveal a nonlinear relationship between the permeability coefficient and salt concentration. It was described before that diffusion of charged particles through PEMs takes place by ”hopping from site to site ” [16, 17]. Increasing the salt concentration increases the number of free sites in polymers. Mobility of ions through PEMs does not depend on the amount of incorporated water, which is a consequence of the swelling of PEMs. However, PAH/PSS do not increase in thickness with ionic strength [16, 18, 19]. Increases in the ionic strength is expected to influence the range and amplitude of electrostatic forces in the polymer layers [16, 20].Generally increases in ionic strength ends in destruction of interpolyelectrolyte complex [16].

Exposure of polyelectrolytes to salt ions results in incorporating them within the lattice expressed at equilibrium between oppositely charged polyelectrolyte and compensated charged polymers by salt ions (relation 1.1).

$$PAH^{+}PSS^{-} + Na^{+}(aq) + Cl^{-}(aq) \rightleftharpoons PAH^{+}Cl^{-} + PSS^{-}Na^{+} \qquad (1.1)$$

5.1.1.1. Choice of Polyelectrolyte Polymers

PAH (Poly (allylamine hydrochloride) and PSS (Polystyrenesulfonate) (Figure 5.2) are one of the most widely used pair of polyelectrolyte in the last decade [14, 16, 18, 19, 21]. When films are made of PAH/PSS, they show a uniform and smooth surface morphology and a linear growth [21]. These polymers show a relatively stable behavior at changes of pH and ionic strength. Previous studies on planar films of polyelectrolyte, using neutron reflectivity, describe no significant swelling in presence of NaCl solutions of concentrations up to 2M [18, 22].

Studies of the effect of salt concentration (between 0-2 M) on swelling of polyelectrolyte multilayers revealed different behavior depending on the type of polymers used. Differences in swelling are due to differences in the degree of association of polymers. The more hydrophobic the polymer is the stronger their association in aqueous conditions and less exposed to swelling.

Poly-(acrylic acid) (PAA) / (PDADMA) films experience hyper swelling at low salt concentration, PSS/poly (diallyldimethylammonium) (PDADMA) pair exhibit a decrease in thickness at low salt concentrations due to possible loss of water molecules in the presence of

high osmotic pressure. PSS/poly (allylamine hydrochloride) (PAH) pair shows the most stable behavior with increasing the salt concentration [19].

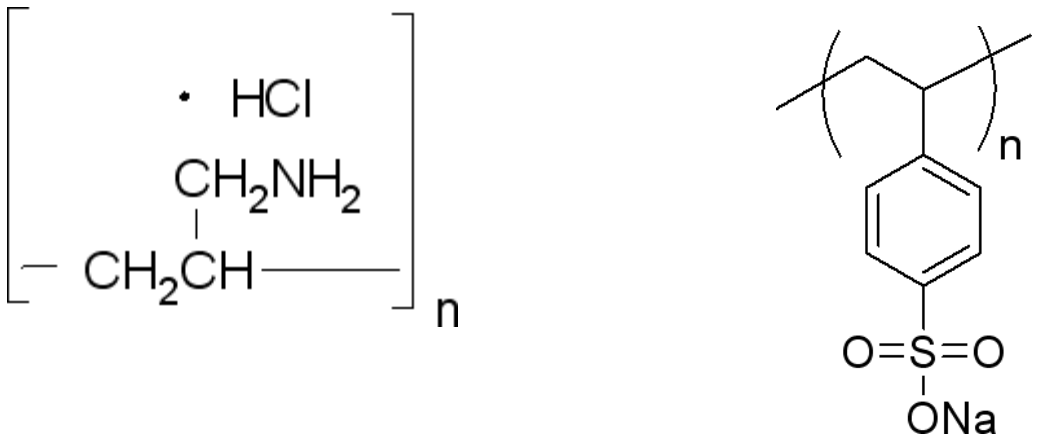

a) b)

Figure 5.2 a) PAH (Poly (allylamine hydrochloride); b) PSS (Polystyrenesulfonate)

Studies of adhesion and viability of varied tissues, grown on these coatings, revealed a high biocompatibility of these materials, which make them suitable for biological applications. Rat retinal cells, seeded on the surface of micropatterned polyelectrolyte multilayer (PEM) lines, showed adhesion 5 hours after seeding, comparable to growing the cells on standard polystyrene

tissue-culture materials .The PEM lines were adsorbed on the surface of a flat oxidized PDMS using a microfluidic channel network.

The microfluidic mask was stripped out after the PEM patterning and the cells were incubated on the PEM/PDMS surface without using blocking agents to prevent adhesion of cells on unpatterned area [14]. It is common to use blocking agents to prevent adhesion of cells in certain areas of the surfaces [14, 24].

Adhesion of bone cells was also observed on PAH (Poly (allylamine hydrochloride); PSS (Polystyrenesulfonate) and poly (L-lysine) [14, 23].

5.1.2. Microfluidics and Micropatterning Techniques

Microfluidics is a relatively new technology from 1990.It allows of a precise control of small volumes of liquids. Applications of microfluidic technology address a wide range of multidisciplinary fields: DNA chips, lab-on–technology, molecular biology, tissue engineering [25- 28]

The field of microfabrication and microfluidics for tissue engineering is a closer field for our application because it provides with necessary conditions to allow growing and investigating the cell behavior in microfluidics. Micro and nanofabrication techniques are currently used to extend the versatility of tissue engineering field. One of the important aims in tissue engineering is to produce tissues and organs containing viable cells for organ replacement [28].

Cell patterning techniques are used to create different patterns of cells on various scaffolds. Among these techniques is photolithography, where cell adhesion materials (polylysine, collagen, matrigel) are being used to pattern the cells [28, 29].

Microfluidic patterning takes advantage of the ability of microchannels to deliver a precise volume of fluids to different areas of a substrate. Minimal diffusion is described across the interface between multiple laminar flows when they are flowing together. This procedure finds application in studies of single cell behavior, when different chemicals are applied to different areas of a cell [28, 30].

Other applications of cell patterning refer to micro fabricating analogs of basal lamina as scaffolds on which cells can be cultured: vascular tissues using a fluid dynamic model for the dynamics of blood flows in the target organ; liver; cartilage; neurons [28].

Microfluidics is a versatile technology for biological applications because it creates the conditions necessary to mimic the *in vivo* environment *in vitro*. Developing a sensor in microfluidics requires taking into consideration mechanical and transport aspects, effective culture volume, effect of material properties on cell culture.

Mechanical aspects refer to the shear stress effects present along the channels, which is represented as a function of fluid viscosity and velocity and position within the channel.

Laminar flows in microchannels could ensure partial treatment of only certain areas of a cell. The mass transport is mainly along longitudinal axis with minimal diffusion across the interfaces. Effective culture volume reflects the capacity of cells to control their

microenvironment .Properties of materials reflect in the biocompatibility and adhesion of the biological specimens [31].

To achieve patterns of lines of polyelectrolyte multilayers with a high resolution, microfluidics channels are employed. Deposition of PEMs is realized either by using layer-by-layer (LbL) deposition cycles [14] or a spin self assembly (SA) .Convective SA is a technique of self-assembling of layers using electrostatic and hydrogen bond interaction between polymers. In principle, the channels are formed by contacting a PDMS mold with hydrophilic substrate. The polymer solution is flowed through the channel and allowed to adsorb. The residual solution is removed by spinning. [32].

5.1.3. Quantum Dots

Quantum dots are a special class of semiconductor nanocrystal materials. Their small size ranging from 2-10 nm makes them tunable for desired color and emission wavelength. As compared to a typical semiconductor, where the energy levels are described as continuous, quantum dots express discrete energy levels with a finite separation between them. Electrons normally occupy the valence band below the band gap. Exposure to a photon flux with enough energy to cross the band gap will propel the electrons to conduction band. In quantum dots, the exciton Bohr radius, which is separation distance between the electron and its hole, approaches the size of semiconductor when the size of quantum dots is small enough. In other words, this situation defines the quantum confinement where the spatial electronic wavefunction is confined to the dot size. The size of the band gap increases with the decrease of the quantum dot size. The outcome of this structure consists in the discrete absorption spectrum of quantum dots, as compared with the continuous absorption spectrum of a classical semiconductor [33].

Typically, synthesis of monodisperse CdSe /ZnS quantum dots employs an organometallic method. The nucleation and crystal growth takes place at high temperature, when CdO and chalcogen elements (selenium) are added to the coordinating TOP (triocthylphosphine) and TOPO (triocthylphosphine oxide) solvents [33]. The TOPO coating prevents the dots from aggregation and continuous growth.

CdSe quantum dots are passivated with a ZnS layer to increase their luminescent quantum yield from 35 to 50 % [34].

5.1.3.1. Biological Application of Quantum Dots

Quantum dots are excellent probes, which linked with recognition elements (antibodies, peptides, nucleic acids, i.e.), find application in various areas of molecular and cellular biology and medical diagnostics research.

To apply the luminescent quantum dots in biological fields, the hydrophobic TOPO coating is replaced through a ligand exchange reaction with various thiol-bearing compunds like mercaptoacetic acid [34, 35], dithiothreitol [36], dihydrolopoic acid [37] or cysteine –containing peptides [35].

As compared to organic fluorophores their quantum confinement results in tunable size and fluorescence emission from visible to infrared wavelengths. Their absorption is more probable at shorter wavelengths and higher energies, which results in a broad excitation band as compared to typical organic fluorophores [38, 39].This property is exploited in designing FRET based biosensors with quantum dots as donors.

The long lifetime of quantum dots (>10s) during recombination of the exciton results in a narrow emission band [39, 40]. Their long lifetime ensures elimination of interferences from short lived auto fluorescent molecules from cells [39].

The ZnS coating of CdSe quantum dots, with a larger band gap than the crystal core, is a strategy to not only increase quantum yield by protecting surface atoms from oxidation and blinking, but also their photostability, as compared to organic fluorophores [39, 45]. This has relevance in long term dynamic biological studies.

Quantum dots are largely used in biotechnology and for tracking and imaging purposes in cell and animal biology (e.g., immunofluorescence assays [42], immunofluorescence labeling of membrane proteins [43], actin) [39, 44].

Quantum dots were also exploited for in *vivo* targeting and imaging of cancer cells in living animals [38], endocytosis by mammalian cells [34]. In eukaryotic cells, quantum dots were finally localized in endosomes [46] or lysosomes [39].

5.1.3.2. FRET Based Quantum Dot Sensor

The purpose of this project is to develop a surface sensor for monitoring the proteolytic activity of pancreatic cells grown in microfluidic channels, using a sensor which is non-invasive, non-toxic and non-destructive.

Incorporating of quantum dots in the sensor design has many advantages: quantum dots are nanometre-sized probes; their higher photo and chemical stability relative to organic dyes make them suitable for biological applications, they are more efficient FRET donors due to their wide excitation enabling selection of an excitation wavelength such to avoid direct excitation of the acceptor, their narrow emission could enable multiplexing.

Lately, several research groups used luminescent quantum dots as donor probes in FRET experiments. For instance, FRET between tetra-peptide RGDC coated quantum dots and rhodamine acceptors which were immobilized on the surface of quantum dots was employed to detect trypsin activity [35]. Single molecule FRET using quantum dots as the donor was used to measure FRET between a single quantum dot and a single organic fluorophore, Cy5. It was possible to perform single molecule studies when the blinking of quantum dots was suppressed by adding thiol containing molecules to the solution. [47].

The utility of Cd-containing quantum dots in the analysis of cells and tissues is limited due to their potential toxicity. However, embedding the quantum dots in polyelectrolyte multilayer films alleviates the toxicity issue and could increase the applicability of quantum dots in bioassays.

Studies on the properties of luminescent thioglycolic acid stabilized quantum dots embedded in polyelectrolytes show an increase in fluorescence intensity of about 31 times and increase in their stability in presence of positive polyelectrolyte PDDA (poly(diallydimethyl-ammonium chloride)) while negative polyelectrolyte PSS didn't affect the emission of quantum dots [48].

5.1.4. FRET in PEMs

FRET in PEMs is commonly employed to investigate the distribution of chromophores within the matrix and evaluate their average separation. First, studies of the distance dependence of energy transfer were performed on Langmuir-Blodgett films doped with fluorescent dyes [49, 50]. Later, inter-layer energy transfer was investigated between 6-carboxyfluorescein and rhodamine B labelled particles where increasing the number of spacer layers between donor and acceptor resulted in less efficient energy transfer [3]; distance dependent fluorescence quenching on gold nanoparticles assembled with PE [51]. The dependence of energy transfer on the properties of the polyelectrolyte [52] or spacer thicknesses was investigated in dye-loaded nano-containers and in self-assembled films of PPV and labelled PAH, respectively.

An advantage of incorporating our FRET based sensor in patterned PEMs lines, using layer by layer deposition in microfluidics, is the flexibility of microfluidics to be customized to provide the necessary conditions to recreate the *in vivo*-like cellular microenvironments *in vitro* [53]. The direct application is in studying biological phenomena [54]. Moreover, incorporating the FRET sensor in PEMs facilitates the culturing of various tissues due to the PEMs biocompatibility and adhesion properties [14, 55].

5.2. Specific Experimental and Technical Details

5.2.1. Materials and Reagents

Poly (sodium 4-styrenesulfonate) was provided by Scientific Polymer Products. Sodium chloride was provided by J. T. Baker. Poly (allylamine hydrochloride) (MW ~70 000), cadmiu oxide, lauric acid, trioctylphosphine oxide, hexadecylamine, lauric acid chloroform, diethylzinc, trioctylphosphine, methanol, selenium powder, were purchased from Sigma Aldrich. Thioglycolic acid; N-(3-Dimethylaminopropyl)-N'-ethylcarbodiimide; N-Hydroxysulfosuccinimide sodium salt; were purchased from Fluka. Phosphate buffered saline was purchased from Gibco. Neurotensin was purchased from American Peptide Company. PDMS, silicone elastomer kit was purchased from Dow Corning Corporation. Dialysis cassettes with 2,000 and 3500 MWCO were purchased from Pierce. Rhodamine Red ^{TM} –X, succinimidyl ester was purchased from Invitrogen. We used UV ultra pure water system from Barnstead. PDMS films were oxidized using a plasma etcher machine (Anatech LTD-Plasma Series). Photolithographic masks were provided by SEM at NIST. Atomic force microscopic measurements were performed using Dimension 5000, Digital Instruments.

5.2.2. Digital Fluorescence Microscopy

An inverted fluorescence microscope (Olympus IX-70) was used to record the emission spectra in FRET measurements. 100-W mercury lamp is used as the light source for excitation. A 20X microscope objective were used to collect the fluorescence. The fluorescence microscope filter cube consisted of a 448±20nm bandpass excitation filter, a 460 nm dichroic mirror and a 475 nm

emission filter. The Roper Scientific software WinSpec 32 was used for spectral data acquisition. The exposure time was 0.1 seconds.

5.2.3. Fabrication Scheme of Microfluidic System

The principle of fabrication of PEMs in a microfluidic system, illustrated in figure 5.3, consists in the alternate deposition of polycations (PAH) (purple line) and polyanions (PSS) (green line) on a charged surface (oxidized PDMS) (figure 5.3C). PDMS, deposited on treated silica glass slides, promotes polyelectrolyte deposition through surface oxidation. Negatively charged PDMS is covered with molded PDMS (figure 5.3 A). The positive polyelectrolyte is flowed through the 5-microchanel network which patterns the PDMS surface (5.3 B). Mercaptoacetic coated quantum dots (yellow line) are deposited onto the positive electrolyte on the top of 2 bilayers.

Deposition of thioglycolic acid stabilized quantum dots onto positive polyelectrolyte is a strategy to avoid the diffusion of quantum dots due to their negative surface charge [56].1μM rhodamine Red-X is conjugated to 1mg/mL PAH solution and alternately deposited at 1, 3, 5, 7 or 9 layers separation from the quantum dots.

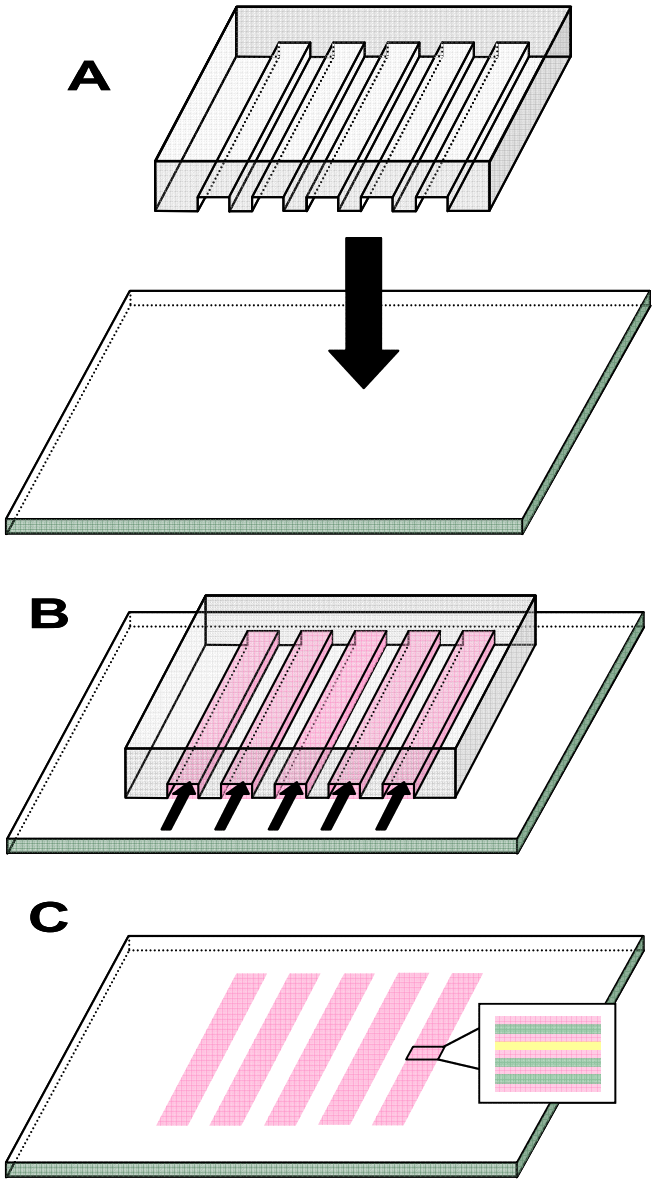

Figure 5.3 Schematic representation of fabrication scheme of PEMs using layer-by-layer deposition in microfluidic system

5.2.4. Fabrication of FRET Sensor in PEMs Using Layer-by-Layer Deposition in Microfluidic System

5.2.4.1. Preparation of Water Soluble Quantum Dots

The CdSe/ZnS quantum dots were prepared according to a modified procedure developed by Peng [57]. It consists in dissolving 12.7 mg CdO in 160 mg lauric acid under nitrogen at>200 ° C in a three necke flask. After cadmium oxide is fully dissolved, 1.94 g TOPO and 1.94 g HDA are added to the mixture and heated to 250-300^{o}C. The mantle is removed and 80 mg of selenium powder in 2mL of TOP is injected into the reaction. After the reaction temperature is decreased to ~200 °C the ZnS coating is formed by injecting into the reaction flask 2 ml TOP solution containing 250 µl hexamethyldisilathiane ((TMS)2S) and 1 ml diethylzinc (Zn(Et)2) into the reaction flask. The reaction mixture was kept at 180°C for one hour. CdSe/ZnS quantum dots were further washed three times with methanol and chloroform.

CdSe/ZnS quantum dots were solubilized through a ligand exchange reaction of TOPO with mercaptoacetic acid [34] (figure 5.4). 2 mL of TOPO coated quantum dots were suspended in 3mL of chloroform and reacted with 2mL of thioglycolic acid overnight with continuous stirring. The water soluble quantum dots were extracted in 7mL of water. To purify, the soluble quantum dots were washed several times with water and chloroform and centrifuged.

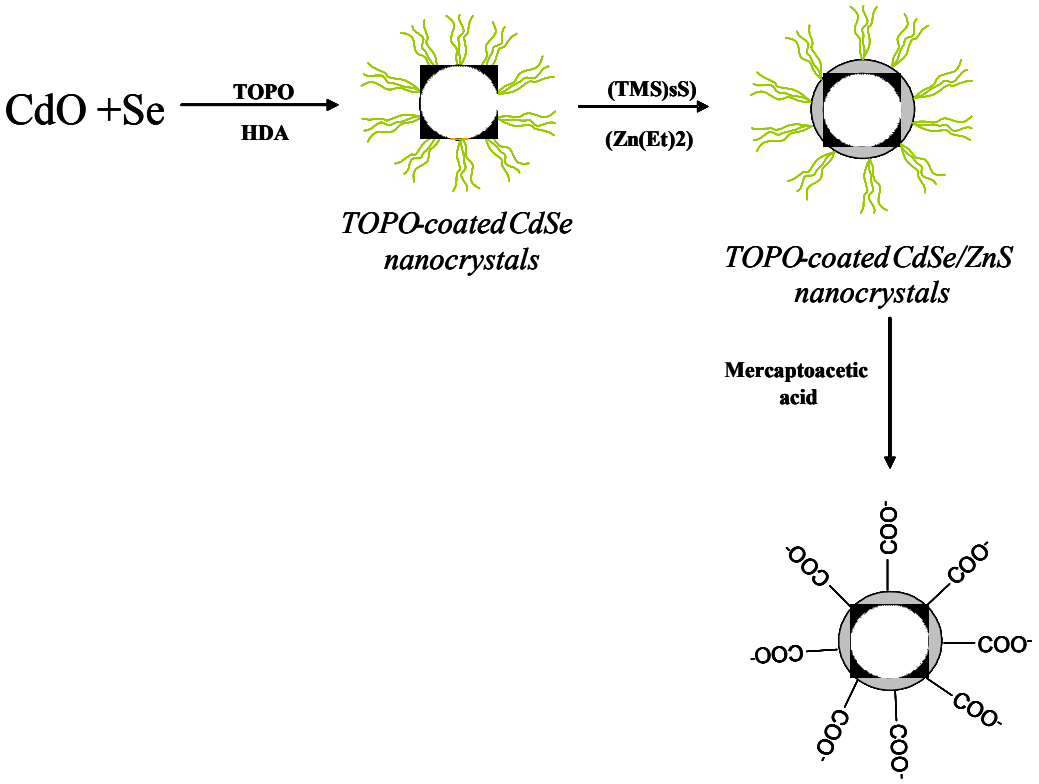

Figure 5.4 Preparation scheme of mercaptoacetic acid coated quantum dots

5.2.4.2. Incorporating of the FRET Sensor in Polyelectrolyte Multilayers

For preparation of conjugated PAH-Rh, 1μM rhodamine Red ^{TM} –X succinimidyl ester was reacted with 2mL 1mg/ml PAH at pH 7.4 for 2 hours with a continuous stirring. The unreacted rhodamine was separated using dialysis cassettes with a molecular weight cutoff point of 3500 Da. 15 μL of 66 μM solution of labelled neurotensin with rhodamine was reacted with 1mg/mL PAH in presence of 20 μM EDC.

The polyelectrolyte solutions of PAH and PSS were prepared at 1mg/ml conc., with 0.1; 0.2; 0.5 mM conc. of salt. The pH was adjusted to 5 for PAH solution and to 6 for PSS. PDMS with microfluidic structures were fabricated according to a procedure described before [14] by pouring the polymer on the glass master and curing at 100^{o}C for 1 h. PDMS without microfluidic channels was fabricated by pouring the polymer on sulfuric acid precleaned glass slides. The unmolded PDMS was oxidized in an O_2 plasma etcher machine for 2min.The oxidized surface was covered with the PDMS patterned with microfluidic channels and filled with positive polyelectrolyte using a vacuum pump and deposited for 30 min.4 alternating layers of polyelectrolyte were flowed through the channels and allow to deposit 5min. Quantum dots were incorporated onto a PAH layer on the top of 2 bilayers. Rhodamine-PAH or Rhodamine embedded in PAH was alternately deposited at 1, 3, 5, 7 or 9 layers of separation from the quantum dot layer. Rhodamine-neurotensin-PAH was deposited at a three layer separation from donor layer (figure 5.5).

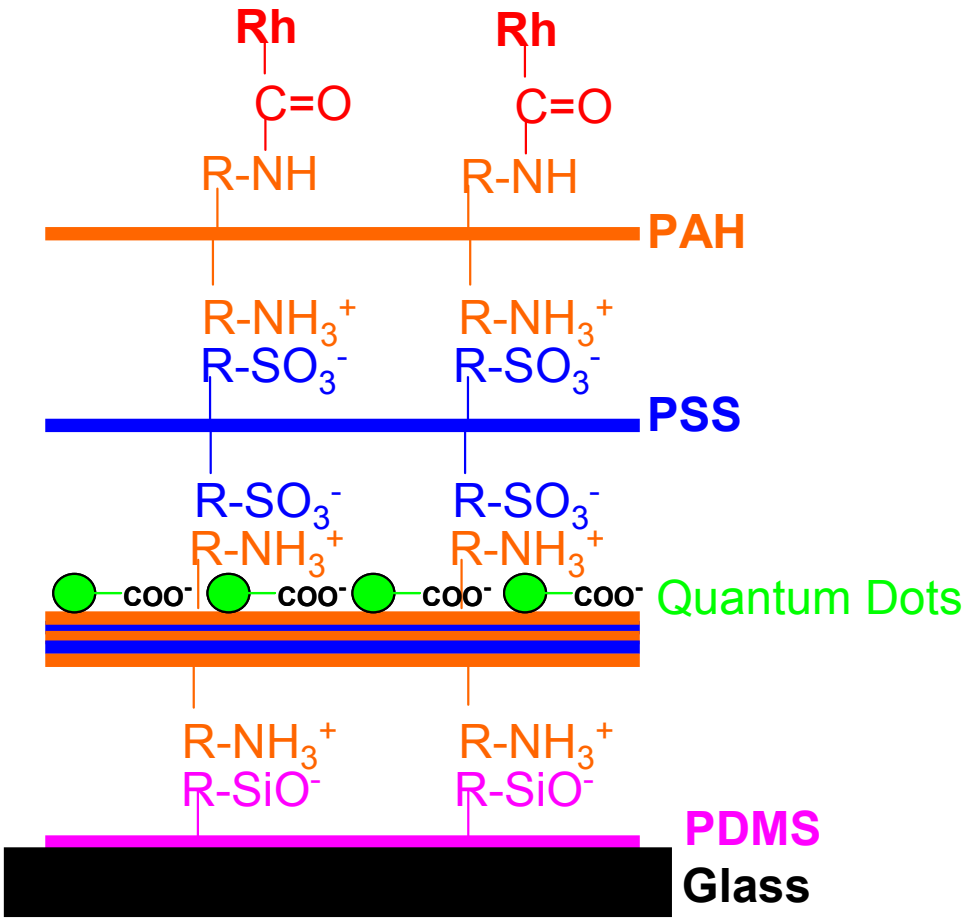

Figure 5.5 Representation of incorporating FRET sensor in polyelectrolyte multilayers

5.2.4.3. Synthesis of FRET Sensor for Enzymatic Activity

Biological application of a FRET system, as a sensor for enzymatic activity, required the labeling of 1mg/mL neurotensin Arg and Lys amine residues with rhodamine Red-X.

To optimize the concentration of rhodamine, 1mg/mL neurotensin was labelled with successive concentrations of rhodamine ranging from 600nM-6.6μM. The labelled neurotensin was then conjugated with 1mg/mL PAH polyelectrolyte and separated from reaction by-products using dialysis cassettes with a cut-off point of 2000 Da. The labelled PAH is then flowed on top of three polyelectrolyte layers separating the quantum dots. FRET measurements revealed that 1.98 μM rhodamine was the optimum concentration of acceptor to result in maximum changes in the Fd/Fa ratio.

15 μL of 66 μM stock solution of labelled neurotensin with rhodamine was reacted with 1mg/mL PAH in presence of 20 μM EDC and 50 μM sulfoNHS for 4 hours at room temperature. The labeled PAH was separated from reaction by-products using dialysis cassettes with a cutoff point of 2000 Da.

The conjugation of labeled peptide to 1mg/mL PAH is followed by deposition to a PSS layer. Neurotensin is a tridecapeptide with brain and gastrointestinal localization. It is secreted in the small intestine where modulates intestinal postprandial motility [58], upper gastrointestinal motor activity [59] etc. The roles of neurotensin in human psychopathology and psychopharmacology are still to be explored as well as its gastric physiology. The bioactivity of

soft-landed trypsin was previously tested using neurotensin as substrate when the digestion fragments were detected by ESI-MS [60].

5.2.5 Cell Culture and Maintenance

The biological application of FRET based quantum dots sensor in microfluidics was investigated using CAPAN-2 tumor-pancreatic cancer cell lines as a biological model for trypsin activity.CAPAN-2 cells secrete a tumor –associated trypsinogen (TAT) and a trypsinogen activity-stimulating factor (TASF) .Expression and activity of TAT enzyme was associated with the degree of invasiveness and metastasis of CAPAN -2 cells. These enzymes could degrade the extracellular matrix and also activate other proteases with relevance in metastasis [61].

CAPAN-2 cells were grown to a confluence in DMEM (Dullbeco's modified Eagle's medium) medium with 10% fetal bovine albumin, 1% antibiotic-antimycotic, 4% L-glutamine and sodium pyruvate. Cells were cultured at 37^{o}C under 5% CO_2.

When the cells reached confluence, they were trypsinized and washed with DMEM. The supernatant was recovered in DMEM and flowed through microfluidic channels. They are allowed to attach. The channels are then flowed with DMEM medium without fetal bovine serum.

Previously, comparative studies on trypsinogen activating effect from supernatants collected from cells cultured 48 hours in DMEM revealed a spontaneous trypsin activity to a lesser extent than when supernatants were incubated with 1μg/ml enterokinase for 60 min to activate the trypsinogen [61].

Control experiments were designed to confirm the trypsin activity. Trypsinogen (0.25mg/ml) was incubated for 60 min at 37 ^{0} C with enterokinase and flowed through microchannel network on top of the enzymatic sensor. Images were collected before and after flowing the solution, separately for quantum dots and rhodamine, using two different filter cubes. A pure inactive trypsinogen solution was flowed through the microchannels as the negative control.

5.3 Results and Discussion

5.3.1. Fluorescence imaging and spectroscopy

Fluorescence images of quantum dots and Rhodamine-PAH micro channels show a green emission for the quantum dot control and a red emission for the rhodamine control (figure 5.6a). Between quantum dots and rhodamine, there are 1, 3,5,7,9 layer separation. The emission colour is orange indicative of FRET between the quantum dots donors and the rhodamine acceptors.

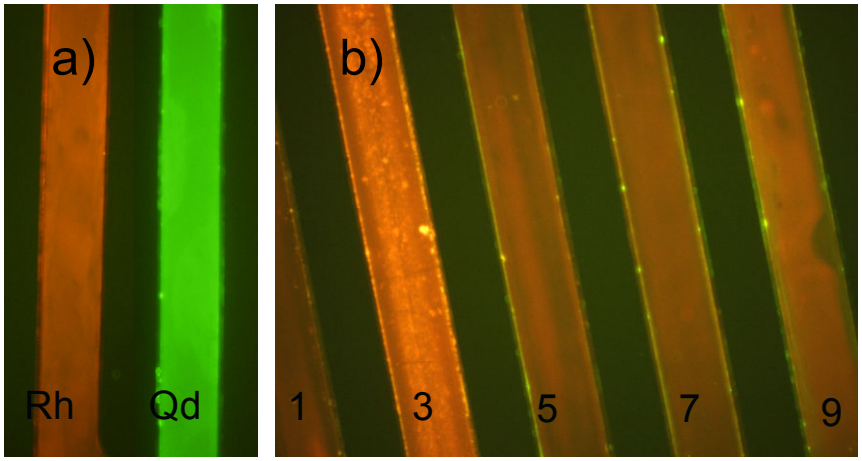

Figure 5.6 a) Fluorescence images of Rhodamine-PAH (red line) and quantum dots (green line); b) quantum dots with 1, 3, 5, 7 and 9 layers separation from Rhodamine-PAH (orange lines) in microfluidic system.

Excitation of the quantum dots at 445 nm results in two clearly separated emission peaks of the quantum dots at 537 nm and of the rhodamine at 588 nm. (Figure 5.7)

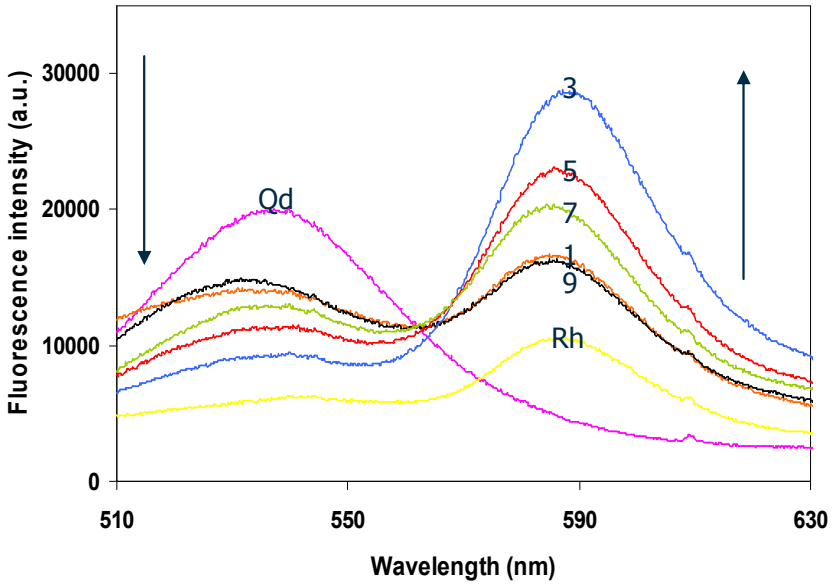

Figure 5.7 Representation of fluorescence spectra from channels containing CdSe/ZnS quantum dots, Rhodamine and quantum dots and rhodamine separated by multiple layers of polyelectrolytes: 1, 3, 5, 7, and 9.

Fluorescence intensity of rhodamine increases while the intensity of quantum dots donor decreases, indicative of fluorescence resonance energy transfer between quantum dots and rhodamine.

5.3.2 Atomic force microscopy (AFM)

The PAH/PSS coatings were analyzed and characterized using AFM (figure 5.9). AFM thickness measurements of patterned PEMs proved that that the height of the PEMs correlate with the thickness obtained previously using the micro patterning convective method [32] and immersion deposition method [14,62,63]. The atomic force microscopy measurements reveal that the thickness of the three layers separating the donor and acceptor molecules was 4.5 nm (~1.5 nm per layer). The film was prepared at low salt concentration (0.1M NaCl). Low salt concentrations are preferably used because the charges of electrolytes repel each other creating a rod-like structure [4, 14]. Additionally, low salt concentrations results in smooth and thin surfaces. Our results are in agreement with previous findings where measurements of PEMs (PAH/PSS) prepared in the same deposition conditions (concentration of polyelectrolyte, salt, and deposition time) revealed a thickness of 19 nm for 13 layers, with 1.46 nm per layer [14].

Image A (Figure 5.8) is a top view image of a 9 layer PEM on a PDMS substrate. The yellow centered line shows the PEM film comprised of (PAH/PSS) 4PAH, formed by using a PDMS microfluidic channel to flow polyelectrolyte sequentially. The left and right brown areas show the bare substrate that was covered during PEM formation and therefore prevented from polyelectrolyte interaction (and hence PEMs formation).

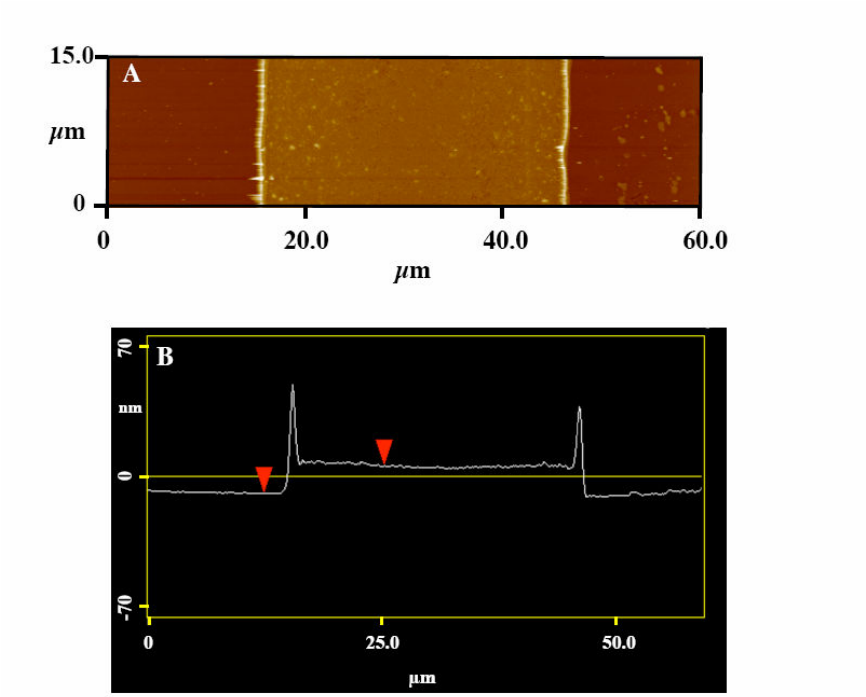

Figure 5.8 A) Atomic force microscopy (AFM) top view image of a 9 layers PEMs on a PDMA substrate. B) Cross-section (average) graph of the image in A.

Image B shows an average height of 14.0 nm. Two other sections of 9 layers lines were analyzed and an average for the three of them obtained (14.2 ± 0.6 nm). The red arrows are pointing at the bare substrate (left) and at the PEMs film (right).

5.3.3. Distribution of Quantum Dots and Their Emission Properties on Polyelectrolyte Multilayers

Distribution of quantum dots within the polyelectrolytes is a function of their degree of solubility in the polyelectrolyte solution and their charge. Thioglycolic stabilized quantum dots with a negative surface charge are less likely to diffusion through positively charged PAH polyelectrolyte. Their negative surface charge ensures a sufficiently strong attraction with PAH electrolyte and a strong electrostatic repulsion with underlying negative electrolyte. The surface charge of quantum dots reflects in their interaction with polyelectrolytes and also modifies of their emission properties [56].

CdTe quantum dots adsorbed on polyelectrolytes and stabilized with mercapto acetic acid showed a decrease in the fluorescence lifetime from 9.58 to 5.78 ns with increasing the thickness of multilayers. This is explained by the increase of exciton recombination relative to surface emission [56].

Investigation of quantum dots distribution on the PAH layer revealed (table1) a relatively homogeneous quantum dots film.

	Average	**Standard dev.**
X axis	45,000	9000
Y axis	33,000	8000

Table1.1 Distribution of quantum dots within the PEMs

Previous studies on photoluminescence properties of CdSe quantum dots embedded in polyelectrolytes revealed that the emission intensity increased 31 times when PDDA

(poly(diallydimethyl-ammonium chloride)) positive polyelectrolyte was added. The explanation consists in passivating the surface defects of quantum dots with PDDA polyelectrolyte and reducing the nonradiative recombination. On the other hand, when PSS negative polyelectrolyte was added to the quantum dots, it resulted in a negligible effect on their emission [48].

It is also described in the literature that [48, 64] the photochemical instability of CdSe quantum dots stabilized with mercaptoacetic acid is due to photooxidation of the quantum dots. Coating of thioglycolic acid quantum dots with a positive polyelectrolyte is thus expected to control the equilibrium of the diffusion of oxygen from the solution to the interface between the crystal and the ligand shell.

However, our studies on the effect of depositing 5 layers of polyelectrolytes on top of quantum dots (green spectrum) on their fluorescence intensity revealed a steady decrease of the fluorescence intensity with every cycle of polyelectrolyte added, with an overall decrease of 10-30% after deposition of polyelectrolyte. This decrease of intensity is due to possible collisional quenching and particle loss during washing steps (Figure 5.9). However, quantum dots incorporated in polyelectrolytes are sufficiently bright and allow measurable signals.

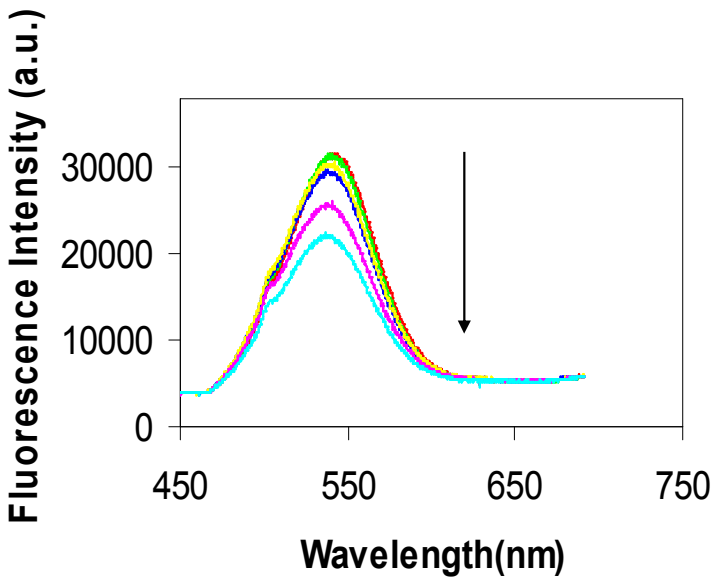

Figure 5.9 Photoluminiscence properties of thioglycolic acid stabilized CdSe quantum dots incorporating in polyelectrolytes

5.3.4. FRET Distribution at Different Salt Concentration of PEMs

The effect of salt concentration between 0.1 and 0.5 M on the FRET efficiency, between the quantum dots and freely diffusing rhodamine molecules at different spacer layer, was further investigated. The Fd/Fa ratio between the quantum dots and the rhodamine acceptors was found to be dependent on the number of polyelectrolyte layers separating between the quantum dots and the rhodamine molecules. Increasing the number of PE layers resulted in less efficient energy transfer corresponding to 5, 7, 9 layers separation between quantum dots and rhodamine.

Increasing the salt concentration from 0.1 to 0.5 M NaCl resulted in a less efficient energy transfer, expressed as Fd/Fa (Figure 5.10) .The 0.1 and 0.2 M salt concentration did not

significantly affect the FRET distribution. On the other hand, the FRET efficiency was less defined with the distance at higher salt concentration (0.5M). This was attributed to the increasing diffusion rate of the rhodamine molecules in the polyelectrolyte film.

As mentioned earlier in this chapter increasing the salt concentration results in an increase of the number of free sites in the polyelectrolyte lattice [16] and subsequently the permeability of freely diffusing molecules.

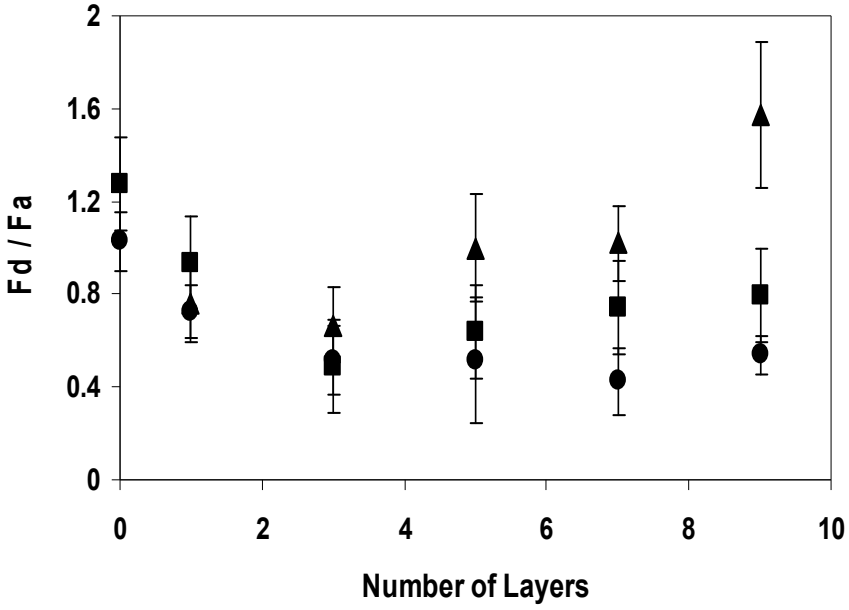

Figure 5.10 Representation of FRET distribution between quantum dots and free diffusing rhodamine in PEMs when salt concentration is (▲) 0.1 M (■) 0.2 M and (●) 0.5M. The data shows a tendency to less defined rate of energy transfer with the distance at increasing the salt concentration.

Conjugation of PAH with rhodamine Red-X is intended to preserve the stability of the sensor and to avoid interferences from permeability of free dye. Immobilization of acceptor molecules resulted in more defined energy transfer rate with distance but a less efficient energy transfer. The less efficient energy transfer is explained by possible perturbations from surface interactions and possible changes in the relative orientation of the donor emission dipole moment and the acceptor absorption dipole moment [65].

Figure 5.11 represents the distribution of FRET with the distance, when PEMs are prepared at 0.5 M salt concentration for freely diffusing rhodamine and PAH conjugated rhodamine. The most efficient energy transfer was observed at three layer separation of quantum dots and rhodamine for conjugated rhodamine.

In literature is also described a comparative study on swelling of polyelectrolyte multilayers in presence of various concentrations of salt (0-2 M). They conclude that the swelling behaviour is highly dependent on the type of polyelectrolyte pairs. However relevant for this study is that PAH/PSS pair of polyelectrolyte showed the most stable behaviour over the range of concentration used [19].

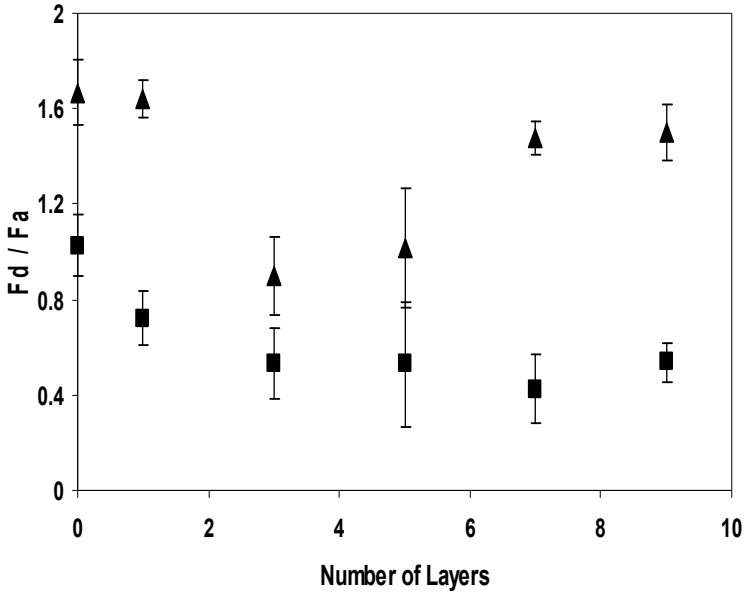

Figure 5.11 Representation of FRET distribution at 0.5M salt concentration of PEMs (▲) with and (■) without fixed rhodamine. The more defined energy transfer is showed at bound rhodamine.

5.3.5. Enzymatic Application of FRET Based Sensor

FRET sensor was designed as a sensor for detecting enzymatic activity from biological fluids and cellular systems which contain tryspsinogen/ trypsin. To fabricate the sensor, we labelled 1mg/mL neurotensin at Arg and Lys amine residues with rhodamine Red-X. The conjugation of labeled peptide to 1mg/mL PAH is followed by deposition to a PSS layer. The FRET efficiency between quantum dots and immobilized rhodamine on neurotensin, as enzyme substrate on the upmost layer of PAH, is expected to decrease due to the tripsin activity which hydrolyzes between Asn-Lys or Arg-Arg residues. The fluorescence intensity of rhodamine decreases while for quantum dots increases after adding tripsin (Figure 5.12).

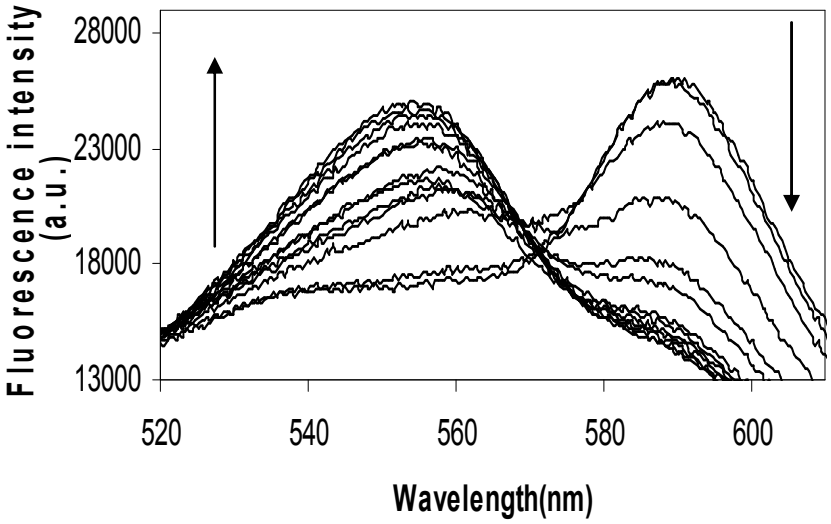

Figure 5.12 Representation of time dependent fluorescence spectra of the quantum dot FRET-based sensor at 0.25mg/mL trypsin

Dynamic studies of time dependent changes of the FRET signal at increasing concentration of enzyme between 0-0.5mg/ml were performed over 65 min. Changes in FRET signals expressed in changes of the ratio F_d/F_a were determined by enzymatic cleavage of the neurotensin molecules which releases rhodamine. Results suggest that at 0.25mg/mL enzyme concentration, F_d/F_a ratio reaches a maximum. At higher concentrations $F_d/F_{a\ is}$ stabilized due to enzyme inhibition effect at higher concentrations (Figure 5.13.).

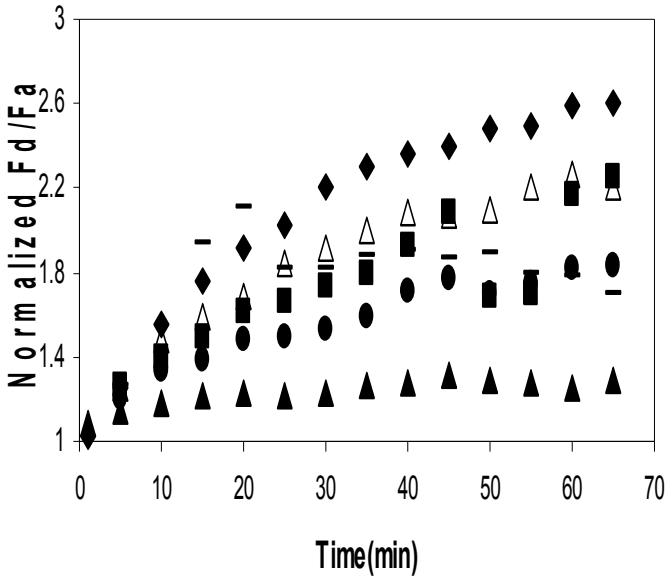

Figure 5.13 Temporal dependence of the rhodamine-labeled neurotensin-PAH sensor at increasing trypsin concentration: ▲0 mg/mL trypsin; - 0.1 mg/mL trypsin; ◆0.25 mg/mL trypsin; ●0.3 mg/mL trypsin ; Δ 0.4 mg/mL trypsin; ■0.5 mg/mL trypsin

Control experiments using rhodamine labeled neurotensin-PAH in microfluidic system in the absence of trypsin suggest minimal changes in the FRET signal (normalized Fd/Fa) during 65 min due to possible desorption of polyelectrolyte polymer in presence of pH shifts (ph7.4), which changes the ratio between positive and negative charges in multilayers.

Digital fluorescence images of microchannels with rhodamine labelled neurotensin-PAH before adding tripsin in Figure 5.14a shows the emission colour in orange characteristic of FRET between quantum dots and rhodamine. Exposure to 0.25mg/mL tripsin results in progressive change in the emission colour of quantum dots from orange to green due to digestion of neurotensin which released rhodamine molecules (Figure 5.14 b, c, d).

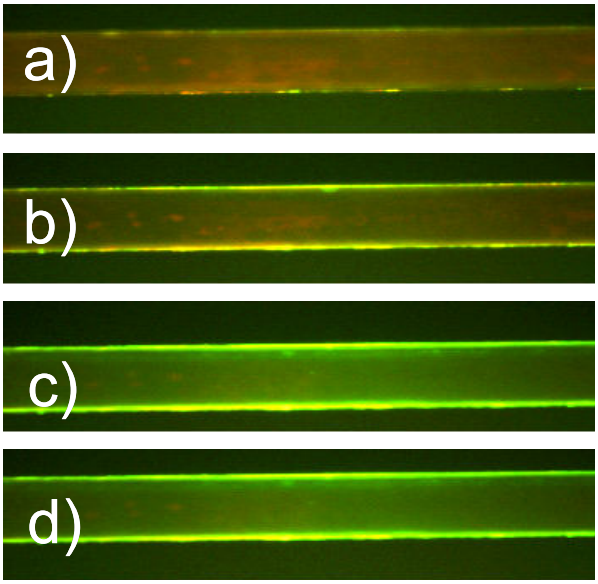

Figure 5.14 Fluorescence images of rhodamine labeled neurotensin-PAH sensor in microfluidic system before and after adding trypsin.

Comparatively is represented in Figure 5.15 the corresponding fluorescence spectra for dynamic measurents of enzymatic activity.

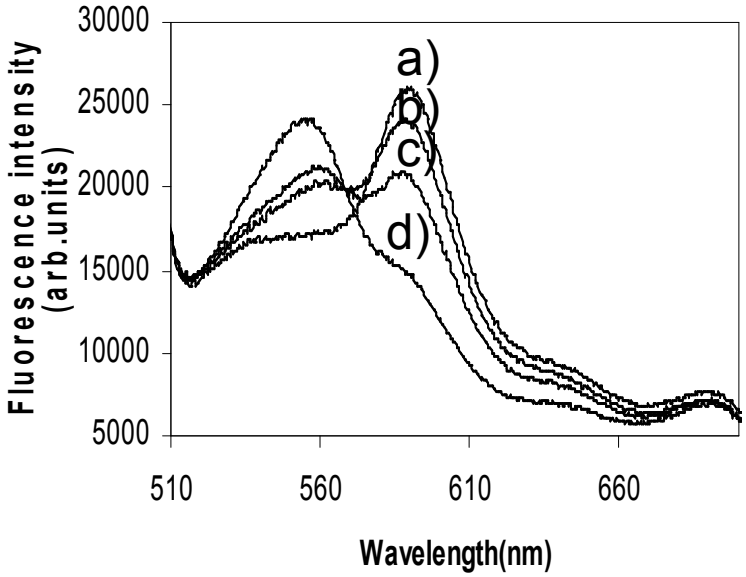

Figure 5.15 Emission spectra of rhodamine labeled neurotensin-PAH in microfluidic system before adding tripsin (a) and 5 min after tripsin (b), 15 min(c), 40 min(d).

5.4 Summary and Conclusions

In conclusion, we have successfully developed a FRET system where quantum dots donor probes and rhodamine acceptor probes were incorporated into polyelectrolytes. The challenges for actual quantum dots sensing probes are to develop a sensor for monitoring enzymatic activity using a method which is non-invasive, non-toxic and non-destructive. Quantum dots embedded in polyelectrolyte multilayer alleviates the toxicity issues which apply the sensor in biological fields.

The FRET based surface sensor for enzymatic activity was developed by incorporating quantum dots as donor and rhodamine labeled neurotensin as acceptor in polyelectrolyte multilayers using layer-by-layer deposition techniques. FRET was employed to investigate the distribution of cromophores within the matrix and evaluate their average separation. The changes in FRET signals between quantum dots and immobilized rhodamine on neurotensin, were indicative of the tripsin activity which hydrolyzes the labeled neurotensin. Developing the sensor in microfluidics provides with necessary tools for precise delivery of reactants to assemble the polyelectrolyte layers and recreate the *in vivo* like cellular microenvironments *in vitro*.

The average distance where the most efficient energy transfer occurs is at three layer separating distance between quantum dots and rhodamine, corresponding approximately to 4.5 nm distance.

Our results are in agreement with the findings of Mattoussi *et al*., who studied fluorescence resonance energy transfer between quantum dots donors and Cyanine dye labeled maltose binding protein (MBP) as acceptors [66]. Enginnered MBP was conjugated with an oligohistidine tail and labeled with acceptor dye Cy3, followed by immobilization on the surface of quantum dots coated with dihydrolipoic acid ligands. Immobilization occurs through electrostatic self-assembly. This association allows of precise control over donor-acceptor separating distance below 10nm.

They treated according to Forster theory, the donor and acceptor as points in the interaction space, even though quantum dots have a finite size and larger than a fluorophore. They approximated the distance between quantum dots center and the position of cyanine molecules on the protein [66]. The measured donor and acceptor distance using different estimates of efficiency, was between 6.5-6.6 nm for 510 nm emission quantum dots; 6.7-6.8 nm for 530 nm emissions of quantum dots and 7-7.1 nm for 555 nm emission quantum dots. These data were in agreement with those approximated from geometrical considerations. X ray scattering and TEM measurements revealed that 555 quantum dots coated with five monolayer of ZnS have a radius of 3-3.1nm, while the spatial extension of protein with location of cyanine dye was of 4nm.Overall the distance was 7-7.1nm [66]. We can approximate that for our quantum dots FRET based sensor for enzymatic activity, the total separating distance was of 7.5 nm which is in agreement with the observations of Mattoussi et al.

Recently, Strouse *et al* [67] introduced another theory about energy transfer when involves nanoparticals and fluorophores. They conjugated a 1.4 nm gold nanoparticle to one end of a DNA strand and fluorescein to the end of complementary DNA strand. As compared to traditional Forster theory, the energy transfer between nanoparticle and fluorescein is a nanosurface energy transfer (SET). It is an interaction between electromagnetic field of the donor dipole and free conducting electrons of the acceptor metal. SET follows $1/R^4$ distance dependence as compared to FRET which is the electromagnetic coupling of two dipoles and follows $1/R^6$ distance dependence. Introducing additional dipoles provides with more coupling interactions and extends the traditional Forster distance beyond 10nm.The application of these optical rulers could extend the measurements of nucleo-protein assemblies of DNA which involves large conformational changes [66]. Our findings, where the most efficient energy transfer was found at three layers of PEMs distance between donor and acceptor, could also be explained through a nanosurface energy transfer between the free conduction electrons of the

semiconductor quantum dots and the dipole moment of the rhodamine acceptor. Nanosurface energy transfers almost double the natural limits of Forster distance.

Investigation of FRET distribution with the distance suggested that the most efficient energy transfer was found at three layer separation distance between donor and acceptor. Increasing the separation distance resulted in less efficient energy transfer. On the other hand, FRET efficiency at distances below 4.5 nm was also minimal because the orientation of the donors and acceptors could potentially prevent the energy transfer when they are located in too close proximity [68].

References

1. Lvov, Y.; Decher, G. & Mohwald, H. *Langmuir* **1993**, 9, 481-486

2. Gong, H.; Garcia-Turiel, J.; Vasilev, K.; Vinogradova& O.I *Langmuir* **2005**, 21, 7545-7550

3. Caruso, F.; Donath, E. & Mohwald, H. *J. Phys. Chem.* **1998***, B* 102, 2011-2016

4. Mc.Aloney, R.; Sinyor, M.; Dudnik, V. & Goh, M. C. *Langmuir* **2001***, 17*, 6655-6663

5. Baur, J.W.; Kim, S., Balanda; P.B., Reynolds, J.R. & Michael F. Rubner, M.F *Adv. Mater*. **1998**, 17, 1452-1454

6.Ball,V.; Hubsch,E., Schweiss, R.; Voegel, J. C.; Schaaf, P.& Knoll, W. *Langmuir* **2005**, 21, 8526-8531

7. Schultz, P.; Vautier, D.; Richert, L.; Jessel, N.; Haikel, Y.; Schaaf, P.; Voegel, J.C.; Ogier, J.& Debry,C. *Biomaterials* **2005**, 26, 2621–2630

8. Kim, H.S.; Sohn, B.H. ; Lee, W.; Lee, J.-K.; Choi, S.J. & Kwon, S.J. *Thin Solid Films* **2002***,* 419, 173–177

9. Shenoy, D.B.; Antipov, A. A.; Sukhorukov, G.B. & Mohwald, H. *Biomacromolecules* **2003***,* 4,265-272

10. Peyratout, C.S. & Daehne, L. *Angew.Chem*. **2004**, 43*,* 3762-3783

11. Sukhorukov, G. B.; Volodkin, D. V.; Gunther, A. M.; Petrov, A. I.; Shenoy, D. B.& Mohwald, H.. *J.Mater.Chem*. **2004**, 14, 2073-2081

12. Roberts, G.G. Plenum Press: New York, 1990; pg.420

13. Antipov, A.A.; Sukhorukov, G.B. *Advances in Colloid and Interface Science* 2004, 111, 49-61

14. Reyes, D.R.; Perruccio, E. M.; Becerra, S. P.; Locascio, L. E. & Gaitan, M. *Langmuir* **2004**, 20, 8805-8811

15. Dong, W-F.; Liu, S.; Wan, L.; Mao, G.; Kurth, D.G.; Mohwald, H. *Chem. Mater*. **2005**, 17, 4992-4999

16. Antipov, A.A.; Sukhorukov,G.B.; Mohwald, H. *Langmuir* **2003**, 19, 2444-2448

17. Qui, X.P.; Leporatti, S.; Donath, E.; Mohwald, H. *J. Phys. Chem*. **2001**, 17, 5375-5380

18. Steitz, R.; Leiner, V.; Siebrecht, R.; v. Klitzing, R. *Colloids Surf, A* **2000**, 163, 63-70

19. Dubas, S.T.; Schlenoff, J.B. *Langmuir* **2001**, 17, 7725-7727

20. Israelachvili, J. Intermolecular and Surface Forces, second edition, Academic Press: San Diego, CA, 1992; Chapter 12

21. Gong, H.; Garcia-Turiel, J.; Vasilev, K.; Vinogradova, O. I. *Langmuir* **2005**, 21, 7545-7550

22. Georgieva, R.; Dimova, R.; Sukhorukov, G.; Ibarz, G.; Mohwald, H. *J. Mater.Chem.* **2005**, 15, 4301-4310

23. Tryoen-Toth, P.; Vautier, D.; Haikel, Y.; Voegel, J.-C.; Schaaf, P.; Chluba, J.; Ogier, J. *J. Biomed.Mater.Res*. **2002**, 60, 657-667

24. Kumar, G.; Wang, Y.C.; Co, C.; Ho, C.-C. *Langmuir* **2003**, 19, 10550-10556

25. Blohm, D.; Guiseppi-Ellie, A. *Curr. Opin. Biotechnol*. **2001**, 12, 41-47

26. Freeman, W.; Robertson, D.; Vrana, K. *BioTechniques* **2000**, 29, 1042-1055

27. Marler, J.; Upton, R.; Langer, R.; Vacanti, J. *Adv. Drug Delivery Rev*. **1998**, 33, 165-182

28. Andersson, H. &Van den Berg, A. *Lab Chip* **2004***,* 4**,** 98-103

29. Healy, K.; Thomas, C.; Rezania, A.; Kim, J.; Mc Keown, P.; Lom, B.; Hockberger, P. *Biomaterials* **1996**, 17, 195-208

30. Takayama, S.; Ostuni, E.; LeDuc,. Naruse, Ingber, D.; Whitesides, G. *Nature* **2001**, *411*, 1016

31. Walker, G. M.; Zeringue, H.; Beebe, D.J. *Lab. Chip.* **2004**, 4, 91-97

32. Jang, H.; Kim, S.; Char, K. *Langmuir* **2003**, 19, 3094-3097

33. Klimov, V. *Los Alamos Science* **2003**, 28, 214-220

34. Chan, W.C.W.; Nie, S. *Science* **1998**, 281, 2016-2018

35. Shi, L.; Rosenzweig,N.; Rosenzweig, Z. *Anal. Chem.* **2007,** 79, 208-214
36. Pathak,S.; Choi, S.K.; Arnheim, N.; Thompson,M.E. J.*Am. Chem. Soc.* **2001**, 123, 4103-4104

37. Mattoussi, H.; Mauro, J.M.; Goldman, E.R.; Anderson, G.P.; Sundar, V.C.; Mikulek, F.V.; Bawendi, M.G.; *J. Am. Chem. Soc*. **2000**, 122, 12142-12150

38. Gao, X.; Cui, Y.; Levenson, R.M.; Chung, L.W.K.; Nie, S. *Nature Biotechnology* **2004**, 22(8), 969-976

39. Michalet, X.; Pinaud, F.F.; Bentolila, L.A.; Tsay, J.M.; Doose, S.; Li, J.J.; Sundaresan, G.; Wu, A.M.; Gambhir, S.S.; Weiss, S. *Science* **2005**, 307, 538-544

40. Efros, A.L.; Rosen, M. *Annu. Rev. Mater. Sci*. **2000**, 30, 475

41. Sukhanove, A. et al. *Anal Biochem*. **2004**, 324, 60

42. Alivisatos, A.P. *Nature Biotechnol.* **2004**, 22, 47

43. Tokumasu, F.; Dvorak, J. *J Microsc*. **2003**, 211, 256

44. Wu, X.Y. et al. *Nature Biotechnol*. **2003**, 21, 41

45. Wang, D.; He, J.; Rosenzweig, N.; Rosenzweig,Z. *Nano Lett* **2004**; 4(3); 409-413.

46. Parak, W.J. et al. *Adv. Mater*. **2002**, 14, 882
47. Honhng, S.; Ha, T. *ChemPhysChem* **2005**, 6, 956-960
48. Zhang, S.; Yu, J.; Li, X.; Tian, W. *Nanotechnology* **2004**, 15, 1108-1112
49. Fromherz, P. ; Reinbold, G. *Thin Solid Films* **1998**, 160, 347-353
50. Richter, B.;Kirsten, S. *Journal of Chemical Physics* **1999**, 111,5191-5200

51.Schneider, G.; Decher, G.; Nerambourg, N.; Praho, R.; Werts, M. H.V.; Blanchard-Desce, M. *Nano Lett*. **2006***,* 6(3), 530 – 536

52. Peralta, S.; Nicol, E.; Moussa, A.; Habib-Jiwan, J.L.; Jonas, A. *Polym. Mat. Sci. and Eng*., **2003**, 89, 267

53. Walker, G. M.; Zeringue, H.; Beebe, D.J. *Lab. Chip.*, **2004,** 4**,** 91-97

54. Andersson, H.; Van den Berg, A. *Lab Chip* **2004,** 4, 98-103

55. Forry, S.P.; Reyes, D.R.; Gaitan, M.; Locascio, L. *Langmuir* **2006***, 22*, 5770-5775

56. Komarala, V.K. et al. *Nanotechnology* 2006, 17**,** 4117-4122

57. Peng, Z.A.; Peng, X. *J. Am. Chem. Soc.* **2001**, 123, 183-184

58. Pellissier, S.; Eribon, O.; Chabert, J.; Gully, D.; Roche, M. *Neuropeptides* **1996***,* 30(5), 412-9

59. Bardella, M.T.; Fraquelli, M.; Peracchi, M.; Cesana ,B.M.; Bianchi, P.A; Conte, D. *Scand J Gastroenterol* **2000***,* 35*,*269-273

60. Ouyang, Z.; Takáts, Z.; Blake, A. T.; Gologan, B.; Guymon, A.J.; Wiseman, J. M.; Oliver, J.C.; Jo Davisson, V.; Cooks, R. G. S*cience* **2003** 301, 1351 – 1354

61. Uchima, Y.; Sawada, T.; Nishihara, T.; Umekawa, T.; Ohira, M.; Ishikawa, T.; Nishino, H.; Hirakawa, K. *International Journal of Molecular Medicine* **2003**, 12, 871-878

62. Decher, G.; Hong, J.-D.; Schmitt, J. *Thin Film Solids* **1992**, 211, 831-835

63. Decher, G.; Schmitt, J. *J. Prog. Colloid Polym.Sci.* **1992**, 89, 160-164

64. Aldana, J.; Wang, Y. A.; Peng, X. J. *Am.Chem. Soc*. 2001, 123, 8844

65. Deniz, A. A.; Dahan, M.; Grunwell, J. R.; Ha, T.; Faulhaber, A. E.; Chemla, D. S.; Weiss, S.; Schultz, P.G *Proc. Natl. Acad. Sci.* **1999***,* 96, 3670–3675

66. Clapp, A. R.; Medintz, I. L.; Mauro, J. M.; Fisher, B. R.; G. Bawendi, G.; Mattoussi, H. *J. Am. Chem. Soc***. 2004**, *126*, 301-310

67. Yun, C. S.; Javier, A.; Jennings, T.; Fisher, M.; Hira, S.; Peterson, S.; Hopkins, B.; Reich, N. O.; Strouse, G. F.*J. Am. Chem. Soc.* **2005**, *127*(9); 3115-3119

68. Joseph R. Lakowicz, Principles of Fluorescence Spectroscopy, Chapter 13: Energy transfer, pg 368, Kluwer Academic /Plenum Publishers, 1999

CHAPTER 6

DISCUSSION

In this dissertation we investigated several techniques to develop new surface optical chemical sensors for studying cellular processes. We employed two techniques to transform the surface properties: covalent immobilization of the sensor on modified glass surfaces or biological molecules and electrostatic immobilization of the sensor by creating multilayer nanometer films. These techniques have inherent advantages and disadvantages intrinsic for each immobilization method.

The nanosurfaces act as sensing materials and transducers which converts the analyte-sensor interaction, i.e. biological or chemical data, into a continuous optical signal corresponding to the analyte concentration for real-time monitoring. These sensors require microliters volumes for sampling “in vitro” specimens.

Chapter 3 and 4 describes a covalent immobilization approach to modify surface properties. Chapter 3 describes the development of zinc sensing glass slides and their analytical properties. To prevent the leakage of the fluorophore, for the first time, a new fluorescent zinc sensing dye, carboxyl-modified ZnAF-2 {6-[N- [N’, N’-bis (2-pyridinylmethyl)-2-aminoethyl] amino-3’, 6’-dihydroxy-spiro [isobenzofuran-1(3H), 9’-[9H]xanthene]-3-one}[1,2] was conjugated to a glass

surface treated with amino silanization agent. ZnAF2 was synthesized from corresponding 6-aminofluorescein. The apparent dissociation constant, *K*d for ZnAF2 is 2.7 nM.

The mechanism of sensing of the chemosensor is based on photoinduced electron transfer. In absence of zinc ions, the fluorescence "switched off" and is "turned on" when zinc ions are added to the solution. The chemosensor absorbs in the visible region of the electromagnetic spectrum and has a high selectivity for Ca , Mg and transition metals. To achieve this selectivity the zinc binding site was designed to accommodate four nitrogens. When zinc ions are added, the four nitrogens of the acceptor form a four coordinative complex with a tetrahedral geometry. The preferred coordination number (CN) for magnesium is six with a predilection for oxygen ligands [4]. The energetic penalty of magnesium ions to change the CN to 4 is high. Calcium ions have a preferred coordination number of 6-9 observed in crystal structures with predilection for oxygen ligands [5].ZnAF-2 also binds to Fe2+ or other transitional metals, but it does not significantly affect the fluorescence intensity, because they do not preferably bind to the pivotal nitrogen of the fluorescence switch, which is the aromatic secondary amine. CN number for Fe2+ is 6 with a sp^3d^2 hybridization which determines an octahedral geometry. CN for group IA like sodium ions is 6 and 4 for potassium for all types of ligands [6].

Characterization studies indicated that the glass slide-based zinc sensors have high sensitivity, selectivity and fast response time to measure zinc ion release events from pancreatic cells.

There are inherent factors which affect the quantitative power of the zinc sensing glass slides. The dynamic range (between 1.25-20nM Zn) in low nanomolar concentrations is inadequate to quantitate micromolar levels of zinc released in secretory events. However the sensor could detect early release events from beta pancreatic cells.

We identified several sources of heterogeneity which resulted in relatively high standard deviation of the calibration curve: physical heterogeneous surface of silica substrate; silanization procedure and the deprotection reaction of zinc binding site. There was also an uncertainty about the level of availability of the zinc binding site after conjugation.

The pivotal nitrogen of ZnAF-2 which belongs to the zinc binding site was typically protected with nossyl group during EDC/sulfo NHS coupling reaction. However, when the conjugation reaction involved an unprotected ZnAF-2, the sensor responded readily in the presence of zinc solutions. To circumvent the possibility of participation of this nitrogen in the reaction, which would negatively affect the zinc sensing properties of ZnAF-2, we usually used the nossyl protected ZnAF2 during the fabrication of the zinc sensing glass slides. The protecting group was removed from the zinc binding site once ZnAF-2 was covalently bound to the glass surface. The success of the deprotection reaction on a solid substrate was also a parameter accounting for the heterogeneity of glass slide zinc sensor.

The film sensor reversibility and reusability was evaluated by alternate exposure to zinc solutions and TPEN chelator solutions. The sensor showed excellent reversibility, it preserved the zinc sensitivity for up to 5 repeated exposures. Reversibility of the zinc sensor could be further exploited in detecting multiple zinc release events from beta pancreatic cells.

The sensor was used for the measurement of glucose-stimulated zinc ion release from beta pancreatic cells with impact in diabetes research. Cells deposited on top of the film sensor maintain their physiological state and respond to glucose stimulation.

Future studies reside in investigation of alternatives to minimize the heterogeneity in the signal of zinc sensing glass slides (e.g., by developing the sensor on a modified PDMS, different silanization approach).

Chapter 4 describes the conjugation of the carboxyl-modified ZnAF-2 to antibody molecules (A2B5) that specifically recognize pancreatic cells. For a targeted measurement of zinc ion release from pancreatic β cells, we synthesized a coating of beta cells with an antibody sensor. For the first time, this enabled the use of targeted zinc sensors to monitor zinc release events from pancreatic cells. Due to a higher dynamic range (0-1μM), the antibody sensor can be used to detect physiologically relevant zinc level in the micromolar range.

The sensor showed biocompatibility with beta cells: coated cells retained the properties of insulin release upon glucose stimulation. Future studies on insulin-zinc release from beta cells using microinjection delivery of secretagogues to the single cells could bring insights in understanding the cell-to-cell signaling mechanisms during exocytosis.

Chapter 5 describes the development, for the first time, of a fluorescence surface sensor to measure the proteolytic activity of pancreatic cancer cells in microfluidic systems. The sensor was fabricated using a Layer by layer (LbL) deposition of polyelectrolytes. The sensor was based on Fluorescence Resonance Energy Transfer (FRET) between luminescent quantum dots as donor probes and rhodamine molecules as acceptor probes that are separated by multi-layers of polyelectrolyte.

The novelty of this technique consists in the capacity to control the surface chemistry such to provide the films with unique properties. Hence, using layer-by-layer method which involves sequential adsorption of oppositely charged polyelectrolyte, it enables the control of the topography, height, charge, functionalities and biocompatibility of the films. The electrostatic deposition of the polymers combined with microfluidics ensures patterns of lines of polyelectrolyte multilayers with a high resolution. Employing distance –dependent fluorescence

resonance energy transfer phenomenon, in the design of the sensor, characterized by enhanced sensitivity and selectivity of fluorescence provided biological sensing with elements inaccessible to fluorescence sensors.

The FRET efficiency between quantum dots and immobilized rhodamine on neurotensin, an enzyme substrate on the topmost layer of PAH, decreased due to trypsin activity which hydrolyzes between Asn-Lys or Arg-Arg residues of the peptide.

The great accomplishment of this surface nanosensor was the ability to provide site specific information due to the proximity of the sensor with the enzymatic activity. Moreover, biocompatibility of these coating materials combined with growing single cells in micro channels provides the fundamental advantages of sampling in microfluidics e.g., study of subcellular processes when different drugs are applied to different area of a cell [3].

In comparison with the covalent immobilization of the sensors on an aminosilanized surface of glass slides, the electrostatic immobilization of the sensor incorporated in PEMs resulted in improved reproducibility of the films.

References

1. Hirano, T.; Kikuchi, K.; Urano, Y.; Higuchi, T.; Nagano, T. *J Am Chem Soc* **2000** , *122*, 12399-12400.
2. Crivat, G.; Kikuchi, K.; Nagano, T.; Priel, T.; Hershfinkel, M.; Sekler, I.; Rosenzweig, N.; Rosenzweig, Z. *Anal. Chem.* **2006**; *78*(16); 5799-5804
3. Andersson, H.; Van den Berg, A. *Lab Chip* **2004,** 4, 98-103
4. Bock, C. W.; Kaufman, A.; Glusker, J. *P Inorg. Chem.* **1994**, 33*,* 419-427
5. Bock, C. W.; Katz, A. K.; Glusker, J. P. *J. Amer. Chem. Soc.* **1995**,117, 3754-37
6. Tunell,I.; Lim,C. *Inorganic Chemistry* **2006**, 45(12), 4811

VITA

The author was born in Judetul Olt, Romania. She enrolled at the University of Bucharest in the department of Biology. Her research thesis, on immunoelectrophoresis techniques was performed at "Dr. Ion Cantacuzino Institute in Bucharest. She worked as a biologist at the Institute for Nutrition, Diabetes and Metabolic Diseases "Nicolae Paulescu "in Bucharest. She was involved in clinical and experimental diabetology and endocrinology research. In 2002 she enrolled in the University of New Orleans' graduate program, in the Chemistry Department. In December 2002 she joined Prof. Zeev Rosenzweig group. The group explores techniques to develop fluorescence based nanosensors with direct application in biological and medical fields. Development of fluorescence based surface sensors for pancreatic activity was a unique opportunity to carry on and make use of previous practice in diabetes research.